安捷伦 7200 GC/Q/TOF 应用文集

The Measure of Confidence

Agilent Technologies

终极性能
AGILENT 7200 四极杆飞行时间气质联用系统

The Measure of Confidence

- 代谢组学
- 食品质控和农药残留
- 天然产物研究
- 人类和动物兴奋剂
- 环境污染物
- 法医/毒理学
- 能源研究和石油化工
- 食品研究、香精和香料
- 材料研究和监测
- 合成物确认和质控
- 国土安全

质量精度稳定

质量误差 < 5ppm
≈ Δ 0.0009Da@188.1405

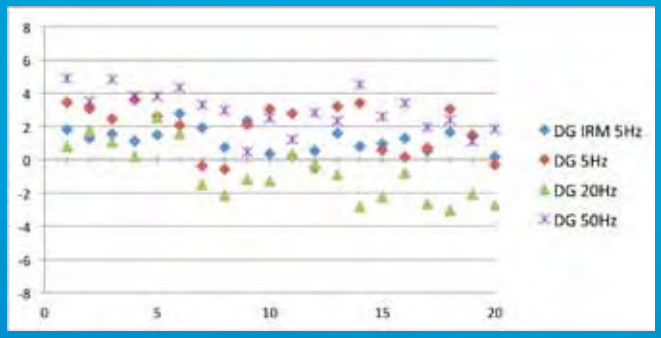

MS/MS 模式的定性分析

分子结构关联计算 (MSC) 工具有助于通过 MS/MS 谱图进行结构解析。

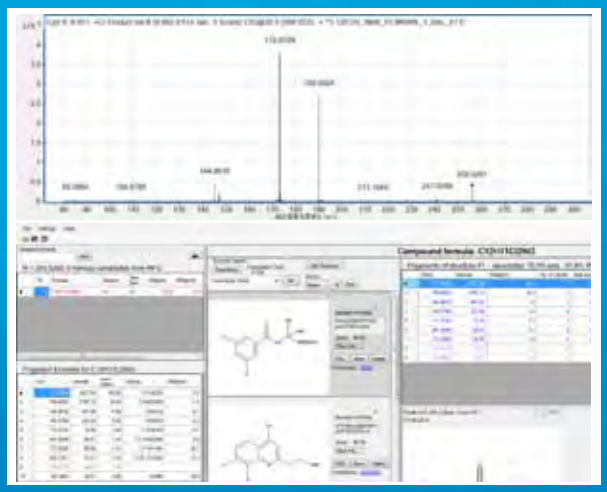

满足定性分析要求的高分辨率

> 13,000 @ m/z 271.9867
（高分辨模式）

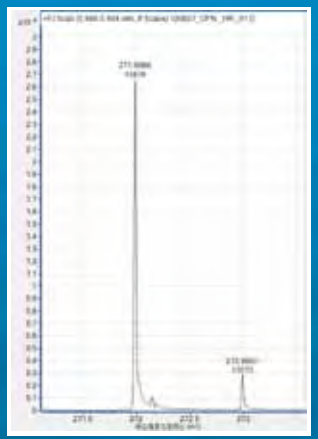

宽线性范围定量分析

> 4 个数量级
（双增益模式）

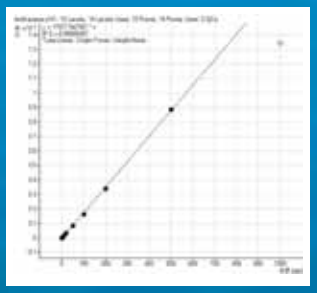

离子源可拆卸

无需放空即可轻松切换离子源

目 录

安捷伦 7200 Q-TOF GC/MS

对最有挑战性的应用实现最有力的定性和定量分析

The Measure of Confidence

最大限度地提高检测的选择性，实现目标物和未知物的准确分析

复杂的基质和痕量分析均要求分析者提供最佳的定性和定量数据。现在，一种新型分析技术的出现可以帮助您找到答案。

安捷伦 7200 Q-TOF GC/MS：使您最棘手的分析获得最高的分辨率、精确的质量数、全谱高灵敏度检测和 MS/MS 级的选择性

安捷伦 7200 Q-TOF 是世界上首款专门针对气质联用系统设计的 Q-TOF（四极杆飞行时间质谱）。它完美结合了分离功能强大的 7890 系列 GC 和 7000 三重串联四极杆 GC/MS 以及 6500 LC/Q-TOF 系统中久经考验的 MS 组件，重新诠释了 GC/MS 分析技术。它具有可靠的 GC/MS 操作平台，出色的选择性、全谱高灵敏度质谱数据采集、高速采样频率、准确的质量信息，极大地简化了分子表征和结构鉴定的过程。

世界首台 Q-TOF GC/MS，集分离功能强大的安捷 7890 GC 和高选择性、高分辨率的 TOF 质谱仪为一体

实现出色的定性*和*定量分析的首选

安捷伦 7200 Q-TOF GC/MS 完美结合了旗舰 GC/MS 系统中最炙手可热的特性与如下先进的功能：

高分辨率和精确的质量数

低至 ppm 级的质量精度，高出单四极杆质谱 15 倍到 50 倍的分辨率，可实现针对目标物、非目标物和未知化合物高度可靠的分析。

低检出限和卓越的线性

高于四极杆质谱的全谱范围的灵敏度可以以最精确的质量数捕集色谱柱上大多数低至 pg 级的化合物。双增益放大模式可将范围扩展至 10^5。

无以伦比的 MS/MS 选择性

高分辨率 MS/MS 的检测选择性远远超越其他 MS/MS 分析仪。此外，具有精确质量数的子离子谱图不但可以帮助鉴定目标物和非目标物，而且还有助于解析未知化合物。

简化对精确质量的 MS 和 MS/MS 数据分析

安捷伦 MassHunter 软件提供有效的工具用于定性、定量分析和结果确认。

- 使用专为 EI 或 CI 数据优化的解卷积软件确定复杂样品中的化合物
- 将谱库检索结果与计算得到的分子离子和碎片离子分子式相结合，确定化合物结构，简化定性过程
- 使用 Mass Profiler Professional，一种质谱数据的化学计量学软件，可在几种数据文件上执行多元统计分析

精确质量数信息可以使您信心十足地进行化合物的定性和定量分析。

久经考验的设计
与尖端科技相结合

7890 GC 全优的性能

包括多模式进样口、高性能反吹功能和快速、低热容的色谱柱技术

高灵敏度的提取离子源

程序升温最高达 350 °C，可长时间经受复杂基质的考验

可加热的石英整体双曲面四极杆

可加热至 200 °C 而没有分辨率或灵敏度的损失，消除高沸点色谱峰的污染

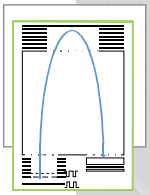

稳定、高性能的 TOF 技术

安捷伦正交 TOF 技术确保成千上万的 LC/TOF 和 LC/Q-TOF 具有高度一致的性能

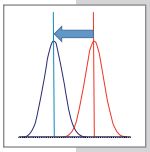

内标质量校正 (IRM)

必要的时候，可以将 IRM 化合物导入系统中进行校正，确保质量精度最大化

可拆卸的离子源

通过计算机控制传输线和真空内锁装置，确保 30 min 内无需排空即可更换离子源而不会引起任何故障

更多有关安捷伦 7200 Q-TOF GC/MS 的性能，
请访问 **www.agilent.com/chem/GCMS_QTOF:cn**

安捷伦 7200 Q-TOF GC/MS 是成熟技术与全新、独特功能的完美结合

二级离子镜改善了二阶时间聚焦，从而提高了质量分辨率

专利设计的 INVAR 飞行管，密封在真空隔绝外壳中，消除了由于温度改变导致的质量漂移，保证了全天候的质量准确度。同时加长的飞行管提高了质量分辨率

4 GHz ADC 电路设计提供更高的采集速率 (32 Gbit/s)，因此提高了低浓度样品检测的分辨率、质量精确度和灵敏度

双增益放大器将动态范围扩大到 10^5

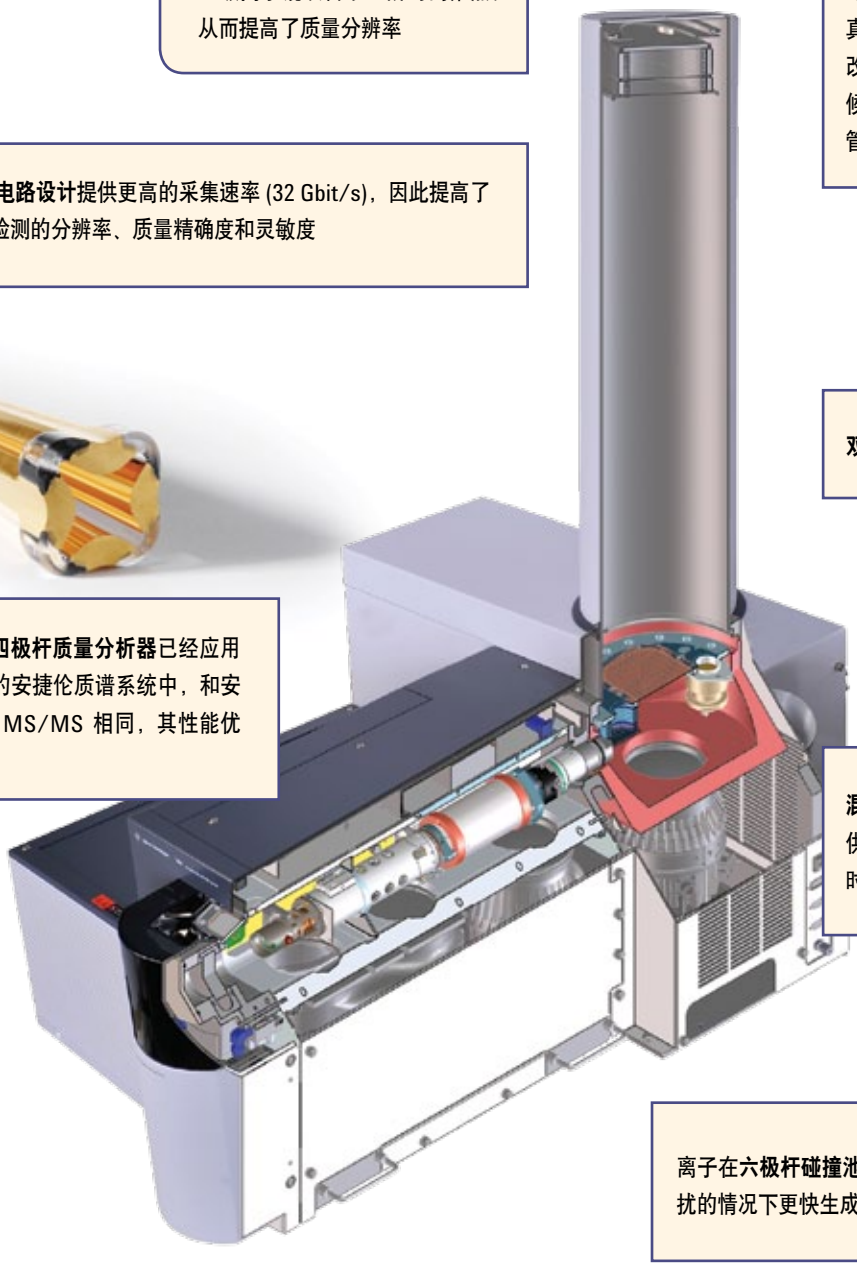

可加热的石英整体四极杆质量分析器已经应用到超过 20,000 台的安捷伦质谱系统中，和安捷伦 7000 四极杆 MS/MS 相同，其性能优势众所周知

混合通道板光电倍增管离子检测器提供单离子级别的检测灵敏度、卓越的时间分辨率和更宽的线性范围

离子在**六极杆碰撞池**中被加速，可以在没干扰的情况下更快生成高质量的 MS/MS 谱图

三个分子涡轮泵，包括两个单级泵和一个用于离子源和四极杆分析器的差分泵，为分析器各区域提供最优的真空条件

卓越的线性和质量精度可以分析目标物、非目标物以及未知化合物

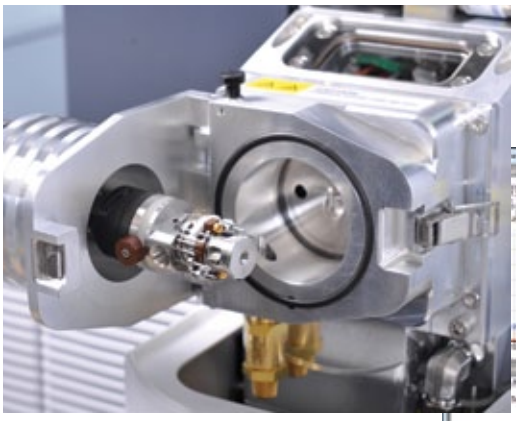

***新型可拆卸离子源（RIS）**，便于快速更换整个离子源组件，包括推斥极、离子体、拉出极和双灯丝，并且 30 min 内可完成，无需对质量分析仪放真空*

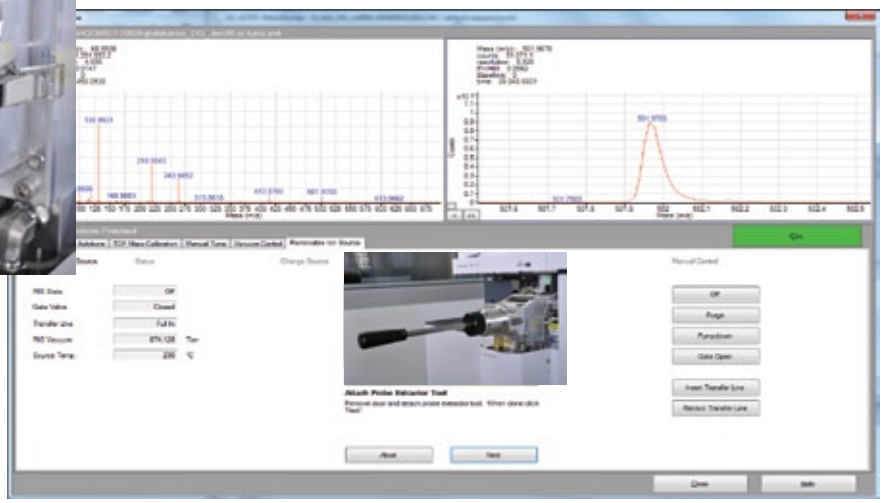

***界面友好的视频和软件**引导用户逐步进行离子源的拆卸和安装，确保整个过程安全无误*

色谱柱上含量 pg	质量误差 ppm	
	2-甲酰噻吩	2-乙酰基噻唑
1	-3.57	-0.79
2	-4.46	-0.79
5	-2.68	-0.79
10	-2.68	0.79
20	-2.68	0.00
50	-0.89	1.57
100	0.00	1.57
200	-1.79	1.57
500	2.68	1.57
1000	1.79	-1.57
平均值	-1.43	0.31

***新型内标质量（IRM）**校正是一种专用系统，用校准化合物在每次扫描中对质量轴进行校正。IRM 可确保大多数复杂谱图条件下低至 ppm 级的质量准确度*

***模拟数字转换（ADC）检测器：**ADC 电路 4 GHz 的采集速率可在高分辨率模式下获得出色的线性。为获得更宽的线性范围，双增益放大器可通过低增益通道和高增益通道同步处理检测器信号，使动态范围高达 10^5*

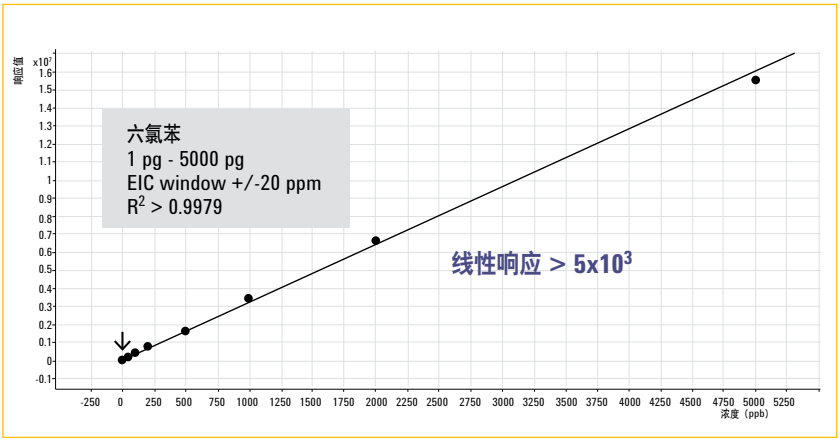

更多有关安捷伦 7200 Q-TOF GC/MS 的性能，
请访问 **www.agilent.com/chem/GCMS_QTOF:cn**

结果证明 GC/Q-TOF 技术使出色的定性和定量分析真实、可行

依靠安捷伦 7200 Q-TOF GC/MS 低至 ppm 级的质量精确度和高分辨率，用户可以降低分析的不确定性，将假阳性减至最低，确认数据库检索结果，得到未知化合物的分子式。

快速、无障碍设置

自动化采集软件指导用户逐步进行调谐和质量校准操作，获得精确的高分辨率和准确的质量数。

极高的分辨率是定性结果高度可信的重要保证

系统高达 13500 (FWHM) 的分辨率可轻松将标称质量均为 240 Da 的两个化合物分离，二者的精确质量数只相差 0.0436 Da。

极高的分辨率对准确识别复杂基质中的化合物是必不可少的。

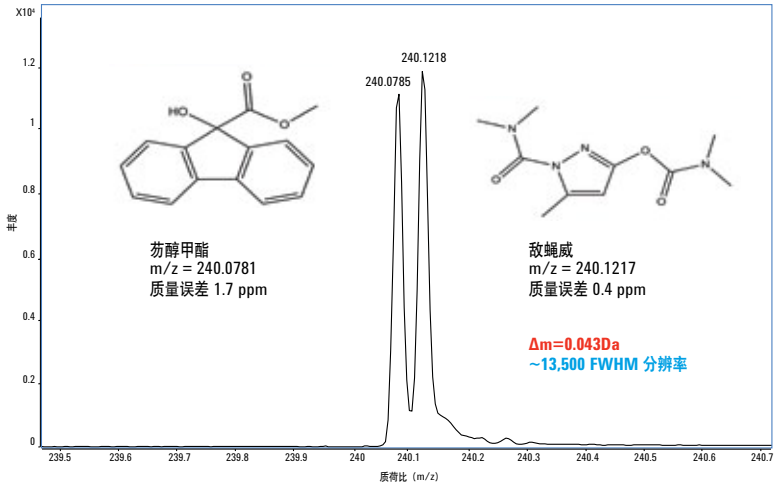

精确的质量数可有效消除基体干扰

使用精确至 0.010 Da 的提取离子窗口，目标物茚虫威的碎片离子 (150.01195 Da) 可轻松从基体干扰物 β-生育酚的离子 (150.06839 Da) 中分离出来，这无疑有利于准确可靠的定量分析。

当分析对选择性要求更高时，可采用精确质量的 MS/MS 技术将目标分析物和基体干扰物进一步分离。

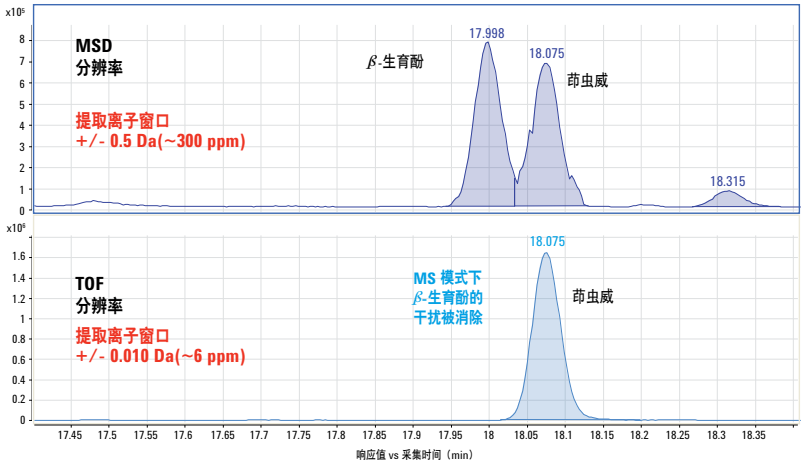

明确的结构鉴定和目标物确认

目标物和未知物的识别可通过多种技术确认：

- 进行 EI 谱库检索
- 在 PCI 模式下测定分子离子峰
- 对多个母离子进行 MS/MS 裂解以记录裂解途径——安捷伦独创
- 通过精确质量数据计算所有离子的分子式

对于非常棘手的复杂分离，如右图中的 α-苹澄茄油萜样品，MS/MS 的选择性同样可生成简化的质谱图以方便鉴定结构。

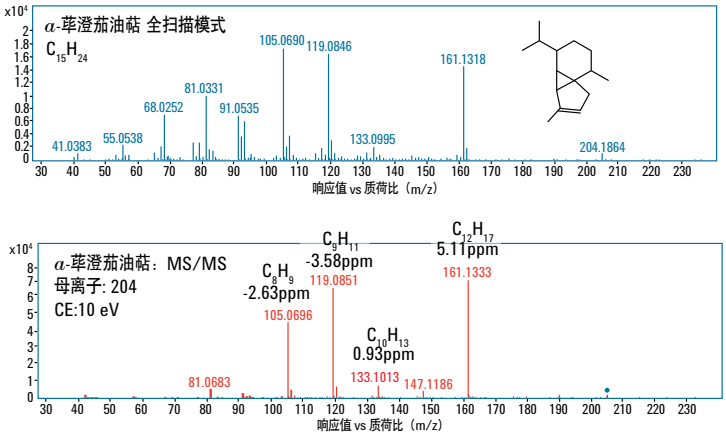

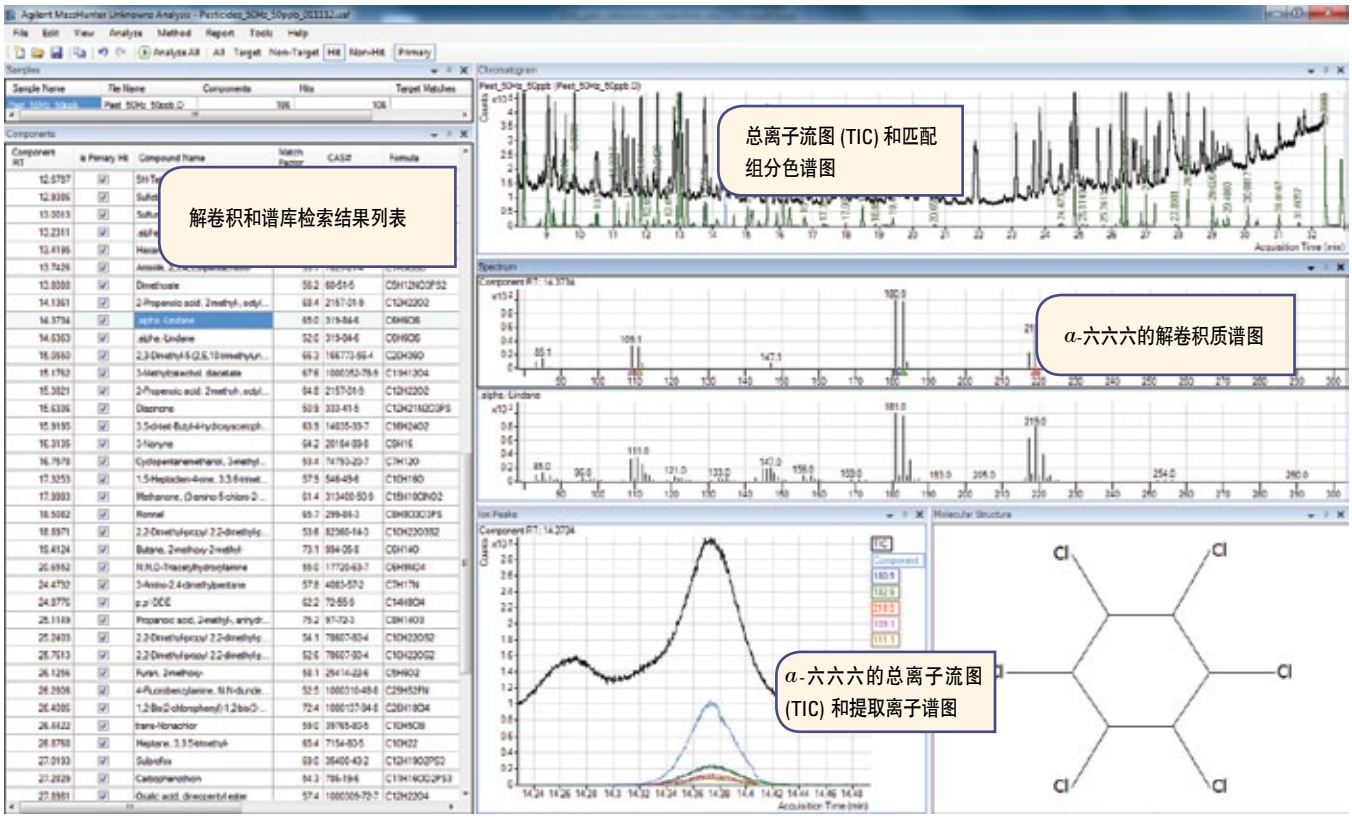

高速谱图采集是 TOF MS 的另一个基本优势。*高达 50 Hz 的采集速率可以使您通过 MassHunter's Unknowns Analysis 软件的色谱图解卷积功能高效地解析大量组分*

更多有关安捷伦 7200 Q-TOF GC/MS 的性能，
请访问 **www.agilent.com/chem/GCMS_QTOF:cn**

代谢组学

分析和推测细胞功能的变化

代谢组学是研究不同条件下代谢变化的有力工具。复杂的代谢研究充分结合 GC/Q-TOF 全扫描技术的高灵敏度和高质量精度以及 MS/MS 的高性能，用于未知代谢物的结构鉴定。7200 GC/Q-TOF 扩展的动态范围使其可以对一个细胞中存在的一系列代谢物同时进行准确的鉴定分析。

对于一个简单实验，安捷伦 7200 Q-TOF GC/MS 可以提供准确的质量信息、全扫描模式下出色的灵敏度和动态范围等必需的基本要素，用于识别和定量代谢通路中研究的所有中间产物，从而准确无误地揭示出受试样品在生化通路中的反应步骤。

Mass Profiler Professional (MPP) 软件用于统计数据的评估，分析内容包括数据筛查，基线校正和显著性检验。该软件的可视化操作工具同样是数据分析不可缺少的因素。

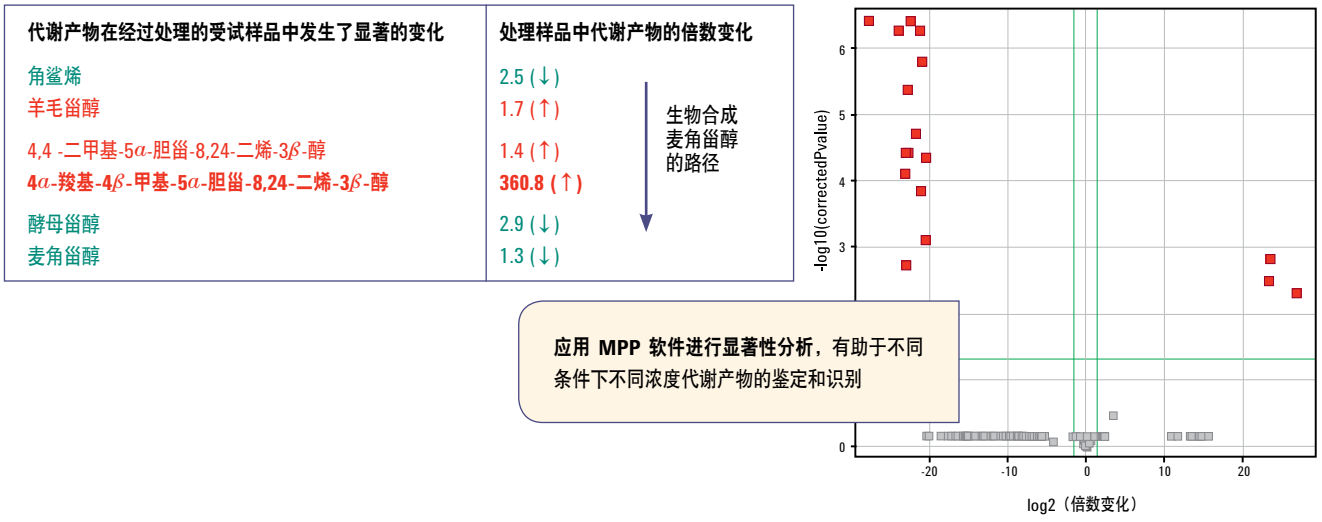

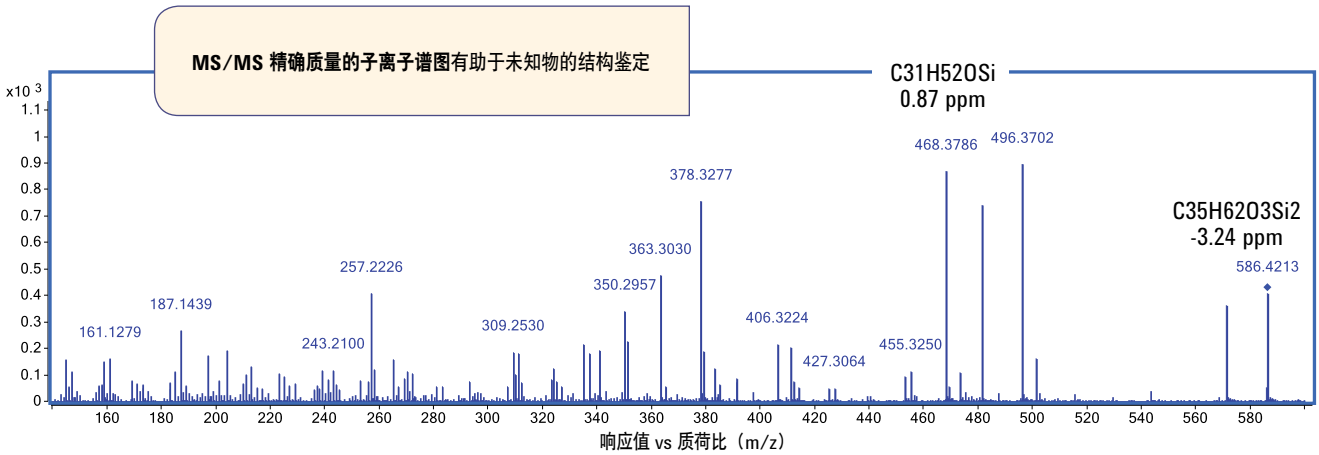

基于精确质量的子离子谱图对代谢产物的可能结构进行确认

代谢组学研究中经常出现大量的非目标物和未知代谢产物，它们对数据的生化解析会产生潜在的重要影响，因此，这些重要代谢产物的结构必须十分明确。安捷伦 7200 Q-TOF GC/MS 和 MassHunter Workstation 软件结合使用是此类研究的理想之选。

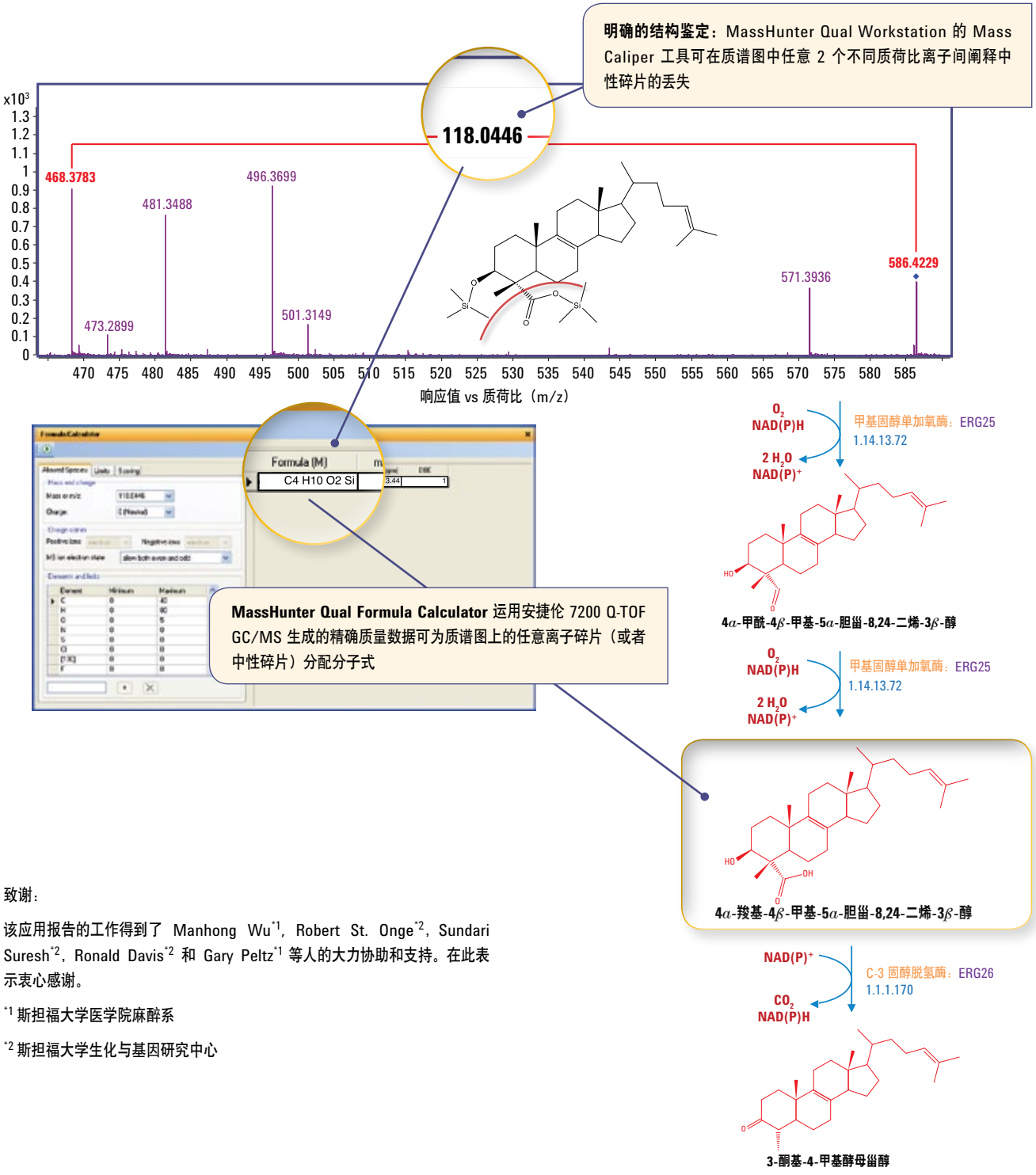

致谢：

该应用报告的工作得到了 Manhong Wu[*1]，Robert St. Onge[*2]，Sundari Suresh[*2]，Ronald Davis[*2] 和 Gary Peltz[*1] 等人的大力协助和支持。在此表示衷心感谢。

[*1] 斯坦福大学医学院麻醉系

[*2] 斯坦福大学生化与基因研究中心

更多有关安捷伦 7200 Q-TOF GC/MS 的性能，请访问 **www.agilent.com/chem/GCMS_QTOF:cn**

在复杂基质中实现可靠的污染物筛查和鉴定

全面的食品安全筛查既包括对常规污染物的定量分析，也包括对非目标物和未知物的定性分析。

分析的成功往往取决于全扫描模式下的高灵敏度，以及用于目标物确认和未知物分析中的精确质量数信息。

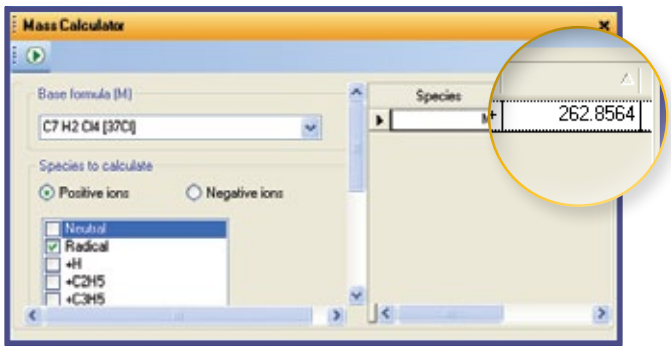

MassHunter Qual Mass Calculator 可用于在 EI 和 CI 两种模式下计算目标物的理论质量数。理论质量数可进一步用于确认定性结果和定量分析

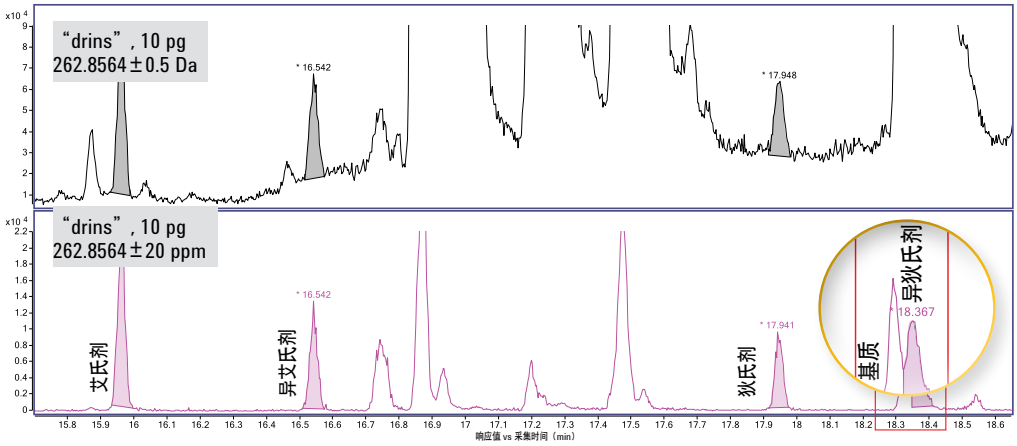

MS/MS 模式下的极高选择性：当高分辨率/高精确质量的单级 MS 不能满足分析的时候，安捷伦 7200 Q-TOF GC/MS 可以轻松解决目标物的共流出基质干扰问题

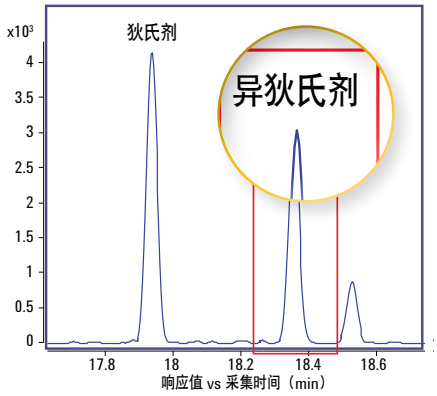

安捷伦 7200 Q-TOF GC/MS 的 MS/MS 模式还可以用于确认复杂基质中的目标物。如下所示：异狄氏剂子离子的质谱图 (m/z 263，CE：20 eV)

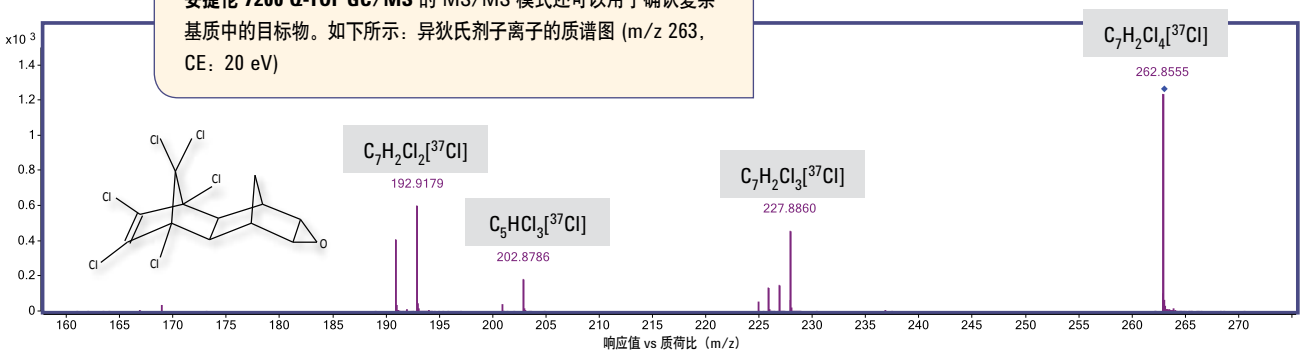

食品检测

特级初榨橄榄油的评估

使用 Mass Profiler Professional (MPP) 软件以 GC/Q-TOF 数据为基础构建一个模型，用于预测一个橄榄油样品是否能通过特级初榨橄榄油感官测试。模型使用 5 种特定化合物预测感官测试的结果。

除了 EI 质谱数据外，正离子 CI 精确质量数质谱对于模型中化合物分子离子的确认也是十分必要的。

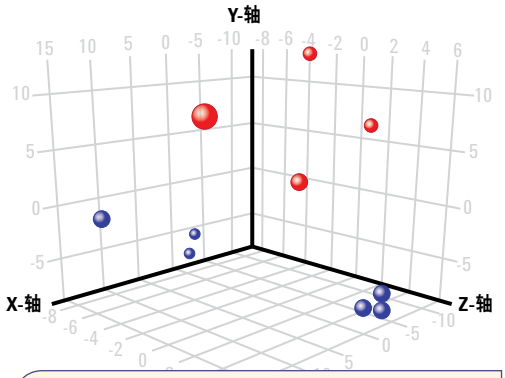

MPP 软件中的主成分分析 (PCA)，显示了数据簇的分布状态。蓝色表示样品顺利通过感官测试，而红色表示未通过

MPP 预测模型正确预测了所有样品的通过与否。未用于构建预测模型的样品在“training”变量一栏中标示为“None”

Prediction Results

Identifier	Grade	Training	Predicted(Class Pre...	Confidence
PAC1-EI-1: Ig2	F	None	[F, Training]	1.000
ESC2-EI-1: Ig2	P	Training	[P, Training]	1.000
ESC1-EI-1: Ig2	P	Training	[P, Training]	1.000
SAC1-EI-1: Ig2	F	None	[F, Training]	1.000
RFC2-EI-1: Ig2	P	None	[P, Training]	1.000
RSA2-EI-1: Ig2	P	None	[P, Training]	1.000
CSC1-EI-1: Ig2	F	Training	[F, Training]	1.000
RSA1-EI-1: Ig2	P	Training	[P, Training]	1.000
EFC1-EI-1: Ig2	P	None	[P, Training]	1.000
FSW2-EI-1: Ig2	F	Training	[F, Training]	1.000

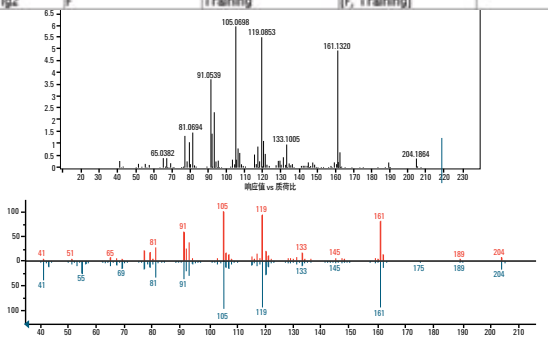

安捷伦 7200 Q-TOF GC/MS 生成的质谱可以在商品化的低分辨质谱库中进行检索

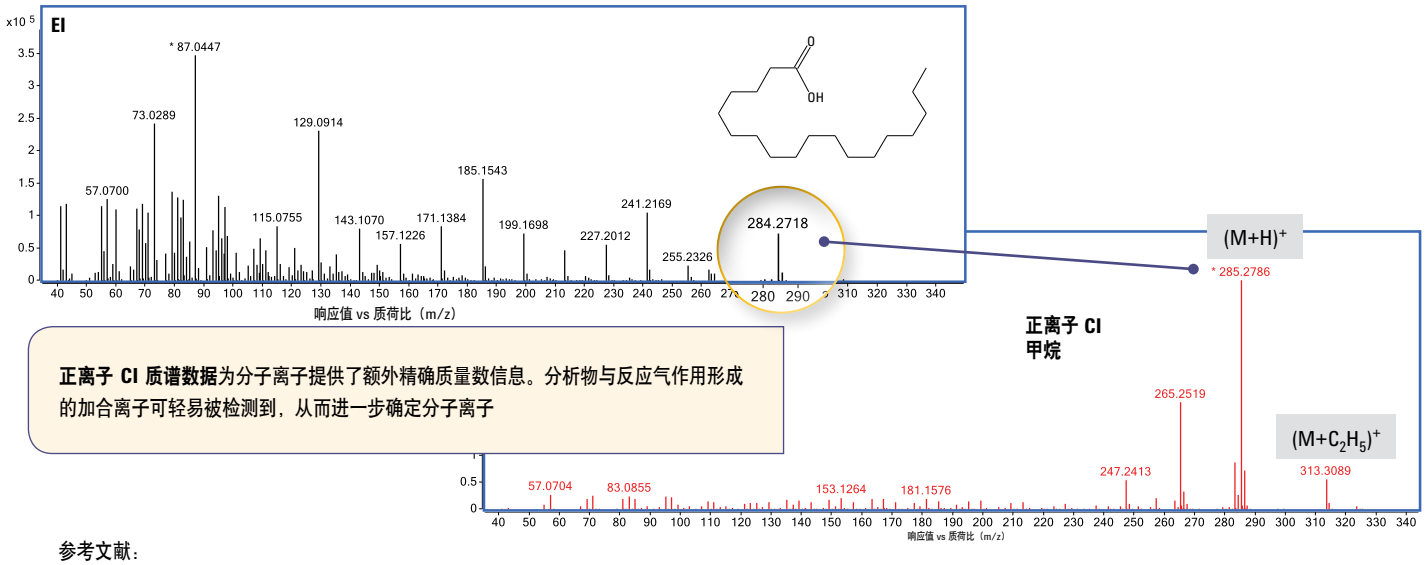

正离子 CI 质谱数据为分子离子提供了额外精确质量数信息。分析物与反应气作用形成的加合离子可轻易被检测到，从而进一步确定分子离子

参考文献：

使用安捷伦 GC/Q-TOF 分析咖啡中的挥发性硫化物：出版号. 5990-9076CHCN

Olive Oil Characterization using Agilent GC/Q-TOF MS and Mass Profiler Professional Software: Pub No. 5991-0106EN

更多有关安捷伦 7200 Q-TOF GC/MS 的性能，请访问 **www.agilent.com/chem/GCMS_QTOF:cn**

环境保护

对目标物和未知物实现可靠的筛查和鉴定

环境分析中最重要的挑战之一是对复杂基质中存在的许多种痕量化合物进行定性和定量分析。对于此类型应用，以下要素是必不可少的：

- 全谱范围内高灵敏的精确质量数采集
- 宽的动态范围
- 易于掌握的自动化定性分析
- 目标物的批量处理功能

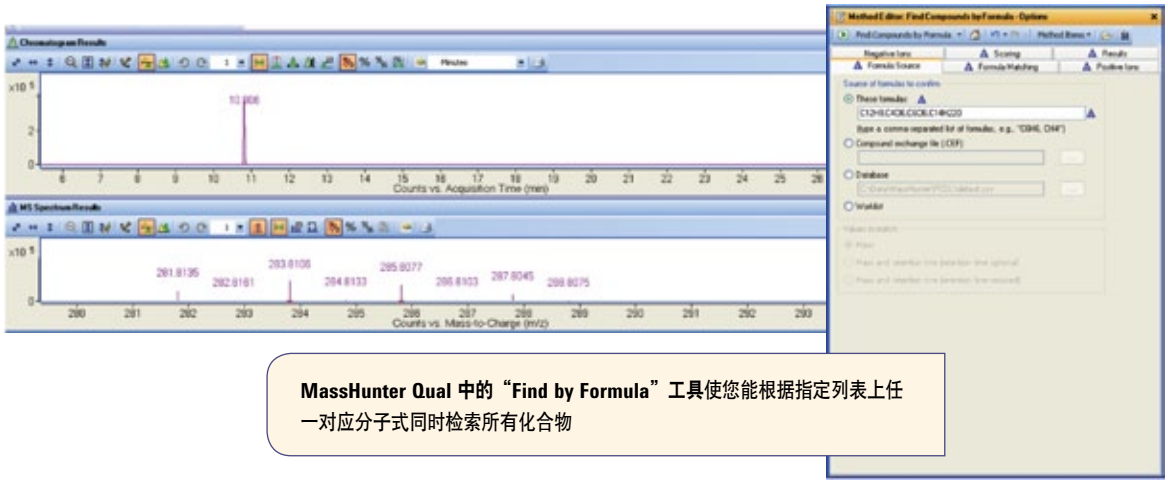

MassHunter Qual 中的“Find by Formula”工具使您能根据指定列表上任一对应分子式同时检索所有化合物

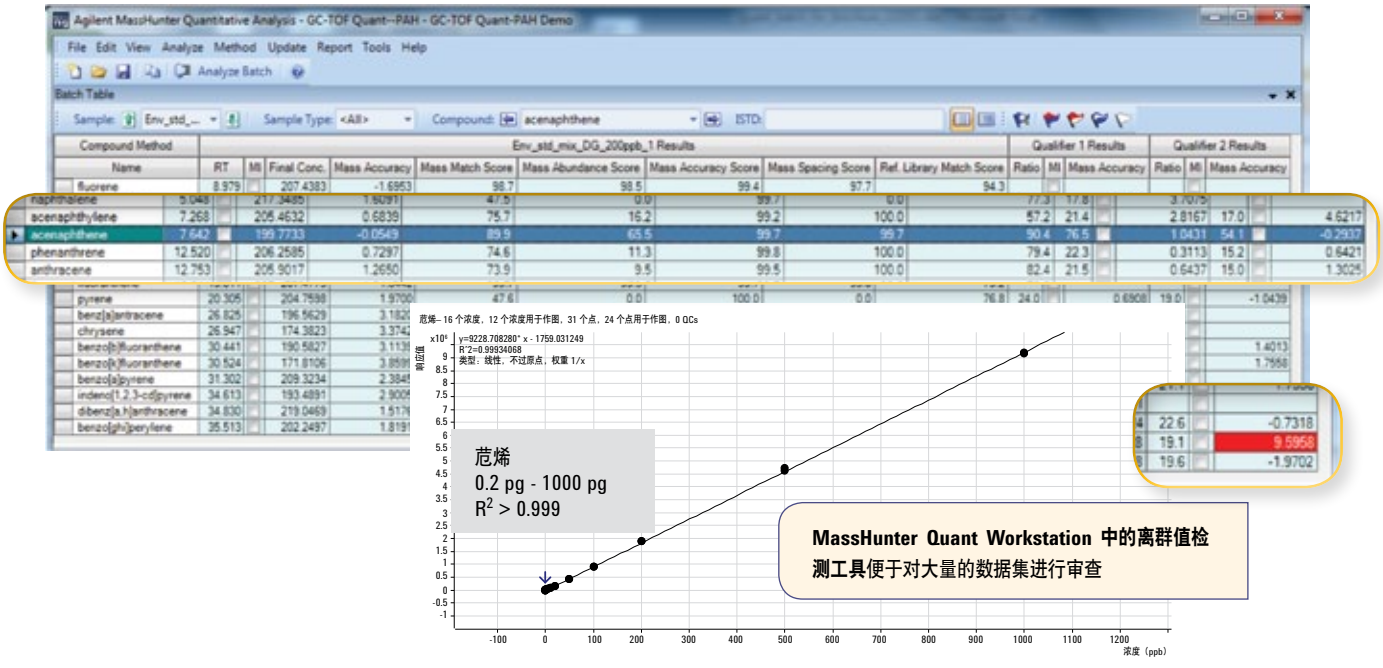

MassHunter Quant Workstation 中的离群值检测工具便于对大量的数据集进行审查

参考文献：

使用安捷伦 7200 Q-TOF GC/MS 分析原油中的生物标志物。

出版号：5990-9477CHCN

天然产物研究

将精确质量数和子离子谱图相结合，明确未知化合物的结构

中草药提取物中含有大量的化合物，需要分别确认。然而，商品化 EI 质谱谱库并非总能提供所研究组分的质谱信息。在这种情况下，安捷伦 7200 Q-TOF GC/MS 生成的精确质量数子离子质谱对于建立碎片离子之间的联系，确定结构相关性具有重要价值。

卡法树萃取液中未知物的鉴定

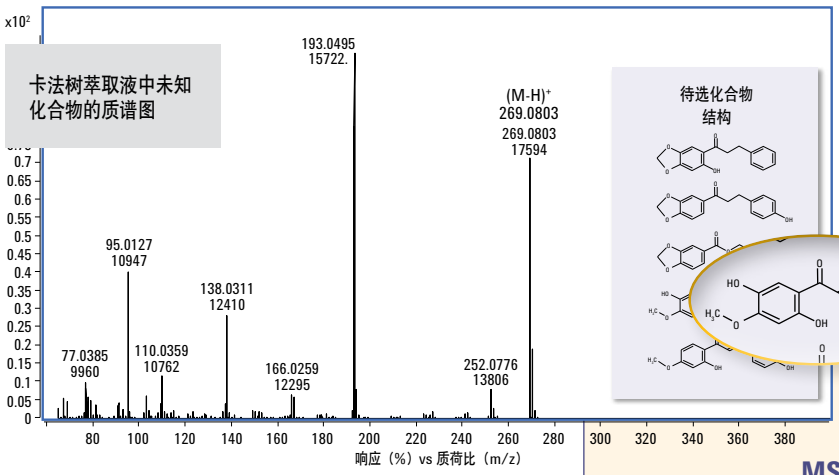

在 5 种待选化合物结构中，只有一种符合 MS/MS 实验中多个母离子碎片鉴定结果

MS/MS 实验测定结果

	m/z（实验值）	分子式	误差（ppm）	匹配程度
$(M\text{-}H)^+$	269.0803	$C_{16}H_{13}O_4$	-1.99	80.7
$(M\text{-}C_6H_5)^+$	193.0494	$C_{10}H_9O_4$	-0.18	96.7
$(M\text{-}CH\text{=}CH\text{-}C_6H_5)^+$	167.0334	$C_8H_7O_4$	-2.9	N/A
$(M\text{-}CH_2\text{=}CH\text{-}C_6H_5)^+$	166.0259	$C_8H_6O_4$	-0.96	N/A
-CO	138.0311	$C_7H_6O_3$	-0.33	98.1
-CO	110.0359	$C_6H_6O_2$	-3.01	N/A
$-CH_3$	95.0127	$C_5H_3O_2$	-0.59	99.5

子离子的精确质量数信息有助于避免在任意两个相同标称质量的中性碎片中产生混淆

可靠的峰鉴别性能和组分数据组合能力使安捷伦 7200 Q-TOF GC/MS 成为以下其它应用的理想之选。

食品检测和香精香料
- 天然产物

能源/化学
- 质量控制
- 石化产品中的痕量目标物分析

法医/毒理学
- 兴奋剂检测
- 尸检筛查、检验和确认

更多有关安捷伦 7200 Q-TOF GC/MS 的性能，请访问 **www.agilent.com/chem/GCMS_QTOF:cn**

可靠、一致的分析源自业内最好的 GC 和 GC/MS 系统

Agilent 7890B 气相色谱仪

- **可靠性能：**安捷伦第五代电子气路控制 (EPC) 和数字电路以及改进的检测器性能，使 Agilent 7890B 气相色谱的可靠性及分析性能达到了前所未有的高度
- **更高的样品分析通量：**快速柱箱降温、新的反吹功能和先进的自动化性能使分析时间更短，每个样品的分析成本最低。所有这些都能容易地整合到您现有的方法中
- **扩展的色谱功能：**灵活的 EPC 设计可进行复杂的分析，可选择第三台检测器（TCD 或 ECD）实现一机多用

安捷伦 5977A 系列 GC/MSD

- **更高的灵敏度：**我们新推出的 Extractor 离子源和调谐方案可提高 MSD 灵敏度，让您可以满怀信心地检测痕量化合物并在常规分析中获得更低的检测限
- **最高的生产率：**全新集成的硬件和软件功能可简化工作流程，帮助您用更少的资源完成更多的工作
- **最好的软件选择：**可以选择使生产率最高的工作流程。继续使用通用可靠的 ChemStation，或者选择成熟的 MassHunter 软件

安捷伦 240 离子阱 GC/MS

- 最广泛的离子化和扫描技术 – EI, CI, MS/MS, MS^n
- 最高的 EI 和 CI 全扫描灵敏度
- 稳健的操作和超长的有效运行时间

安捷伦 7000 系列三重串联四极杆 GC/MS

- 唯一一款装备可加热石英四极杆分析器的三重串联四极杆 GC/MS，该四极杆分析器为专利技术，专为气相色谱分析而设计
- 常规检测可达 fg 级的灵敏度和优越的选择性
- 每秒多达 500 MRM 转换

安捷伦 GC 和 GC/MS

- 随时可用的成套工作流程解决方案适用于 60 多种主要应用
- 出厂前经预装并通过特定应用方法及相应混标测试

终身确保仪器的最佳性能——最大限度地提高您实验室的分析通量

作为世界色谱行业的引领者，安捷伦始终定位于带给用户最具创新性的样品前处理产品、GC 色谱柱和消耗品，帮助客户满足最苛刻的分析挑战。

从最少的重复样本中获得准确、重现的结果

只有安捷伦提供完整的样品制备产品线以满足您的仪器分析所需。

- **安捷伦 Bond Elut 聚合物 SPE 产品**可提供最洁净的萃取操作，选择性地将干扰物从复杂基质中清除。由超过 40 种固定相组成 30 多种产品形式，种类之多居当今市场之首
- **安捷伦出品的行业领先的 QuEChERS 前处理包**是一种经济有效的工具，使样品制备更加快速、简单、可靠

更多信息，请访问 **www.agilent.com/chem/sampleprep:cn**

信心十足地进行痕量分析

安捷伦超高惰性气相色谱解决方案的各组件共同为分析创造出惰性的样品流路，使您可以获得 ppb 或者 ppt 级的检出限，以满足当今分析所需。

- **安捷伦 J&W 超高惰性气相色谱柱**经过行业最严格的混合标样测试，确保一致的柱惰性和出色的低柱流失
- 无论带或不带玻璃毛，安捷伦的**超高惰性衬管**都提供了稳健、可重复并且可靠的惰性流路

更多有关确保 GC 惰性流路的信息，请访问
www.agilent.com/chem/ultrainert:cn

在您实验室的一切努力背后，都有安捷伦为您提供无与伦比的专业知识、服务和信息

安捷伦的承诺

依赖 10 万多个成功的认证案例和几十年的认证测试实践经验，您有理由相信可以依靠安捷伦的系统认证和仪器校准证明顺利通过法规认证。

实时技术支持和预警

每台安捷伦仪器内装的“智能系统”对仪器可能出现的故障提前预警，使工作效率和分析通量达到最大化。

安捷伦 OpenLAB

随着食品、药品、土壤和水样分析生成的数据日益复杂和庞大，您迫切需要将大量原始数据转化成可操作的信息。安捷伦 OpenLAB ELN 和 OpenLAB ECM 帮助收集、分析并共享您的结果，在促进合作的同时保护并归档您的知识财产。

安捷伦的价值承诺

我们*承诺*自购买之日起至少 10 年的仪器使用保证，或者我们可以折价为您提供升级产品。

安捷伦的服务保障

在安捷伦服务协议范围内，只要您有要求，我们承诺为您的仪器提供维修或者免费更换服务。

使用安捷伦 GC/Q-TOF 分析咖啡中的挥发性硫化物

食品检测

安捷伦 7200 GC/Q-TOF 系统的分辨率、灵敏度和质量精度为咖啡中痕量硫化物的检测提供了简单、快速、可靠的分析解决方案。

咖啡中释放出来的挥发性硫化物对咖啡的香气和味道起着非常重要的作用。由于许多香味化合物都是以痕量水平存在，对怡人的咖啡香气进行完全表征是一项比较困难的事情。复杂食物基质中痕量水平（低 ng/mL 级）硫化物的定性和定量通常需要耗时的样品制备过程和高分离度的复杂仪器，如 2D GC/MS 联用仪。使用高分辨率、高灵敏度和快速分析的安捷伦 GC/Q-TOF 系统，可以通过最少量的样品制备和 1D GC 标准方法得到高质量、一致性的结果。

对于 GC/Q-TOF 方法，只需对样品进行简单的液液萃取，即可进行咖啡中挥发性硫化物的分析。具有低质量误差的高分辨率的质谱图有助于在严重基质干扰下对目标化合物进行识别和分析。7200 GC/Q-TOF 具有低 pg 级的方法检出限，质量精度误差小于 5ppm。基质中检测的线性范围高达 3 个数量级，线性相关系数大于 0.995。对 ng/mL 级的 2- 噻吩甲醛和 2- 乙酰基噻唑成功运用了标准加入法进行测定，这个浓度是咖啡萃取物中的天然浓度水平。

总之，安捷伦 7200 GC/Q-TOF 可对复杂食物基质中的化合物进行痕量水平分析，无需复杂繁琐的样品制备和分离方法。

方法由来自 Gerstel K.K. 的 Nobuo Ochiai 和 Kikuo Sasamoto 以及安捷伦科技有限公司的 Ryo Ogasawara 和 Sofia Aronova 建立。

主要优势：

- 安捷伦 7200 GC/Q-TOF 为复杂食物基质中的硫化物常规分析提供了快速、简单的解决方案
- 系统的高灵敏度可使咖啡中挥发性硫化物的定性和定量水平低至 1 pg 柱上进样量
- 安捷伦 7200 系列 GC/Q-TOF 卓越的分辨率和质量精度为复杂食物基质中的目标组分定量分析提供足够高的选择性
- 覆盖 3 个数量级浓度范围的线性确保目标物在宽浓度范围内满足定量要求

使用安捷伦 GC/Q-TOF 分析咖啡萃取液中的挥发性硫化物

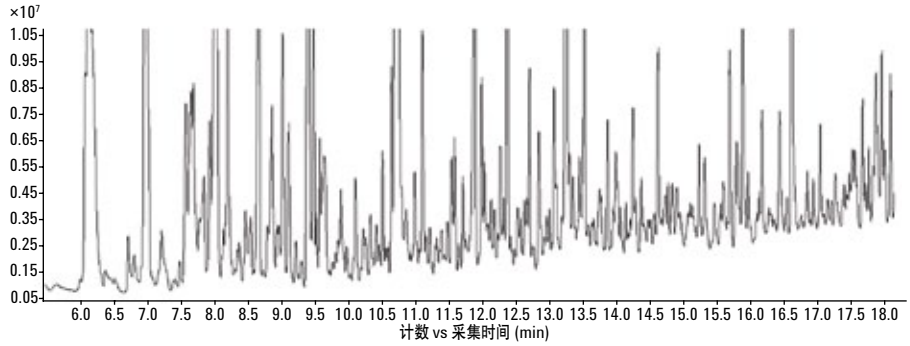

图 1. 咖啡萃取液的 TIC 谱图（未添加硫化物标准品），充分证明了基质的复杂性

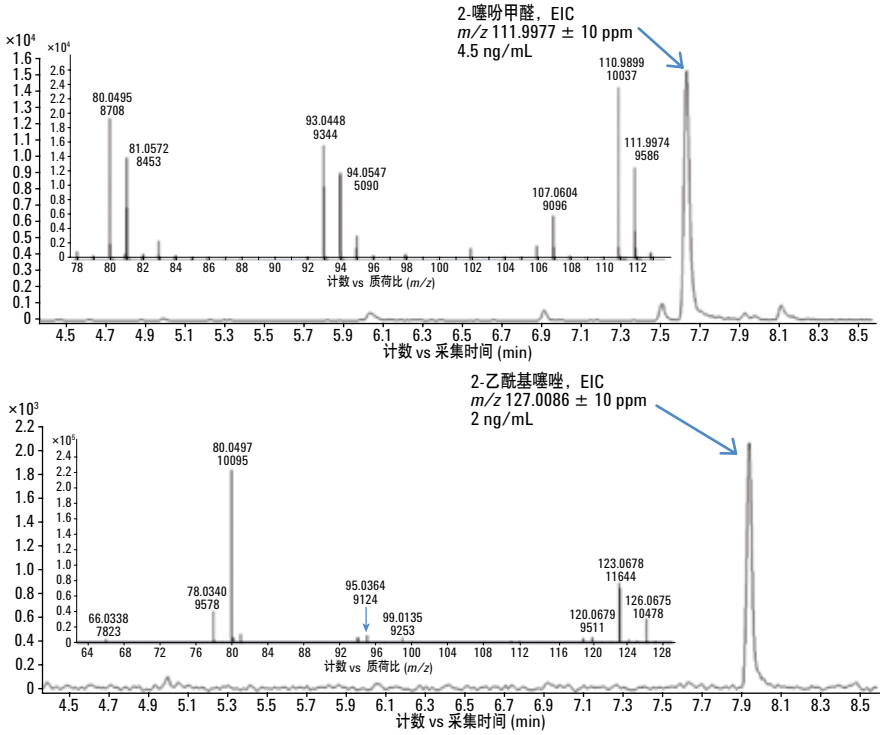

图 2. 咖啡基质中，天然浓度水平的加标 2- 噻吩甲醛和 2- 乙酰基噻唑的 EIC 和质谱图

表 1. 2- 噻吩甲醛和 2- 乙酰基噻唑的咖啡加标萃取液中的质量误差

	质量误差，ppm	
柱上量 pg	**2- 噻吩甲醛**	**2- 乙酰基噻唑**
1	-3.57150	-0.78735
2	-4.46438	-0.78735
5	-2.67863	-0.78735
10	-2.67863	0.78735
20	-2.67863	0.00000
50	-0.89288	1.57470
100	0.00000	1.57470
200	-1.78575	1.57470
500	2.67863	-1.57470
1000	1.78575	-1.57470
Average	2.32148	1.10229

使用安捷伦 GC/Q-TOF MS 和 Mass Profiler Professional 软件表征橄榄油

应用简报

食品检测与农业

作者

Stephan Baumann,
Sofia Aronova
安捷伦科技有限公司
Santa Clara,
加利福尼亚
美国

摘要

本研究建立了一种预测橄榄油能否通过特级初榨感官测试的模型。使用的仪器为安捷伦 7890A GC 和安捷伦 7200 系列精确质量 Q-TOF 质谱联用系统，同时在电子轰击电离源（EI）和正化学电离源（PCI）模式下，检测发现了橄榄油中存在大量的化合物。使用 Mass Profiler Professional 软件进行统计分析并建立分类模型，该分类模型利用 5 种特定化合物可以准确预测一种橄榄油能否通过感官测试。

引言

在美国，对地中海食物和橄榄油健康效应的日益追捧使橄榄油的需求快速增长。到 2013 年，美国市场预期将超过 18 亿美元 [1]。橄榄油被认为与欧洲南部人口的长寿和心脏病低发率有关。事实上，食品与药品管理局（FDA）已经批准橄榄油中单不饱和脂肪酸降低冠心病风险的健康声明。最近有研究表明，橄榄油的消炎作用主要来源于第一次压榨得到的特级初榨橄榄油（EVOO），很少有食物含有如此丰富的抗氧化物和消炎成分。

国际橄榄油理事会（IOC）和美国农业部（USDA）已经建立了 EVOO 的分类标准，包括由品鉴小组进行的感官测试和化学测试。然而，最近的研究 [2] 表明，占美国 EVOO 市场 99% 的进口橄榄油往往通不过 EVOO 类别的感官测试，加之感官测试是昂贵和主观的。

基于美国市场 EVOO 强大的市场份额和对 EVOO 日益增长的需求，非常值得开发一种可以预测橄榄油能否通过感官测试的化学筛查法。这样，生产厂商只需提交那些通过几率高的橄榄油产品进行感官测试。这样的化学筛查同样可以降低鉴别和认证的费用和时间，同时提高市场上 EVOO 的品质。

该应用报告证明了开发一种模型预测橄榄油能否通过感官测试的可行性。该模型使用一种类似于近期红酒分类报告 [3] 中应用的非目标化合物分析方法，同时采用电子轰击电离源（EI）和正化学电离源（PCI）模式采集数据，使用安捷伦 7890A GC 和安捷伦 7200 系列精确质量 Q-TOF 质谱联用系统，安捷伦 MassHunter 软件用于谱图的解卷积，Mass Profiler Professional（MPP）软件用于深度统计分析和建立分类模型。橄榄油样品中的 5 种特定化合物与感官测试失败有关。

实验

试剂和标准品

环己烷，色谱纯，来自 Sigma-Aldrich 公司。

样品

一共 10 种橄榄油样品均来自 UC Davis Olive Center。所有样品均接受了由 IOC 授权小组执行的感官测试确定它们是否符合 EVOO 标准。样品室温下避光保存，用环己烷按 1:10 的比例进行稀释，以 1:10 分流比进样到气相色谱中，按随机顺序进行分析。

仪器

研究使用的仪器是安捷伦 7890A GC 和安捷伦 7200 系列 GC/Q-TOF 联用系统。仪器的操作条件列于表 1。

表 1.　　GC 和 MS 仪器条件

GC 仪器参数设置	
色谱柱	DB-5 MS，30 m x 0.25 mm x 0.25 µm（部件号 122-5532）
进样量	1 µL
MMI 进样口	50 °C 保持 0.01 min， 600 °C/min 升到 300 °C
吹扫分流出口	60 mL/min @ 1 minute
柱箱升温程序	45 °C 保持 4.25 min， 5 °C/min 升到 75 °C，保持 0 min， 再以 10 °C/min 升到 320 °C，保持 10 min
载气	氦气，1.3 mL/min 恒流
传输线温度	290 °C
MS 仪器参数设置	
离子化模式	EI，正 CI（20% 甲烷气体）
离子源温度	230 °C
四极杆温度	150 °C
m/z 范围	40 ~ 800 *m/z*
质谱采集速率	5 Hz，同时以曲线图模式和棒状图模式采集

数据处理和统计分析

使用 MassHunter 定性分析软件（版本 B.05 SP1）进行数据处理，其中的谱图解卷积工具用于色谱峰定性。通过调整质量和化合物过滤器，可以鉴定 100~300 个化合物。使用 MassHunter 的输出工具创建 CEF 文件将解卷积数据输入到 MPP。

使用 Mass Profiler Professional 软件（版本 2.1.5）进行统计分析，数据处理步骤如下：

1. 设置导入过滤器和对齐参数
2. 选择归一化准则
3. 定义样品组
4. 设置数据过滤器
5. 用主成分分析（PCA）图对数据进行聚类评估

一旦这些步骤完成后，就使用倍率变化和显著性分析等统计工具对数据进行评估。最后的分析步骤是建立和测试分类模型。进一步的数据处理还包括使用质谱数据库检索和分子式估算排布对化合物进行定性。

结果和讨论

数据采集和处理

使用 GC/Q-TOF 对 EVOO 样品中的化合物进行鉴定。使用 MassHunter 中的谱图解卷积（图 1）通常情况下可识别大约 150 个色谱峰。使用冷柱头分流进样，进样口温度从 50 °C 程序升温至 300 °C，将热分解降至最低。为了能较好分离早出峰的化合物，将柱温箱初始升温速率设为 5 °C/min。

使用 MassHunter 的解卷积对色谱峰进行识别，然后利用 MassHunter 的输出工具生成可以导入到 Mass Profiler Professional（MPP）软件的 CEF 文件。

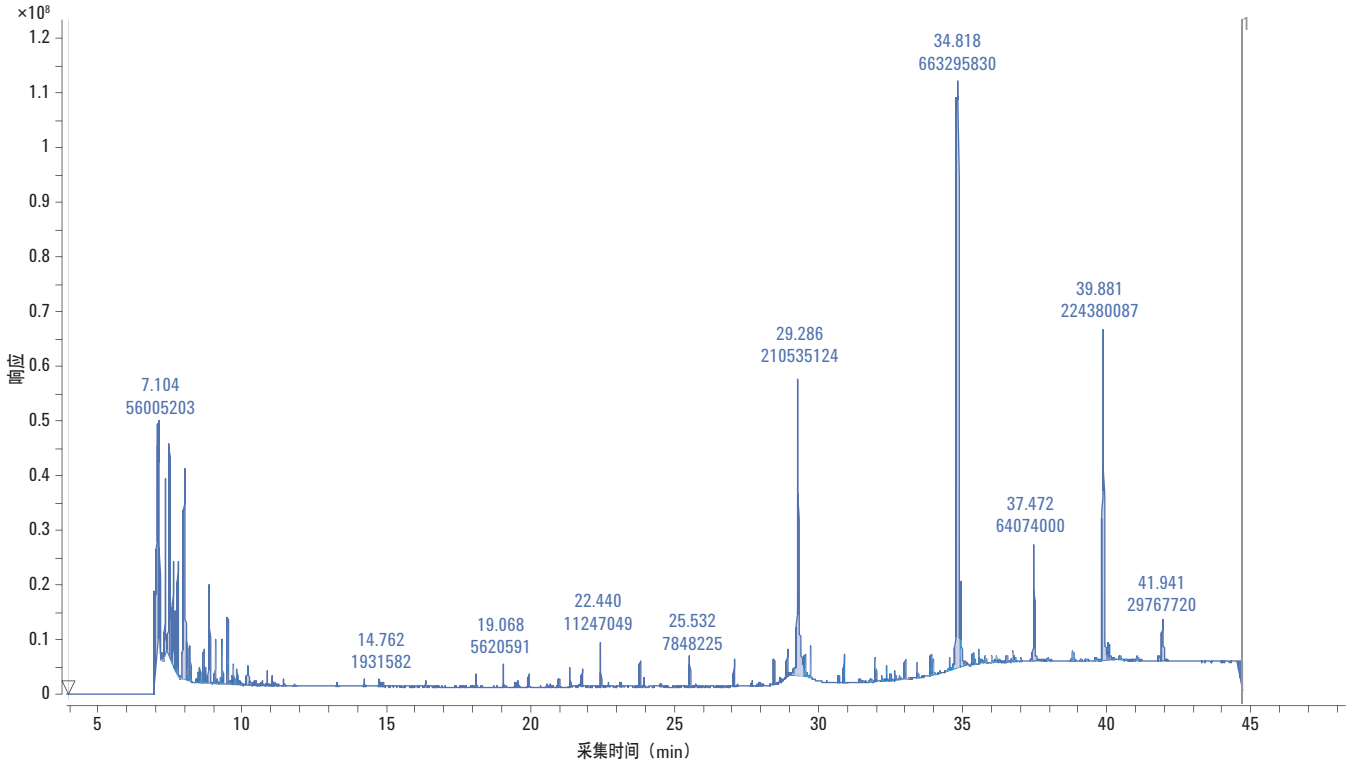

图 1.　通常情况下，利用谱图解卷积可以识别约 150 个色谱峰，峰面积筛选器为最大峰峰面积的 0.1%

MPP 软件匹配了以谱图类型和保留时间为基础的提取离子色谱（EICs）。提取离子谱图要求交叉相关系数为 0.6，保留时间匹配到 0.05 min，才认为是同一个化合物。图 2 中的质量和保留时间曲线显示橄榄油中共识别出 442 个独特的实体（化合物），它们中的大多数只出现过 1 到 2 次，并且在数据过滤时被筛选掉。

定义了样品组后，在 MPP 中设置数据过滤器。实体过滤可以生成更高质量的数据集，使后续多元分析更有意义。第一次过滤确定了哪些实体（化合物）100% 时间都在至少一个样品组中出现（频率分析）。该频率过滤器将初步标记物从 442 个降到了 91 个。

统计分析

当使用复杂的统计软件经编写以处理 ASCI 或文本类型的结果时，标记物发现的统计分析往往会非常繁琐和费时。MPP 软件是有效利用复杂而“嘈杂”的数据，进行复杂的数据管理、筛选、统计分析、解释、模型创建和预测的理想选择。它提供了一个易于遵循的指导工作流程，帮助用户决定如何最好地去评估数据。专家级用户可以直接进行所需的数据处理（详情见 Mass Profiler Professional 产品样本 5990-4164CHCN）。

主成分分析（PCA）是一种经常采用的非监督多元分析技术，它可对数据进行降维处理，同时保留数据中的鉴别能力。

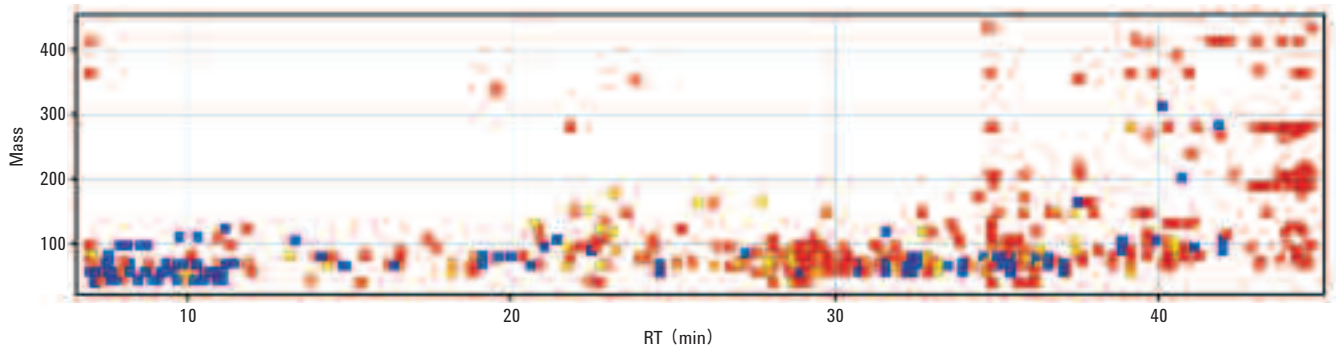

图 2.　质量和保留时间曲线表明经谱图解卷积识别了 442 个独特的化合物。它们中的大多数只出现过 1 到 2 次，会被 MPP 过滤掉。低频的化合物以红色表示，高频的以蓝色表示

PCA 通过把测量的变量转化为不相关的主成分，每个主成分是一个原始变量的线性组合。它作为一种质量控制工具，分析数据如何聚类并确定离群样本。实体（化合物）PCA 在通过和未通过感官测试样品之间分析数量上的不同，进一步确定了数据分组的差异性（图 3）。

倍率变化和统计学意义

一旦确定了橄榄油样品通过和未通过感官测试这两大分类，即进行统计学分析。首先，测定任何指定化合物的浓度倍率变化（上升），这项分析识别选定数组之间丰度差异大的实体（化合物），即通过和未通过的 EVOO 样品中那些浓度相差 2 倍、3 倍、4 倍或更多的实体（化合物）。

下一步，利用方差分析（ANOVA）确定那些满足倍率变化标准的化合物间是否具有统计学上显著性差异。使用概率值 P=0.01，频率筛选得到的 91 个实体减少到 5 个重要化合物。倍率变化分析和 ANOVA 分析的结果以火山曲线（图 4）表示。选定 P 值最低和倍率变化最大的 5 个化合物用于创建分类模型。

分类模型

分类的目的是以几个变量描述并且已知分类信息识别的一套训练样品为基础，建立一种一般性假设。任务是通过前者映射后者。为实现此目的，大量基于统计或人工智能的技术被开发出来 [4]。本研究的目的就是以 5 种与不能通过感官测试有关的化合物为基础预测哪个橄榄油样品不能通过感官测试。

偏最小二乘（PLS）分析尤其适合于这种观察对象，这里指样品数量比测量变量（如检测实体，*m/z*）少的情况。因为它具有处理大量相关及嘈杂变量的能力，应用越来越广泛。偏最小二乘判别分析法（PLSDA）用于锐化不同观察组别之间的分区，从而获得最大化的分类，已经成为代谢组学数据分类强有力的工具 [4]。因此，PLSDA 被用于建立橄榄油分类模型。

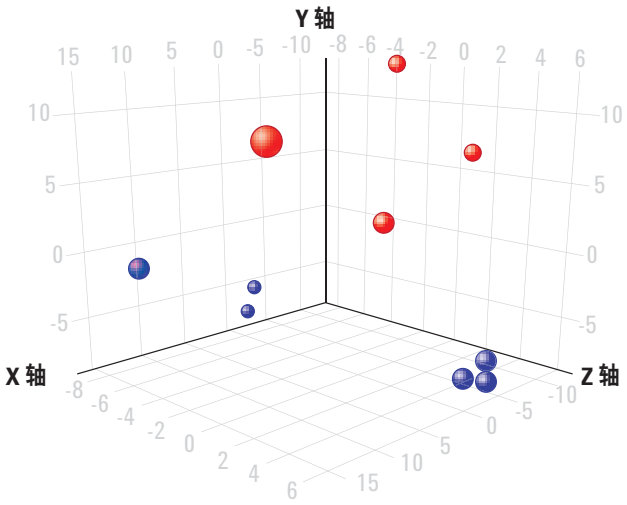

图 3. *主成分分析（PCA）显示数据如何聚类。红色表示未通过感官测试的样品，蓝色表示通过感官测试的样品*

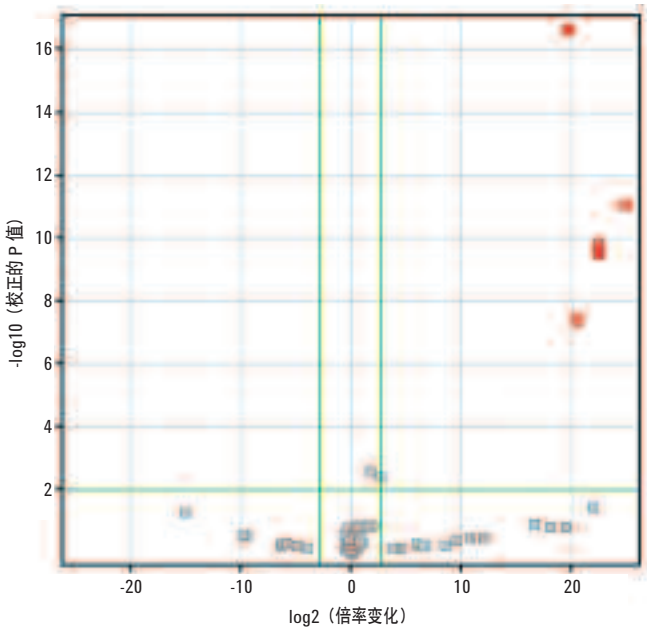

图 4. *火山曲线表示了 X 轴上每个实体的倍率变化和在 Y 轴上的显著性差异。这 5 种化合物聚积在未通过感官测试的样品中*

根据 MPP 筛选出的 5 种化合物将数据分为 2 类，下一步是创建一个模型来预测一种橄榄油样品能否通过感官测试。建立分类模型的第一步是用数据对模型进行训练（图 5）。

为测试模型，要使用相同但未包括在创建模型中的训练数据和样品，虽然有些多余，但这是一个有效的统计过程。采用同样的分类预测模型验证训练模型。包括那些不用于构建模型的有限数量的样品，模型的准确度均为 100%（图 6）。这些结果表明了创建一个模型用于准确预测一个 EVOO 样品能否通过感官测试的可行性。

Identifier	Training	Predicted(Training)	Confidence
CSC1-EI-1: Ig2	[F, Training]	[F, Training]	1.000
FSW2-EI-1: Ig2	[F, Training]	[F, Training]	1.000
ESC1-EI-1: Ig2	[P, Training]	[P, Training]	1.000
ESC2-EI-1: Ig2	[P, Training]	[P, Training]	1.000
RSA1-EI-1: Ig2	[P, Training]	[P, Training]	1.000

图 5.　代表了 PCA 中 3 个聚类的 PLSD 训练集

Prediction Results

Identifier	Grade	Training	Predicted(Class Pre...	Confidence
PAC1-EI-1: Ig2	F	None	[F, Training]	1.000
ESC2-EI-1: Ig2	P	Training	[P, Training]	1.000
ESC1-EI-1: Ig2	P	Training	[P, Training]	1.000
SAC1-EI-1: Ig2	F	None	[F, Training]	1.000
RFC2-EI-1: Ig2	P	None	[P, Training]	1.000
RSA2-EI-1: Ig2	P	None	[P, Training]	1.000
CSC1-EI-1: Ig2	F	Training	[F, Training]	1.000
RSA1-EI-1: Ig2	P	Training	[P, Training]	1.000
EFC1-EI-1: Ig2	P	None	[P, Training]	1.000
FSW2-EI-1: Ig2	F	Training	[F, Training]	1.000

图 6.　模型准确预测了所有样品的通过与否，包括那些未参与模型创建的样品，这些样品没有用于构建预测模型，在“Training”变量中以“None”表示

化合物定性

安捷伦 7200 系列 GC/Q-TOF 这类仪器的优势在于可以以 EI、CI 和产物离子扫描模式采集数据。这些正交操作模式有助于信息确认。EI 可以进行谱库检索并提供碎片数据；CI 可以提供经验公式方面的信息；产物离子 MS/MS 扫描生成的数据可用于精确质量的子结构检索，应用到 EI 或 CI 产物离子上。

然而，没有必要知道分类模型中使用的化合物是什么，但化合物鉴定可以了解那些化学组分直接或间接对橄榄油感官质量产生副作用的机理。安捷伦 7200 系列 GC/Q-TOF 可以提供精确质量的结构信息，对化合物鉴定（ID）具有强大的优势。

使用安捷伦 MassHunter 定量软件进行精确质量谱图解卷积并从干扰峰中提取干净谱图。然后，根据 NIST 数据库对 EI 质谱数据进行检索（图 7）。除了最后一个化合物，所有 EI 数据均发现有相应的匹配度。虽然碎片形成模式是一样的，但和四极杆仪器得到的数据相比，该匹配因子相对较低，因为 NIST 谱库中大部分数据均来自于四极杆质谱。这两种质谱仪在不同的质量范围内体现的最佳性能各有不同：四极杆质谱的响应在低质量范围内优于飞行时间质谱。

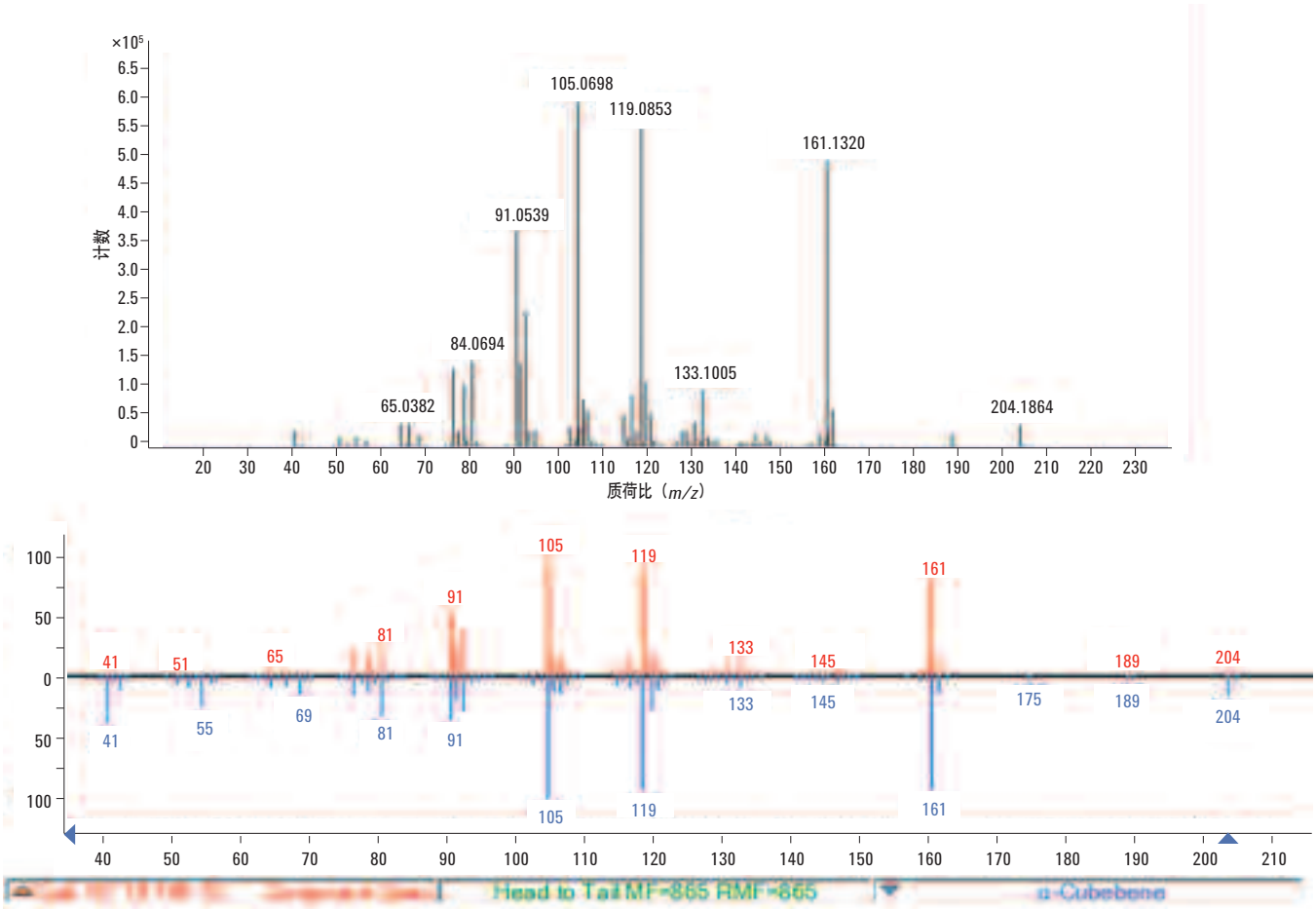

图 7.　EI 商业谱库如 Wiley 和 NIST 可以进行精确质量 EI GC/Q-TOF 数据检索确定化合物

EI 离子的精确质量信息有助于聚积化合物的初步定性，除了一个缺少主导分子离子的化合物外（图 8），对其他所有化合物质量准确度均低于 5 ppm。

利用正 CI 精确质量数据，每个标记物都可以生成分子式（图 8）。根据观察到的碎片形成模式，数据对第 5 个化合物（最底行）的分子式进行了确认。除了 227 *m/z* 处的预期峰和它的（M+C_3H_5）+ PCI 加合物外，还观察到一个 209 *m/z* 的碎片峰，这和丢失 H_2O 分子的结果一致。191 *m/z* 的碎片峰的形成表明了第二个水分子的丢失。从这些数据可以推测该化合物为一个经验分子式为 $C_{14}H_{26}O_2$ 的二醇类物质，它的质量准确度正好大于 8 ppm，符合低信号强度。对 NIST 谱库检索确定的另外 4 种化合物的研究表明，它们都具有影响橄榄油味道的气味，从而导致无法通过感官测试（图 9）。

MPP ID	初步 NIST 检索 ID	NIST 匹配度	分子式	CAS	EI、M*+			PCI、[M+H]+		
					计算值	测定值	质量偏差（ppm）	计算值	测定值	质量偏差（ppm）
55.0@27.546	n-棕榈酸	789	$C_{16}H_{32}O_2$	57-10-3	256.2397	256.2385	4.7	257.2475	257.2470	1.9
73.0@29.750	硬脂酸乙酯	703	$C_{20}H_{40}O_2$	111-61-5	312.3023	312.3008	4.8	313.3101	313.3091	3.2
81.0@35.731	角鲨烯	831	$C_{30}H_{50}$	111-02-4	410.3907	410.3904	0.7	411.3985	411.3987	0.5
105.0@20.906	α-荜澄茄油烯	880	$C_{15}H_{24}$	17699-14-8	204.1873	204.1883	4.9	205.1951	205.1945	2.9
71.0@27.260	NIST 谱库不存在	N/A	$C_{14}H_{26}O_2$	N/A	226.1927	ND	ND	227.2006	227.1987	8.4

图 8.　PCI 质谱数据提供了精确质量信息，用于确定积聚在未通过测试的橄榄油样品中的化合物的分子离子。最下一行是在 EI 谱图中没有发现主导性分子离子碎片的化合物信息

MPP ID	初步 NIST 检索 ID	NIST 匹配度	分子式	CAS	气味	来源
55.0@27.546	n-棕榈酸	789	$C_{16}H_{32}O_2$	57-10-3	淡油	Bedoukian Research
73.0@29.750	硬脂酸乙酯	703	$C_{20}H_{40}O_2$	111-61-5	蜡	Good Scents 公司
81.0@35.731	角鲨烯	831	$C_{30}H_{50}$	111-02-4	花香	Good Scents 公司
105.0@20.906	α-荜澄茄油烯	880	$C_{15}H_{24}$	17699-14-8	草药香	Good Scents 公司

图 9.　4 种和感官测试失败有关的化合物气味列表

使用 Molecular Structure Correlator 进行结构确认

Q-TOF 产物离子谱图可以帮助确认所有生成的碎片离子和所提议的结构异构体建立联系。Molecular Structure Correlator 可以对子结构进行 ChemSpider 数据库检索并且将结果和所有可能的异构体建立联系。每个碎片离子按与建议分子式的质量误差和生成该建议分子式需要断裂多少个化学键的罚点排序。将每个碎片离子的得分加权平均，同时考虑每个碎片离子的强度和质量数，得到一个异构体的个体兼容性评分（Compatibility Score）（图 10）。

该工具作为 EI 谱库的补充，清晰地鉴定出 29.75 min 的峰为一种乙酯类化合物，最佳匹配化合物为硬脂酸乙酯。Molecular Structure Correlator 表明，312 *m/z* 母离子的产物离子和硬脂酸乙酯有很好的相关性，兼容性评分为 98（图10）。此外，碎片的精确质量和建议质量相关性良好，所有碎片的质量误差在 5 ppm 之内，这为化合物鉴定提供了额外的确认信息。

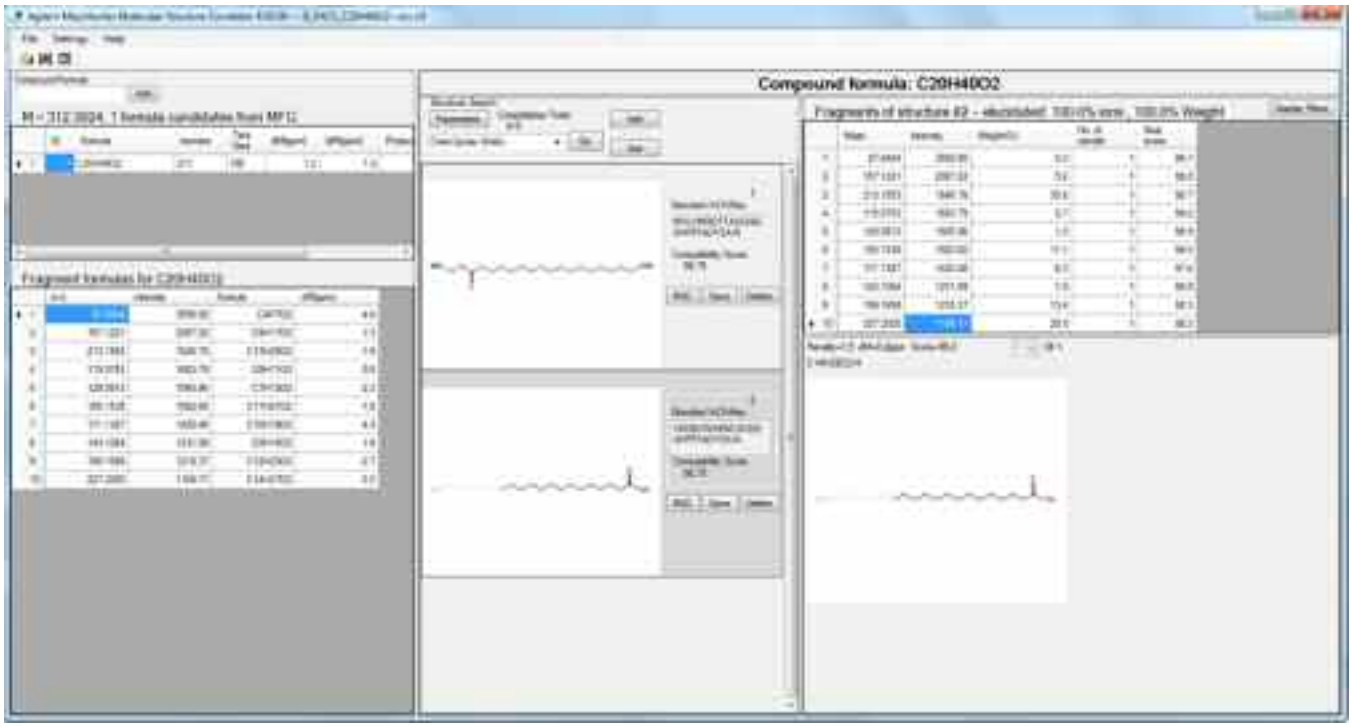

图 10.　Molecular Structure Correlator 将 Q-TOF 产物离子的谱图和结构异构体经验公式的谱图相比，确定哪个产物离子和异构体的碎片相关，从而得出兼容性评分

结论

使用 Agilent GC/Q-TOF 系统的精确质量 EI 源和正 CI 源扫描数据建立了一个模型，用于准确预测一种橄榄油样品是否能够通过感官测试。虽然只是使用小样本创建的模型，但也充分证明了这种方法的可行性。使用增大的样本量构建的预测性模型将为橄榄油厂商提供一种经济、快速的测试方法预测他们的产品能否通过感官测试，从而，避免了对劣质油进行感官测试花费的时间和金钱。对没有通过感官测试的 EVOOs 中聚积化合物的识别与通过味道识别劣质橄榄油一样可靠。这种方法还可以被创造性地用于构建另一种模型，以预测一种橄榄油是否被掺杂了廉价替代品。

参考文献

1. Olive Oil in the U.S., 3rd Edition, Apr 1, 2009, a marketing report from Packaged Facts (http://www.packagedfacts.com/Olive-Oil-Edition-2071654/)
2. E. N. Frankel, R. J. Mailer, C. F. Shoemaker, S. C. Wang, J. D. Flynn, "Tests indicate that imported "extra virgin"olive oil often fails international and USDA standards" UC Davis Olive Center, July 2010 (http://olivecenter.ucdavis.edu/news-events/news/files/olive%20oil%20final%20071410% 20.pdf)
3. L. Vaclavik, O. Lacina, J. Hajslova, J. Zweigenbaum. "The use of high performance liquid chromatography-quadrupole time-of-flight mass spectrometry coupled to advanced data mining and chemometric tools for discrimination and classification of red wines according to their variety.", *Anal Chim Acta*. **685**, 45-51 (2011)
4. J. Boccard, J. L. Veuthey, S. Rudaz. "Knowledge discovery in metabolomics: an overview of MS data handling." *J Sep Sci*. **33**, 290-304 (2010)

更多信息

此数据仅代表典型结果，有关我们产品和服务的更多信息，请访问 www.agilent.com/chem/cn。

使用安捷伦 7200 GC/Q-TOF 分析原油中的生物标志物

应用简报

石化和环保

作者

Frank David
色谱研究所
Kennedypark 26，B-8500 Kortrijk，
比利时

Sofia Aronova
安捷伦科技有限公司
Santa Clara，CA，
美国

摘要

在油源特征分析和溢油源勘探等多种石化应用中常常需要对原油中的生物标志物如（烷基）二苯并噻吩、藿烷和甾烷等进行分析。经过复杂的样品制备和分馏后，采用 GC-MS 方法对其进行分析。

稀释后的样品无需分馏即可使用飞行时间质谱仪进行分析，感兴趣的生物指标可通过提取精确质量来实现高选择性的测定。

系统出色的灵敏度可对二苯并噻吩、烷基化二苯并噻吩和藿烷进行选择性测定。使用安捷伦 GC/Q-TOF 的 MS/MS 模式还可对低浓度的甾烷进行选择性测定。

前言

生物标志物包括烷烃、多环脂肪烃、多环芳烃等一系列碳氢化合物，这些化合物均为永久性环境污染物。这些生物标志物可用于包括油源特征分析等在内的多种石化应用中，作为油品成熟度和油品老化的指标。生物标志物也可被用于勘探造成环境污染的油泄漏源 [1、2]。

典型的生物标志物多为杂环多环芳香烃类如烷基化二苯并噻吩、五环三萜类如藿烷和甾醇衍生的多环烷烃如甾烷（例如胆甾烷）。通常使用 GC-MS 法测定这些生物标志物。分析前，样品先经液液萃取、气相色谱柱和/或固相萃取，将烷烃类化合物和芳烃类化合物分离。最后，萃取液经气相色谱分离，使用质谱的选择离子监测（SIM）模式进行检测。由于监测的标志物数量庞大，经常需要采取多次运行，每次运行针对一组特定的生物标志物。

该篇应用中，使用安捷伦 7200 Q-TOF 直接对原油稀释液中的二苯并噻吩（DBTs）、藿烷和甾烷进行测定。飞行时间质谱将高灵敏度、分辨率与精确质量测定相结合，为复杂基质中的痕量组分检测提供了独一无二的选择性。GC/Q-TOF 方法不只局限于几种预选的分析物（如 SIM 和 MRM 模式分别用于单级四极杆和三重四极杆），还可以通过提取精确质量的离子色谱的模式对不同种类的生物标志物进行检测、鉴别和定量。此外，MS/MS 模式还对全扫描下低选择性的痕量组分有更高的选择性。

实验

化学试剂和样品

选择 NIST SRM 2260a（LGC，Molsheim，法国）二苯并噻吩参比溶液用于仪器性能测试，检测液为正己烷的 10 倍稀释液。二苯并噻吩的最终浓度为 0.38 ng/µL。

原油样品来自法国道达尔。称取 100 mg 原油，用 10 mL 正己烷超声提取。再将溶液离心，上清液用正己烷稀释 10 倍（原油最终浓度为 1 mg/mL）。

GC 和 MS 条件

使用配置 SSL 的安捷伦 7890A GC 和 7200 Q-TOF 的气质联用系统进行分析。

分析条件见表 1。

表 1.　GC/Q-TOF 条件

进样口	进样口类型	分流/不分流
	模式	不分流
	温度	300 °C
	进样体积	1 µL
色谱柱	DB-5MS，30 m x 0.25 mm，0.25 µm	
载气	1.5 mL/min，氦气，恒流	
GC 柱箱	50 °C（1 min）- 10 °C/min - 320 °C（8 min）	
检测器	电离模式	EI
	MS 模式	扫描范围 40–500 Da
	采集速率	5 Hz
	MS/MS 模式	扫描范围 40–500 Da CE : 10 eV
	离子源温度	280 °C
	四极杆温度	150 °C

结果和讨论

首先对二苯并噻吩浓度为 0.38 ng/µL 的参比液进行分析。色谱图（分析窗口范围为 5–23.5 min）如表 1 所示。DBT 在 16.3 min 出峰，其质谱图见图 1B，基峰离子为 *m/z* 184.0338，与精确质量的分子离子（$C_{12}H_8S, M^{\bullet+}$ = 184.0341）相比，质量误差小于 2 ppm。

接着，用相同方法对原油样品进行分析。图 2a 为总离子流图。谱图轮廓显示为典型的正构烷烃同系物峰。二苯并噻吩的出峰位置用箭头标出。采用单级四极杆 MS 提取 *m/z* 184 ± 0.5 amu 的离子谱图，可以检出二苯并噻吩，如图 2b 所示。但同时其他几个化合物也能够被检测到，尤其在 14–18 min 的时间窗口内尤为明显。这些化合物（可能为 C4-萘, $C_{14}H_{16}$, MW = 184）可能会干扰选定生物标志物的测定。

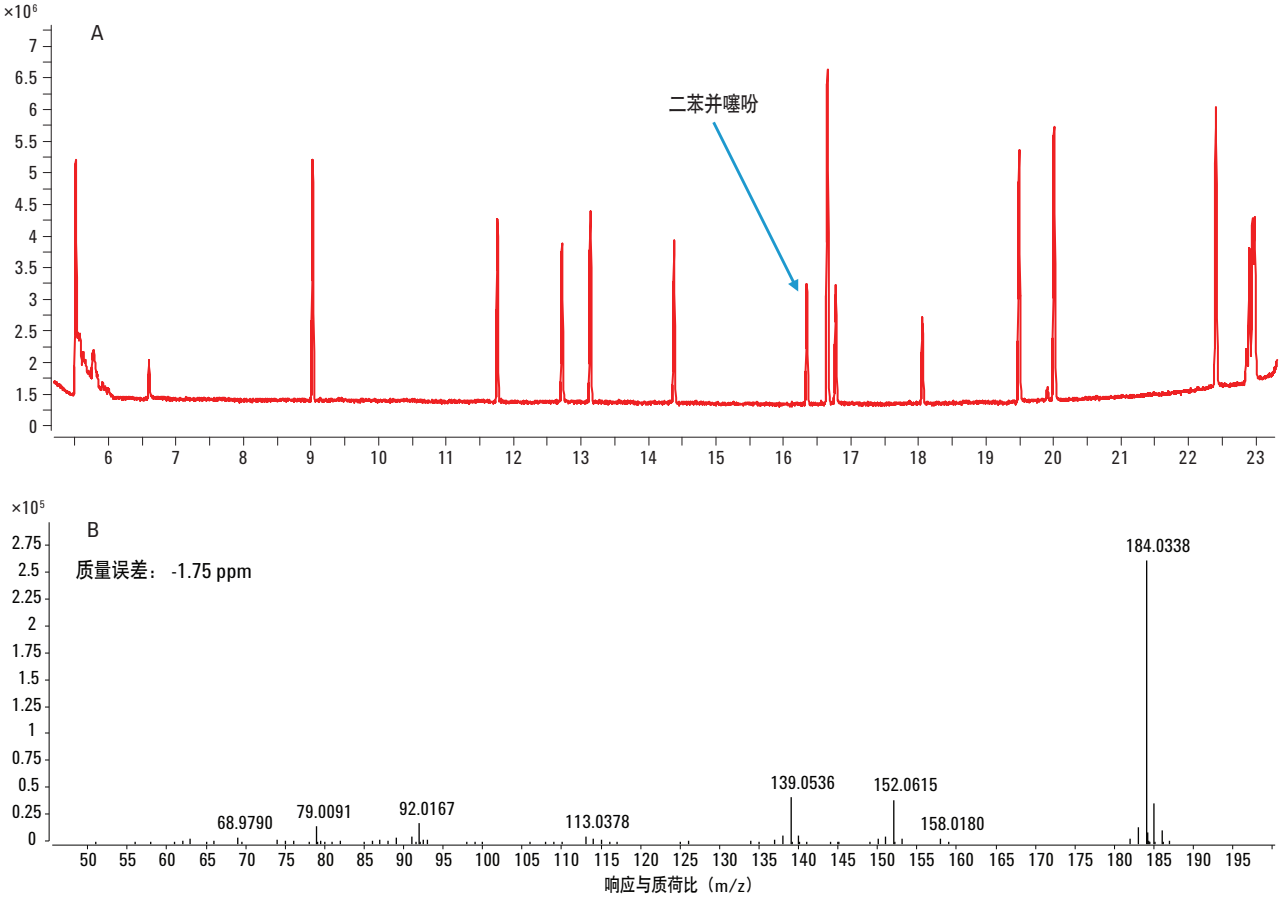

图 1.　　芳香烃混标的 GC/Q-TOF 分析（0.38 ng 二苯并噻吩（$C_{12}H_8S$, $M^{\bullet+}$ = 184.0341）的质谱图如 B 所示）

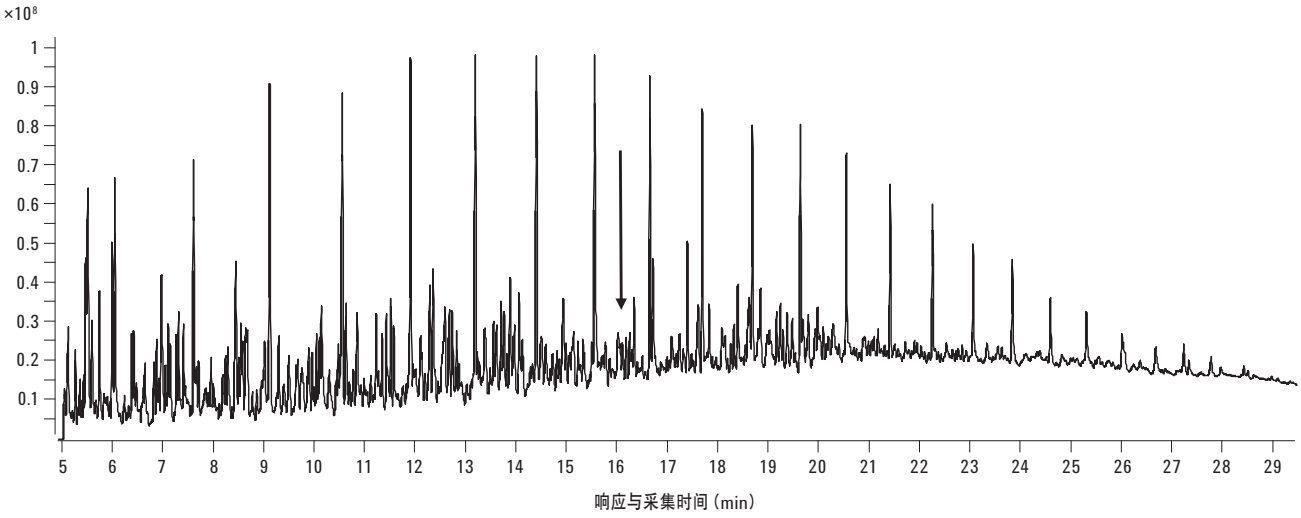

图 2a.　　原油的总离子流图（DBT 的流出时间用箭头标出）

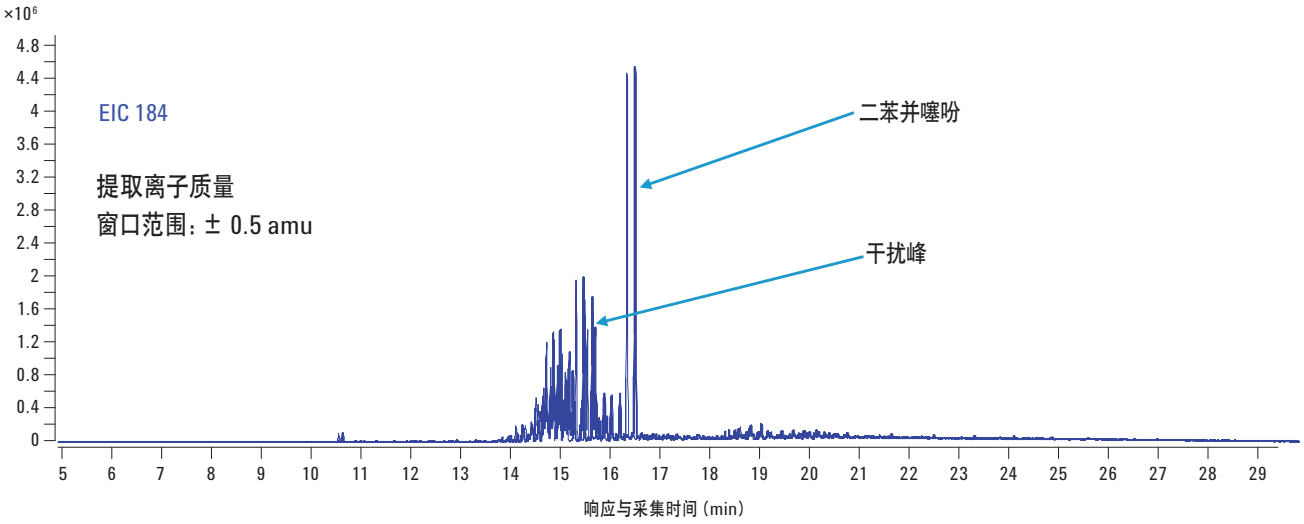

图 2b.　　184 ± 0.5 amu 的提取离子谱图

通过提取精确质量离子（184.0341 ± 5 ppm）的离子谱图，可有效消除所有干扰，大大提高分析的选择性，如图 2c 所示。16.32 min 的质谱图如图 2d 所示。复杂基质中 DBT 的精确质量（*m/z* 184.0339）未受到明显影响，质量误差小于 2 ppm。

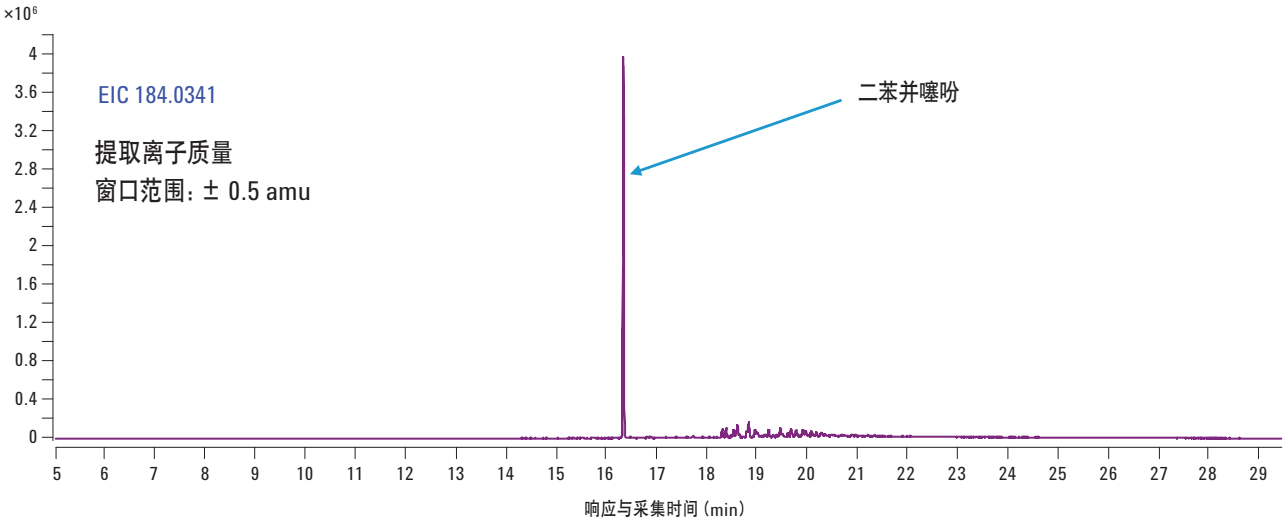

图 2c.　　184.0341 ± 5 ppm 的离子提取谱图

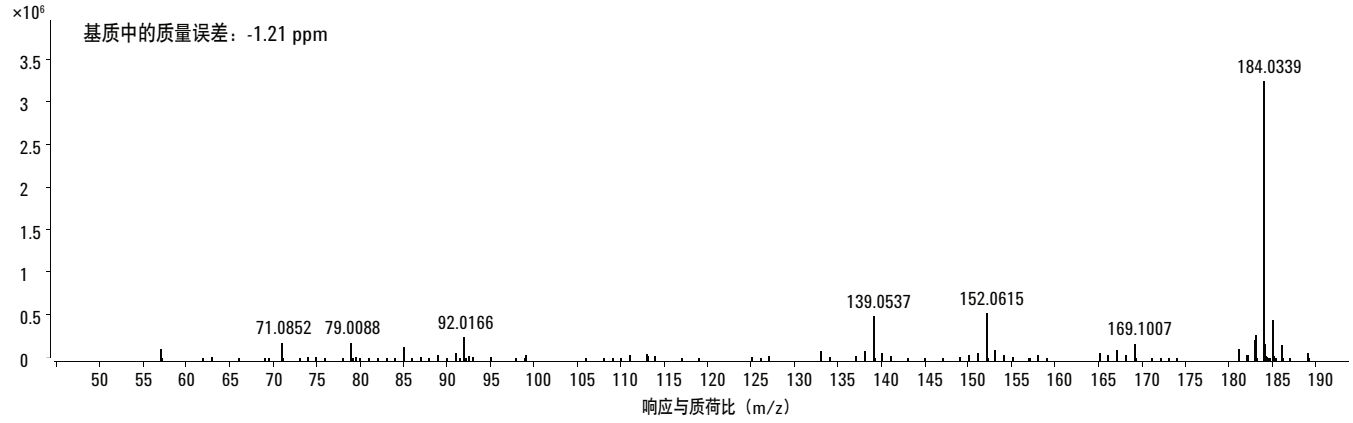

图 2d.　　原油中二苯并噻吩的质谱图

同样原理，可对甲基-二苯并噻吩（C1-DBT，4 个同分异构体，只得到了 3 个异构体的谱图）提取 *m/z* 198.0498 的离子谱图，对 C_2-二苯并噻吩提取 *m/z* 212.0645 的离子谱图。这些 DBT 标志物可轻松检出，如图 3 所示。

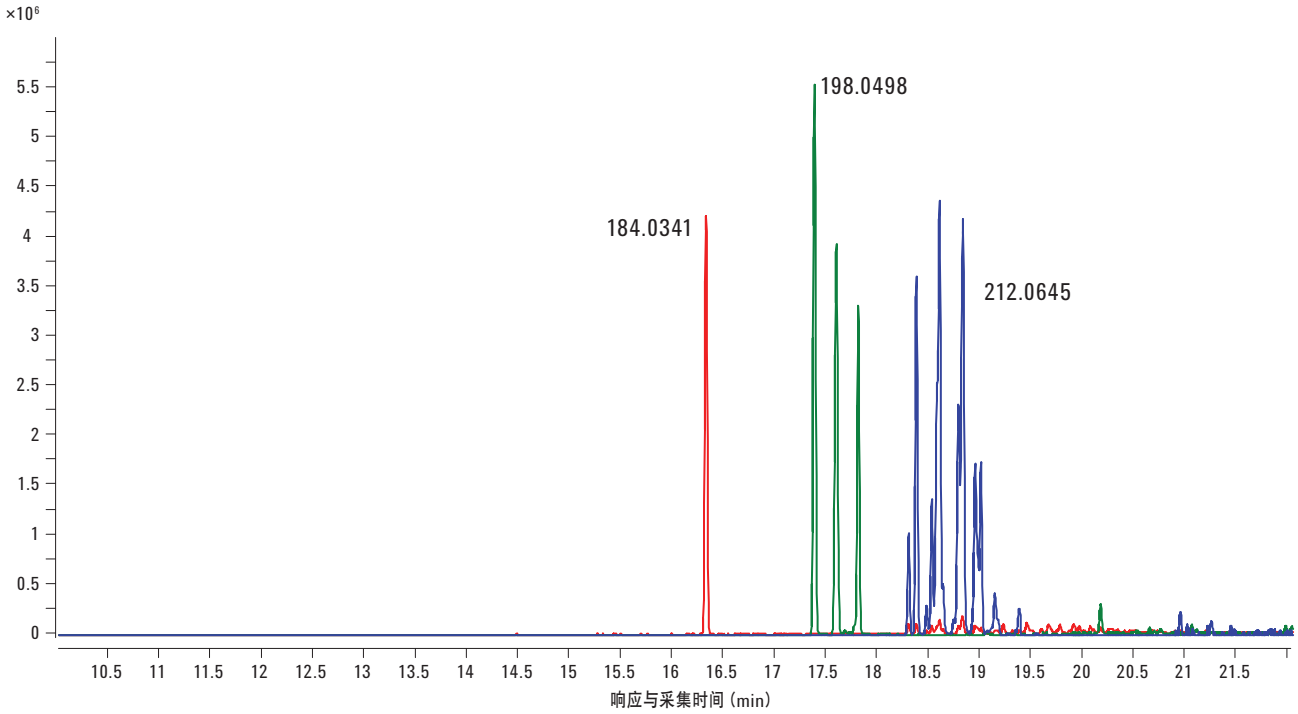

图 3.　　检测 DBT（m/z184.0341）、甲基-二苯并噻吩（m/z 198.0498）和 C_2-二苯并噻吩（m/z 212.0645）所得到的精确质量（± 5 ppm）提取离子谱图

除了含硫的多环芳烃外，藿烷和甾烷同样为重要的生物标志物。同样可以提取精确质量离子的离子谱图，对复杂原油基质中的这些化合物进行选择性检测。图 4 为 191 ± 0.5 amu（顶部）和 191.1794 ± 10 ppm（底部）条件下提取离子的谱图对比。使用精确质量检测无疑可获得更高的选择性和更高的信噪比。在时间窗口 26 min 到 30 min 的范围内可检测出几种藿烷。27-28 min 的大峰可能为降-藿烷（$C_{29}H_{50}$, MW = 398）。

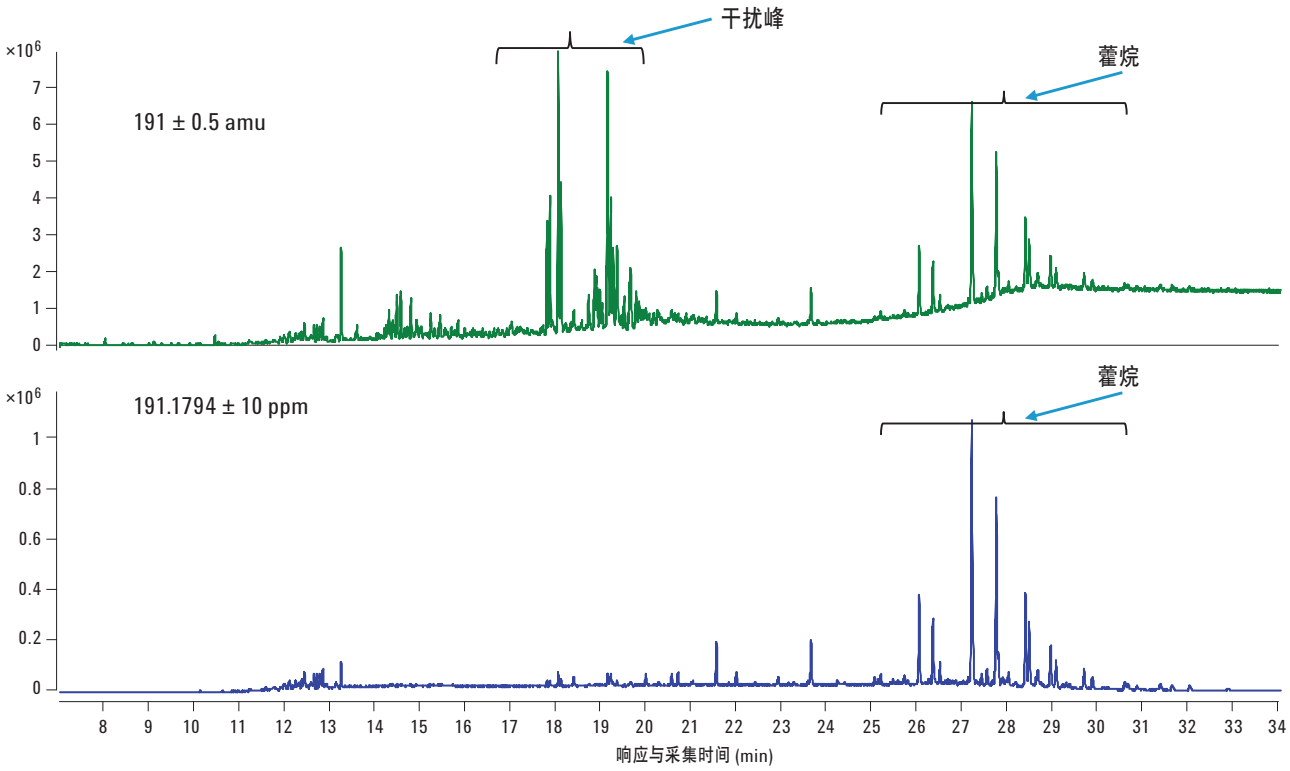

图 4.　检测藿烷在 191 ± 0.5 amu（顶部）和191.1794 ± 10 ppm（底部）条件下的提取离子精确质量谱图

最后进行甾烷特征离子的提取。因为这些分析物在样品中的浓度很低，如图 5 所示，即便使用精确质量提取离子图谱，依然容易受到基质离子的干扰。而 GC/Q-TOF 还可以采用 MS/MS 模式，可以以离子 400 为母离子（$C_{29}H_{52}$, $M^{\bullet+}$ = 乙基胆甾烷）再次提取子离子谱图。子离子在 217.1951 时的提取离子谱图表明，乙基胆甾烷测定的选择性有了显著提高，如图 6 所示。

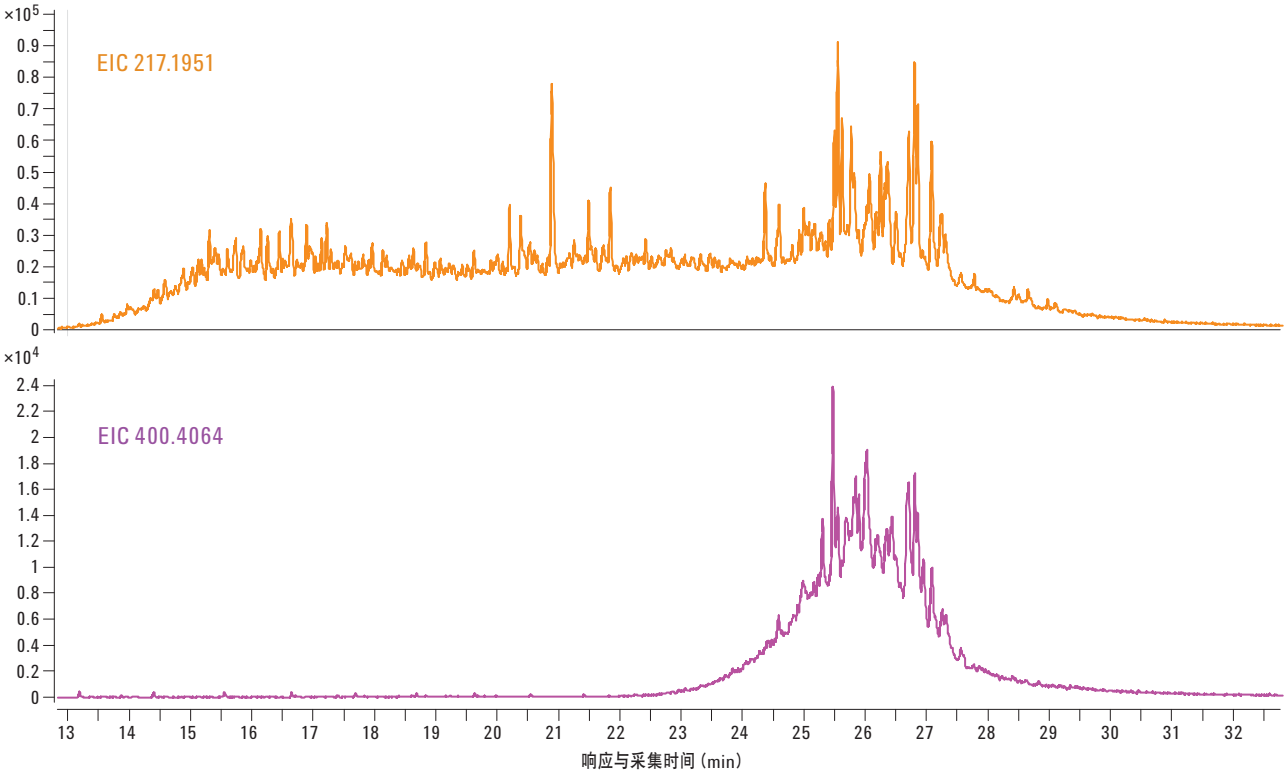

图 5.　　甾烷的精确质量提取离子谱图（217.1951 ± 10 ppm 和 400.4064 ± 10 ppm）

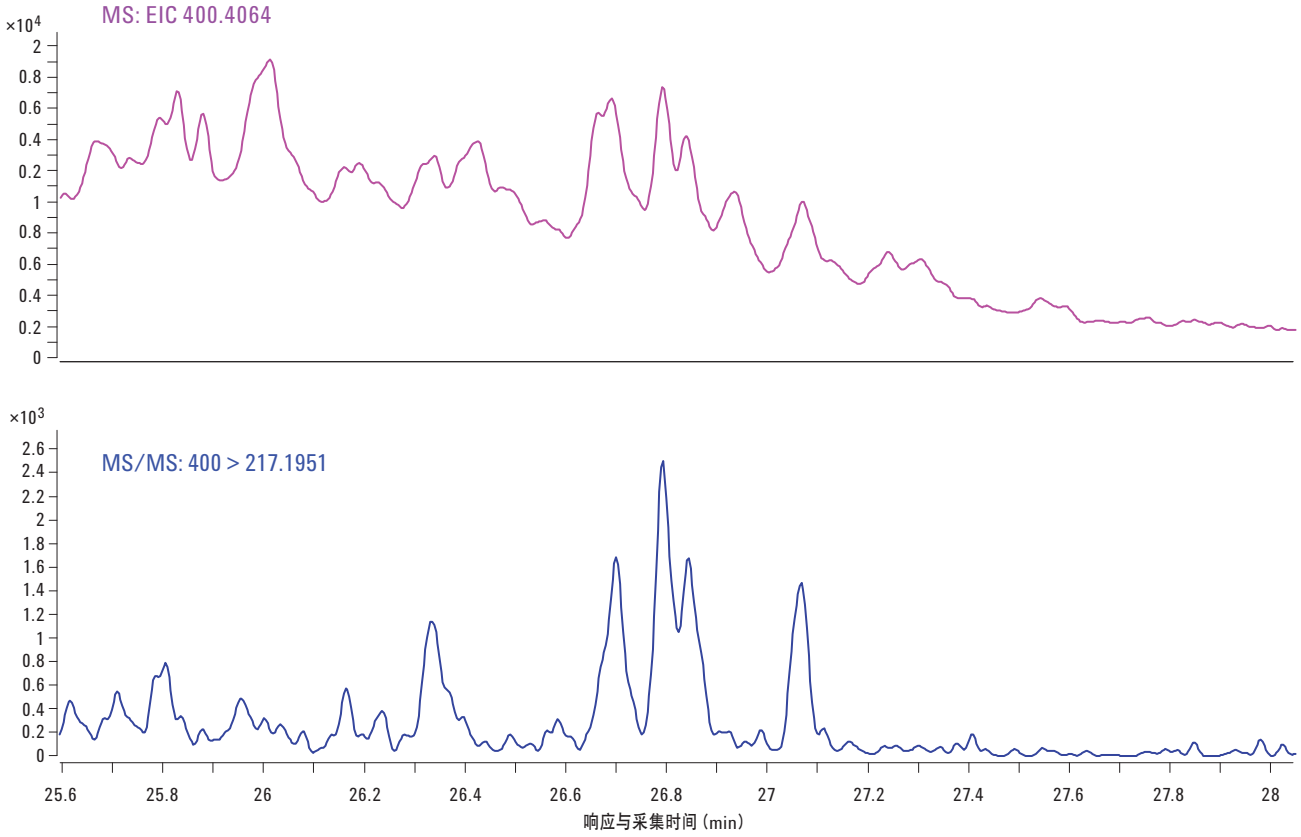

图 6. *检测甾烷在全扫描模式下精确质量（400.4064 ± 10 ppm）离子的提取离子谱图（顶部）和 MS/MS 模式下精确质量（400 > 217.1951 ± 10 ppm）产物离子的提取离子谱图（底部）的对比*

结论

安捷伦 7200 Q-TOF 可对原油中的各种生物标志物进行分析，无需进行预分馏。稀释后的原油可直接用于测定，利用精确质量的提取离子谱图和窄化的提取窗口可对二苯并噻吩和藿烷等生物标志物进行高选择性监测。

7200 Q-TOF 在 MS/MS 模式下同样可对痕量甾烷进行选择性检测。

总之，安捷伦 7200 GC/Q-TOF 系统可应用在石油特征勘察中，对目标和非目标生物标志物均可进行有效的分析。

参考文献

1. Z. Wang and M. Fingas, Developments in the analysis of petroleum hydrocarbons in oils, petroleum products and oil-spill-related environmental samples by gas chromatography, *J. Chromatogr. A* 774 (1997) 51-78.
2. Z. Wang, M. Fingas, C. Yang and B. Hollebone, Biomarker Fingerprinting: Application and Limitation for Correlation and Source Identification of Oils and Petroleum Products, Prep. Pap.-*Am. Chem. Soc., Div. Fuel Chem*. 49 (1) (2004) 331-334.

更多信息

有关我们产品和服务的更多信息，请访问 www.agilent.com/chem/cn。

使用 Agilent 7200 系列 GC/Q-TOF 进行酵母类固醇的代谢轮廓分析

应用报告

代谢组学

作者

Manhong Wu, Robert St. Onge, Sundari Suresh, Ronald Davis, and Gary Peltz
医药和生物化学学院
基因研究中心
斯坦福大学
Stanford, CA
美国

Sofia Aronova and Stephan Baumann
安捷伦科技有限公司
Santa Clara, CA
美国

摘要

使用安捷伦 7200 系列 GC/Q-TOF 系统和 Mass Profiler Professional（MPP）软件对酵母类固醇进行了代谢轮廓分析，用来精确测定新型潜在抗真菌药物的靶酶。将相对浓度的麦角甾醇生物合成中间体的靶标分析和非靶标分析相结合，再赋予精确质量的高分辨 GC/Q-TOF 技术，可以获得最全面的结果。电子电离（EI）的全采集模式质谱图结合 MS/MS 产物离子质谱数据，进一步确保了酵母中药物治疗蓄积化合物定性的准确性。

前言

芽殖酵母酿酒酵母因为其简单而且菌株可适用于基因组中所有基因的个体缺失而成为一种广受欢迎的模式生物。本研究使用酿酒酵母对新型抗真菌药物进行评价。这一药物家族以麦角甾醇，一种真菌细胞膜的重要组成部分为作用靶标。麦角甾醇和动物细胞中的胆固醇功能相似。虽然如此，但很多参与酵母类固醇生物合成的酶在结构和特异性上与哺乳动物细胞中相应的酶有很大的差别。因此，那些抑制麦角甾醇生物合成路径的药物通常具有抗真菌的治疗潜力。这些药物可以通过互补性遗传和分析方法确定。作为分析通量最高的方法，曾有文献进行过 Haploinsufficiency Profiling（HIP）筛查 [1]。HIP 涉及了基因缺失的酵母对药物的生长，造成菌株灵敏度升高，表明杂合位点的产物可能是抑制剂的靶标。除此之外，还可使用精确质量高分辨气相色谱/四极杆-飞行时间质谱（GC/Q-TOF）联用进行酵母类固醇代谢物轮廓分析并与遗传学相结合专用于潜在药物的靶酶鉴定。

本应用报告描述了使用安捷伦 7890 气相色谱和 7200 系列 Q-TOF 质谱联用仪通过定性药物治疗后，蓄积的化合物对新兴抗真菌药物的靶标物进行可靠的鉴定。首先用两种明确效果的抗真菌药物对方法进行验证，接着对有潜在治疗特性的新兴药物进行测定。较宽的仪器线性范围允许在酵母细胞的浓度范围内同时量化脂类代谢产物。

以麦角甾醇生物合成路径中的靶中间体以及药物治疗蓄积的非靶代谢物对非治疗样本的相对水平为基础，提出了几种潜在抗真菌药物作用于酵母中固醇代谢的机理。此外，使用 MS/MS 产物离子的精确质量谱图结合 Molecular Structure Correlator（MSC）工具对某些蓄积的代谢产物进行结构确认。

实验

试剂和标准品

标准品和试剂	来源
特比萘芬	Sequoia Research Products
氟康唑	Sigma-Aldrich
桃柘酮	Sigma-Aldrich
NCE 1181-0519	ChemDiv
MSTFA（N-甲基-N-三甲基硅烷-三氟乙酰胺）+ 1% TMCS （三甲基氯硅烷）	Sigma-Aldrich
甲氧基胺盐酸盐	Sigma-Aldrich
无水吡啶	Sigma-Aldrich

仪器

本研究在 7890A 和 7200 系列 GC/Q-TOF 上进行。仪器条件列于表 1。

表 1.　GC 和 MS 仪器条件

GC 条件	
色谱柱	HP-5 MS UI，30 m × 0.25 mm，0.25 µm（部件号 19091S-433UI）
进样量	1 µL
分流比	20:1
分流/不分流进样口温度	250 °C
柱箱程序升温	60 °C 保持 1 min，以 10 °C/min 升至 325 °C，保持 3.5 min
载气	氦气，恒流，1 mL/min
传输线温度	290 °C
MS 条件	
离子化模式	EI
离子源温度	230 °C
四极杆温度	150 °C
扫描范围	50 ~ 600 *m/z*
质谱采集速率	5 Hz，centroid 和 profile 模式
MS/MS 模式碰撞能量	15 V

样品制备

用抑制 10% 增长率的药物浓缩液对 6 个含有 5 mL 野生型酵母培养液（BY4743）的平行样进行培养，当 OD_{600} 值约为 1 时进行收集（约 3 × 10^7 细胞/mL）。用 Folch 法提取酵母油脂 [2]。相当于原培养液 2.5 个 OD_{600} 单位的下层有机相通过快速抽真空干燥，用 40 mg/mL 甲氧基胺盐酸盐的吡啶溶液进行衍生化，再用 MSTFA+1%TMCS 混合溶液进行硅烷化，溶液的最终体积为 100 µL。取 1 µL 用于气相色谱进样。

数据分析

使用安捷伦 MassHunter B.05 进行定量。所有谱图均使用 Mass Hunter Qualitative Analysis B.05 进行解卷积，感兴趣的代谢产物通过与 NIST11 谱库比对确定结构。

使用多元软件包 Mass Profiler Professional（MPP）对解卷积后的数据进行统计评估（数据过滤、统计学意义分析、确定痕量水平的特异性化合物和结果可视化），测定药物治疗样本中浓度显著不同于对照样本的化合物。此软件可以进行多个非预期代谢产物的检测。

结果与讨论

数据分析

得益于精确的质量数信息，GC/Q-TOF 数据的谱图解卷积可以区分具有相同标称质量碎片离子的共流出化合物。MassHunter Qualitative Analysis 软件按以下 4 步进行解卷积：

1. **噪声分析：**为每个离子的谱图计算噪声因子
2. **化合物预测：**噪声分析结果和保留时间一起对每个谱图组分进行峰形模型预测
3. **谱图解卷积：**用最小二乘法创建每个组分的质谱图
4. **化合物识别：**对每个组分进行 EI 谱库检索和比对

无偏方法的优势之一是无需考虑目标离子进行解卷积。在“**化合物预测**”步骤中确定的色谱峰形可以识别相邻扫描中具有相似的峰形和峰顶的组分。

色谱峰解卷积还有助于区分具有相同经验公式的不同化合物。图 1 表明 3 种化合物的分子式均为 $C_{29}H_{48}O$，但只有右侧的谱图具有和 4,4-二甲基-8,24-胆甾-二烯醇相匹配的 EI 谱图结构。根据下面的 9 步向导工作流程，确定 4,4-二甲基-8,24-胆甾-二烯醇是这些化合物中唯一符合 Mass Profiler Professional（MPP）多元统计软件包设定的倍率变化和显著性标准的化合物。

一旦谱图完成解卷积，即创建了化合物交换格式（.CEF）的文件。然后用 MPP 软件测定那些浓度因药物发生显著变化的化合物。MPP 统计评估步骤如下：

1. 定义实验类型、工作流程和生物体
2. 选定数据源为 MassHunter Qualitative Analysis
3. 从 Qualitative Analysis 导入 .CEF 文件
4. 设置丰度和模型离子过滤器

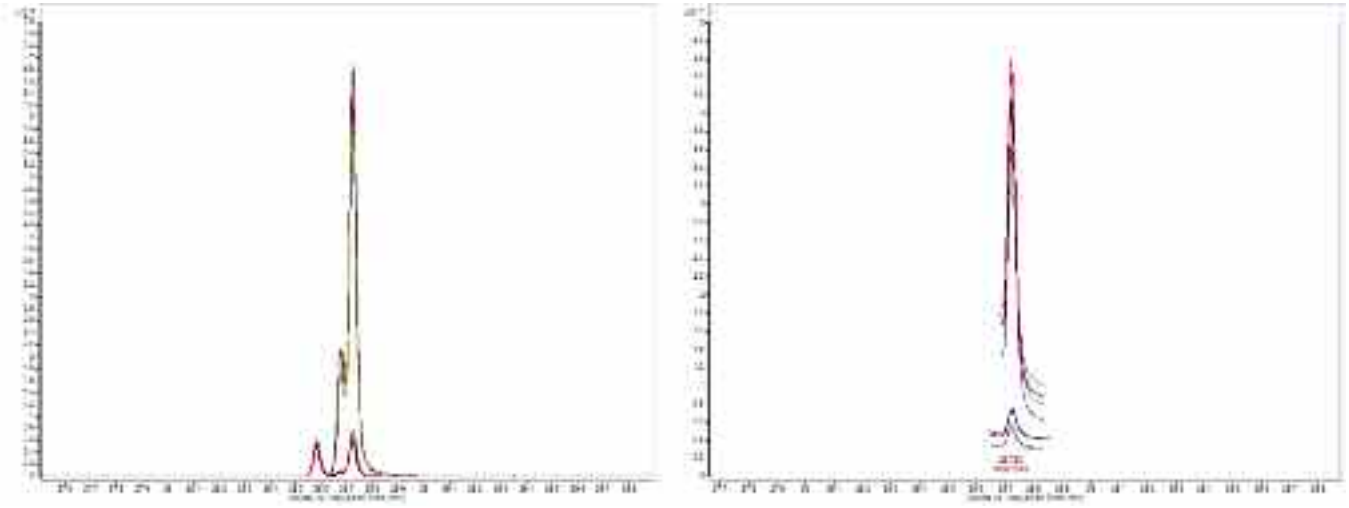

图 1.　谱图解卷积可以区分具有相同标称质量碎片离子的共流出化合物。左侧的谱图为提取离子叠加谱图（EICs），说明一些共流出化合物具有相同的碎片离子。右侧的谱图为经 MassHunter 解卷积治疗后，其中一种化合物 4,4-二甲基-8,24-胆甾-二醇的谱图

5. 定义保留时间和匹配因子定位参数
6. 选择校准类型
7. 选择基线校准
8. 设置条件筛选标志
9. 火山曲线过滤。其结合了显著性（$p < 0.05$）的 Student's t 检验结果和阈值为 2 的倍率变化结果

概念验证

使用先前所述的抗真菌药物和易于理解的靶酶来论证使用精确质量高分辨 GC/Q-TOF 分析酵母类固醇代谢轮廓的可行性。特比萘芬和氟康唑都是广泛使用的抗真菌药物，在麦角甾醇的生物合成路径中的靶标为完全不同的过程，且抑制机理成熟。特比奈芬抑制 ERG1 的基因产物鲨烯环氧酶，从而防止角鲨烯转化成路径上的后续中间体，角鲨烯环氧化物。酵母细胞一直在持续生成角鲨烯但却不能有效地将之转化成下游中间体，从而导致了角鲨烯的蓄积。氟康唑抑制 ERG11 的基因产物细胞色素 P450 14α-去甲基化酶或者羊毛甾醇去甲基酶，这时，就会形成羊毛甾醇的蓄积。研究对相关类固醇在药物治疗样本和非治疗样本中的代谢物丰度变化进行了对比和评估（图 2 和图 3）。

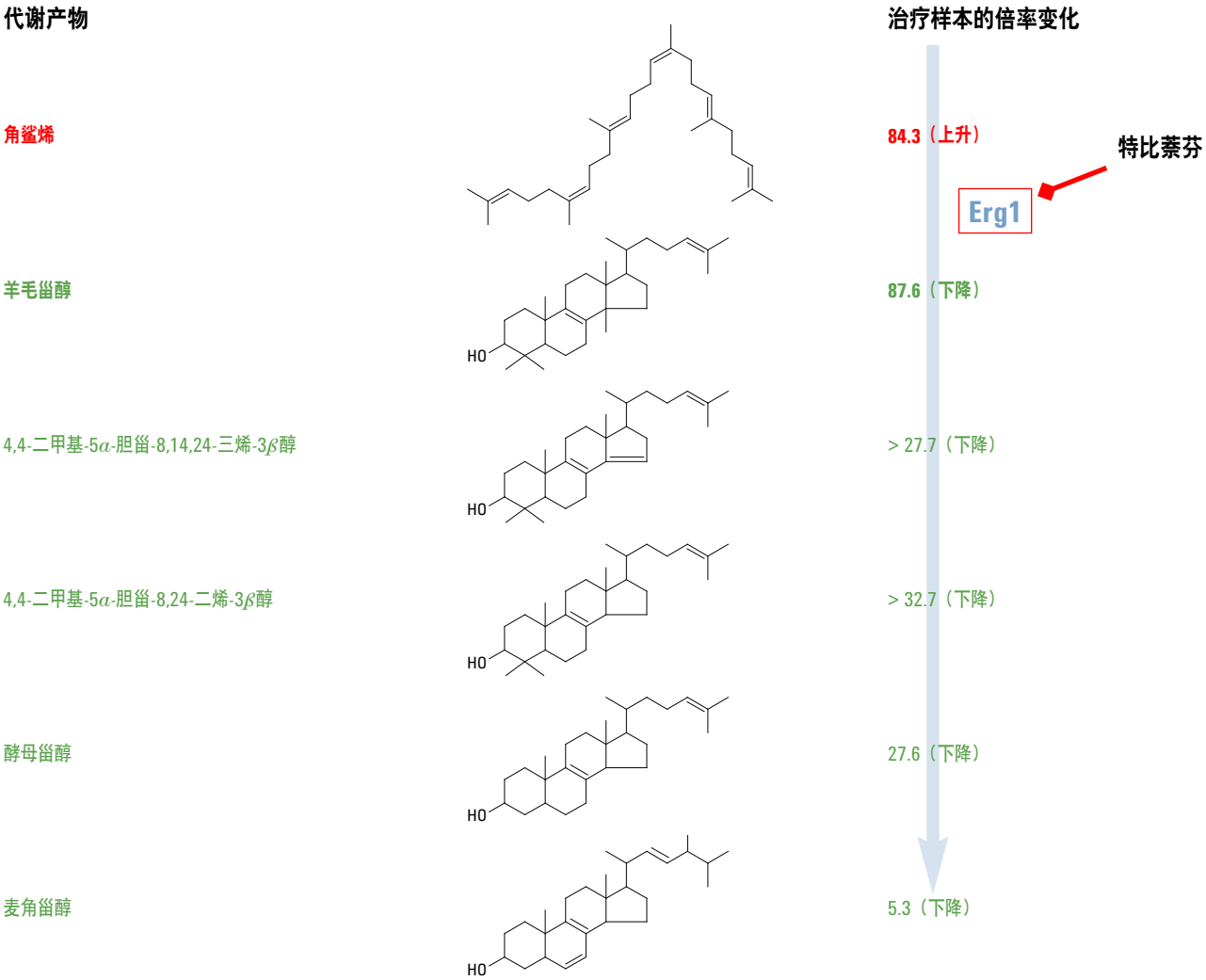

图 2.　经特比萘芬治疗后，不同类固醇代谢产物丰度的倍率变化，包括因为抑制 ERG1 基因产物角鲨烯环氧酶造成的角鲨烯蓄积

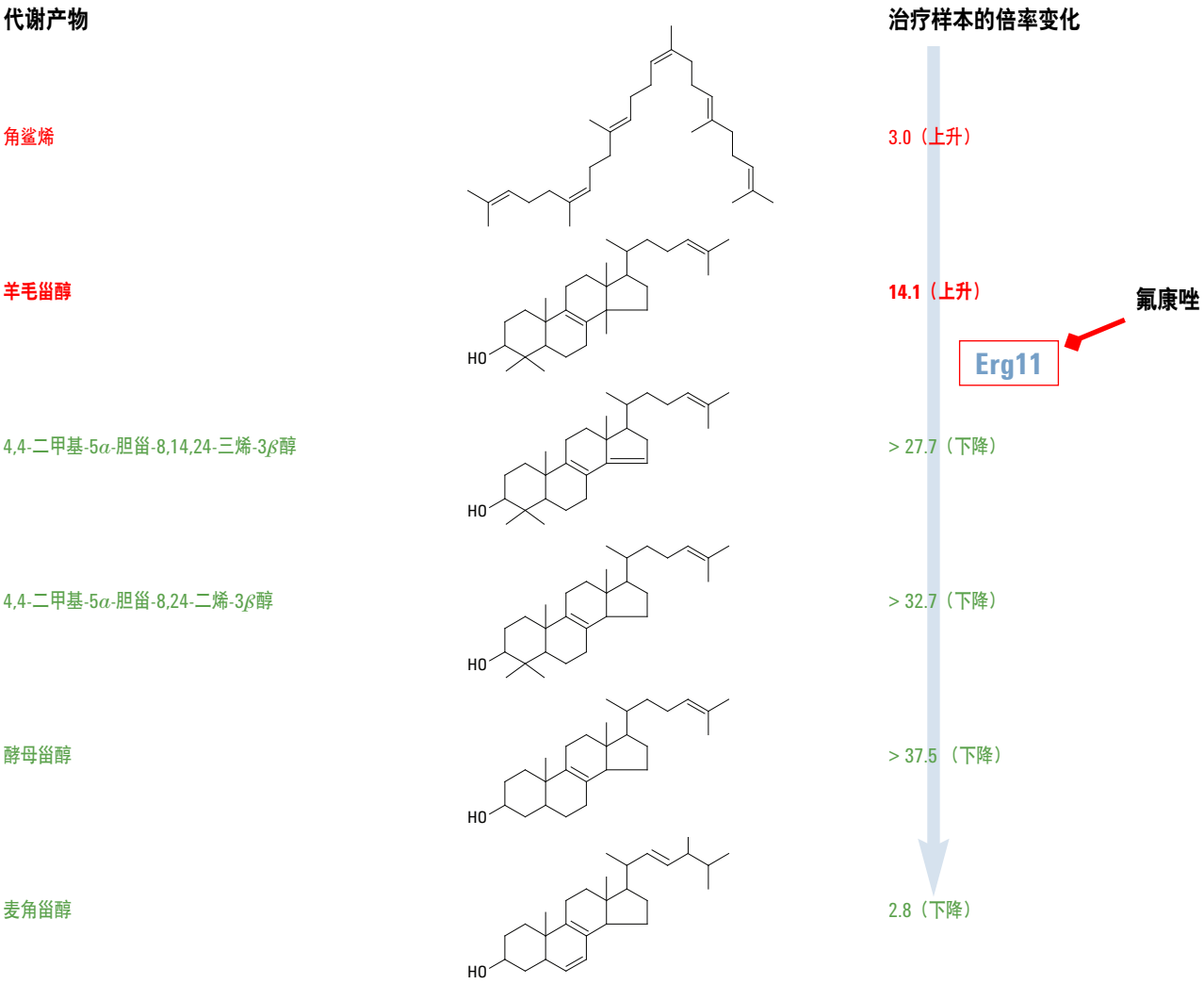

图 3.　经氟康唑治疗后，不同类固醇代谢产物丰度的倍率变化，包括因为抑制 ERG11 基因产物 14α-去甲基化酶造成的羊毛甾醇蓄积

正如预期的那样，分别在特比萘芬和氟康唑治疗的样本中发现了角鲨烯和羊毛甾醇的蓄积。使用 MPP，发现在氟康唑治疗的样本中因 14α-去甲基化酶的活性受到抑制而导致几种 14α-甲基类固醇的蓄积。非靶标分析得到的结果显示麦角甾醇生物合成路径上的某些下游酶表现得更加“混杂”，这样可以使用蓄积的类固醇和额外的甲基官能团作为他们的培养基。14α-甲基类固醇的经验公式可以通过 EI 碎片谱图和精确质量信息（表 2）确定。碎片离子的精确质量进一步确保了化合物定性的可靠性。

表 2.　　氟康唑的非靶标分析结果

组分（*m/z* @ RT）	化合物	分子式	衍生化产物 MI (*m/z*)	MI 精确质量 (*m/z*)	质量误差 (ppm)
469 @ 28.08	14-α-去甲基粪甾醇	$C_{29}H_{48}O$	484.4095	484.4101	1.24
379 @ 28.26	14-α-去甲基- 4-α-甲基酵母甾醇	$C_{29}H_{48}O$	484.4095	484.4107	2.48
467 @ 28.39	14-α-去甲基-3-酮基-α-甲基酵母甾醇	$C_{29}H_{46}O$	482.3938	482.3931	–1.45

RT = 保留时间

MI = 分子离子

新型抗真菌药物的代谢轮廓特征分析

根据基因筛查结果，选择了一些麦角甾醇生物合成路径的潜在抑制剂如桃柘酮和一种新型化学实体（NCE）1181-0519 进行研究。为了更好地了解新型潜在药物诱导的酵母中的代谢变化，同时采用了靶标分析和非靶标分析比较治疗样本和非治疗的样本中代谢产物的蓄积水平。

此外，MS/MS 实验结果提供的结构信息对药物治疗造成的蓄积代谢物的结构鉴定至关重要。结果清晰表明，NCE 1181-0519 和桃柘酮的靶标分别是 Erg25 和 Erg26。

用 MPP 进行统计分析有助于轻松识别不同变化差异的组分（图 4）。

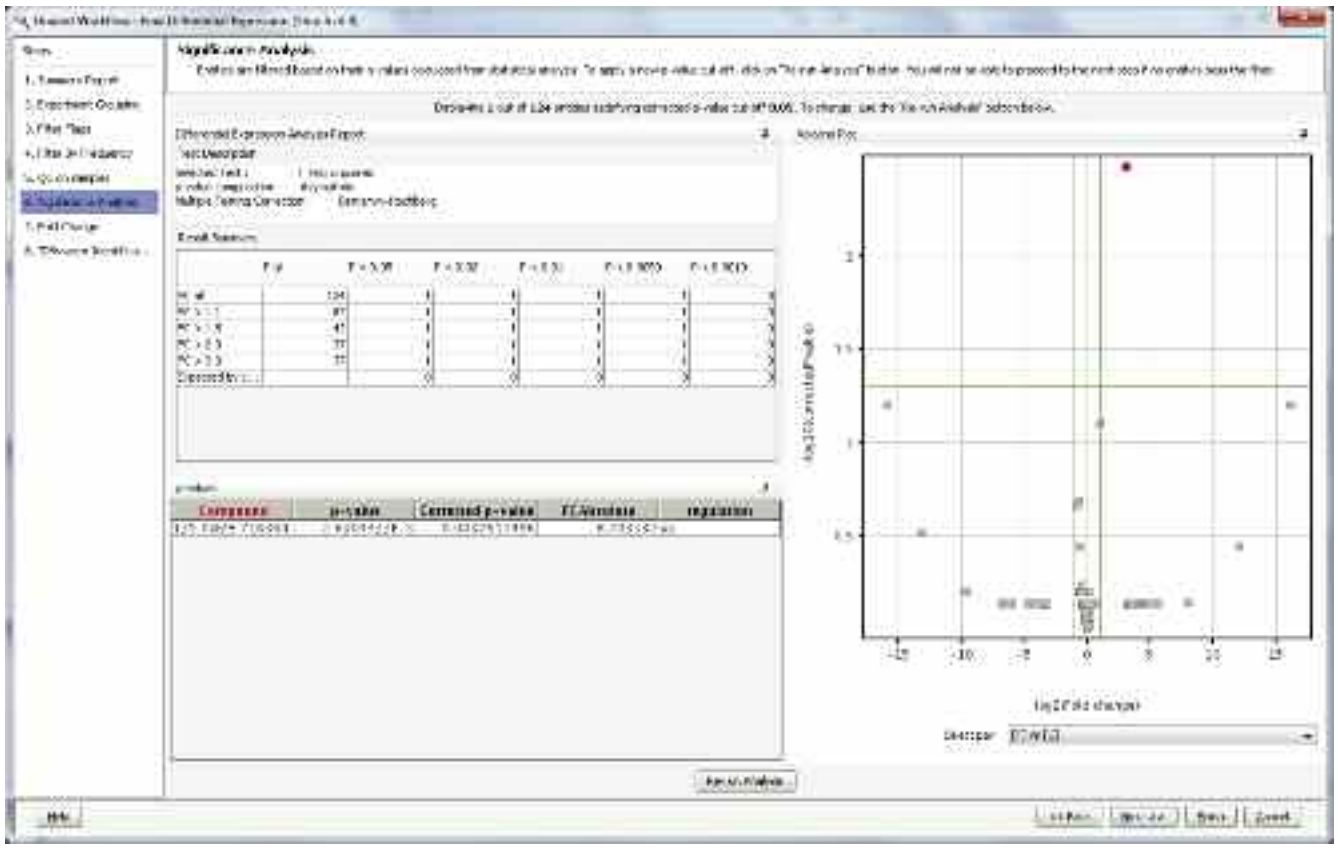

图 4.　　MPP 的显著性分析表明，NCE 1181-0519 治疗的样本中，只有一种化合物（4,4-二甲基-8,24-胆甾二醇）的倍率变化存在显著性差异

在 NCE 1181-0519 样本中，只有 4,4-二甲基-8,24-胆甾二醇满足显著性检验标准，即倍率变化的 $p < 0.05$，说明 NCE 特异性作用于 Erg25，下游中间产物的衰减同样有力地支持了这一结论（图 5）。

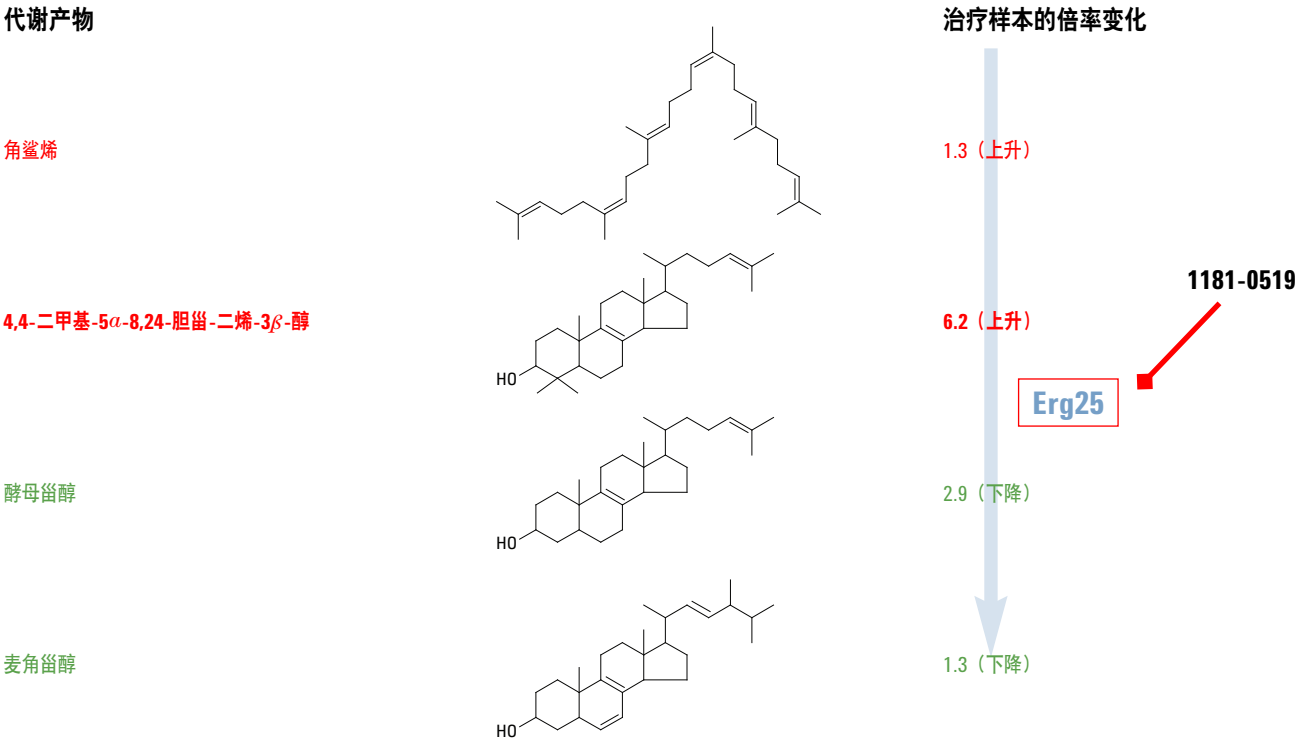

图 5.　经氟康唑治疗后，不同类固醇代谢产物丰度的倍率变化，包括 4,4-二甲基-8,24-胆甾二烯醇的蓄积和下游中间体的下降，确定 Erg25 为药物靶标

桃柘酮造成 4α-羧基-4β-甲基-5α-胆甾-8,24-二烯-3β-醇的蓄积，这和 Erg26 作为桃柘酮的靶标结果一致（图 6），因为它是一个生物性质不稳定的中间体，通常不检测该化合物，本实验未将其作为原始靶标物，只能通过非靶标分析揭示桃柘酮会导致其蓄积。

这一代谢物的结构通过精确质量产物离子谱图信息（图 7）确认，Molecular Structure Correlator 软件用于进一步确认 MS/MS 生成碎片的结构，并生成匹配度分值表，以此确定蓄积化合物最佳的结构式（图 8）。

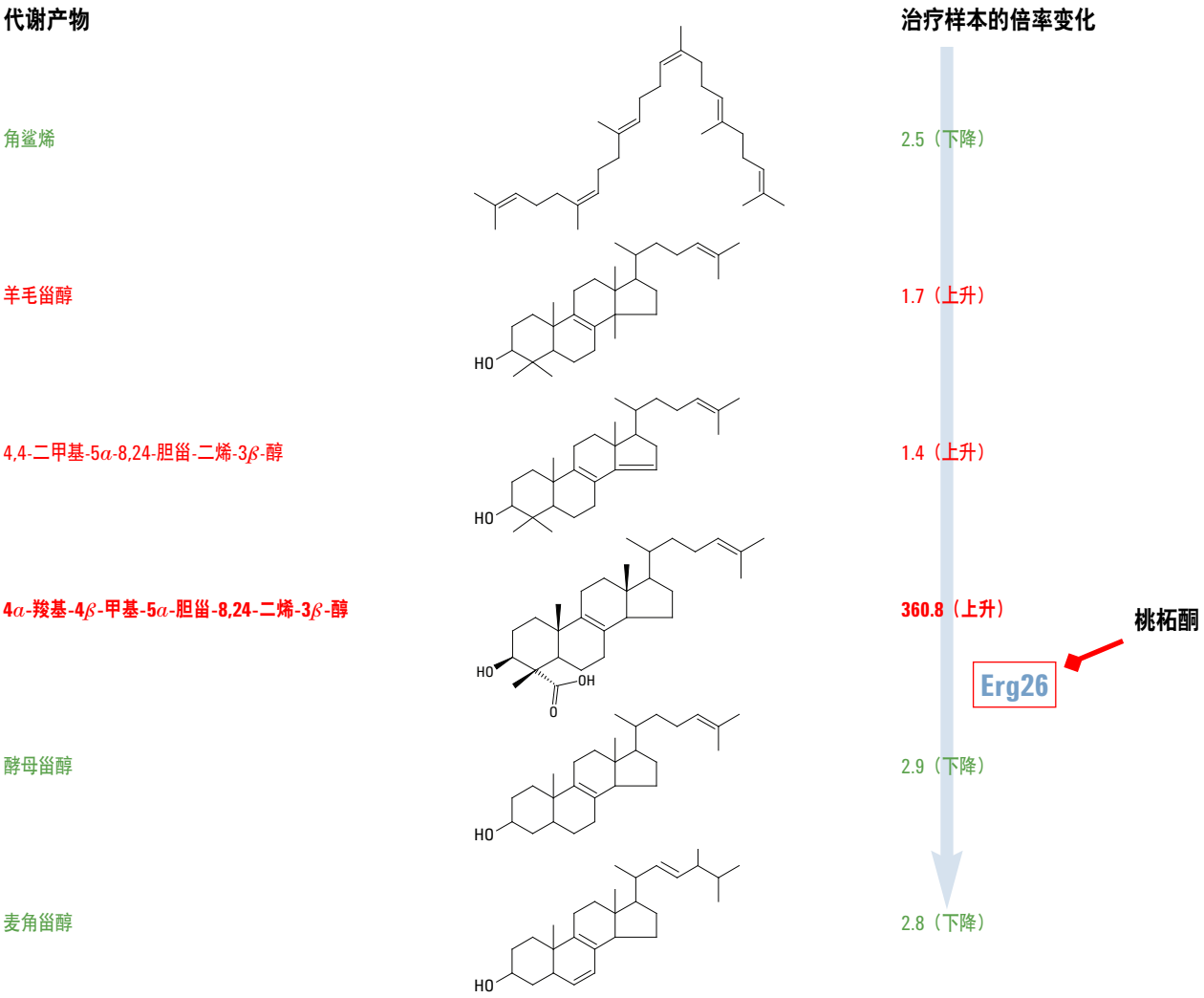

图 6.　经桃柘酮治疗后，4α-羧基-4β-甲基-5α-胆甾-8,24-二烯-3β-醇丰度的倍率变化，Erg26 为桃柘酮的特异性靶标

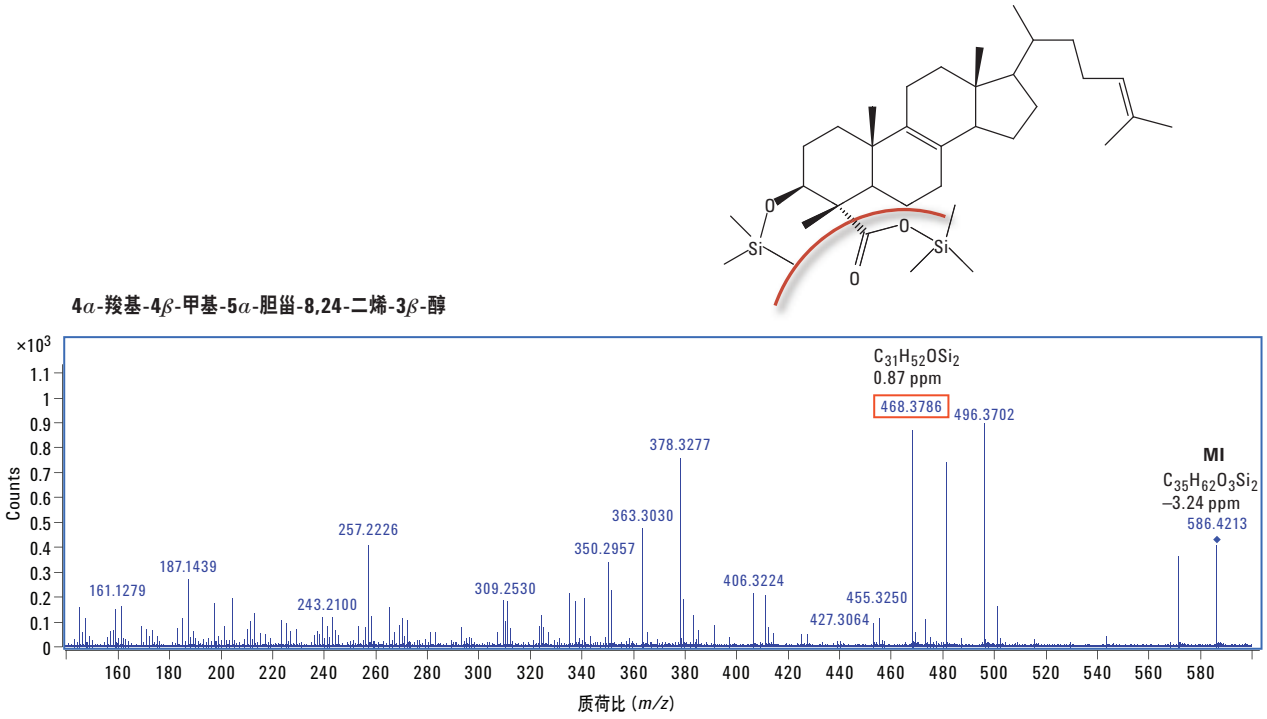

图 7. *MS/MS 产物离子谱图帮助进一步确认非靶标方法确定的蓄积物结构，4α-羧基-4β-甲基-5α-胆甾-8,24-二烯-3β-醇*

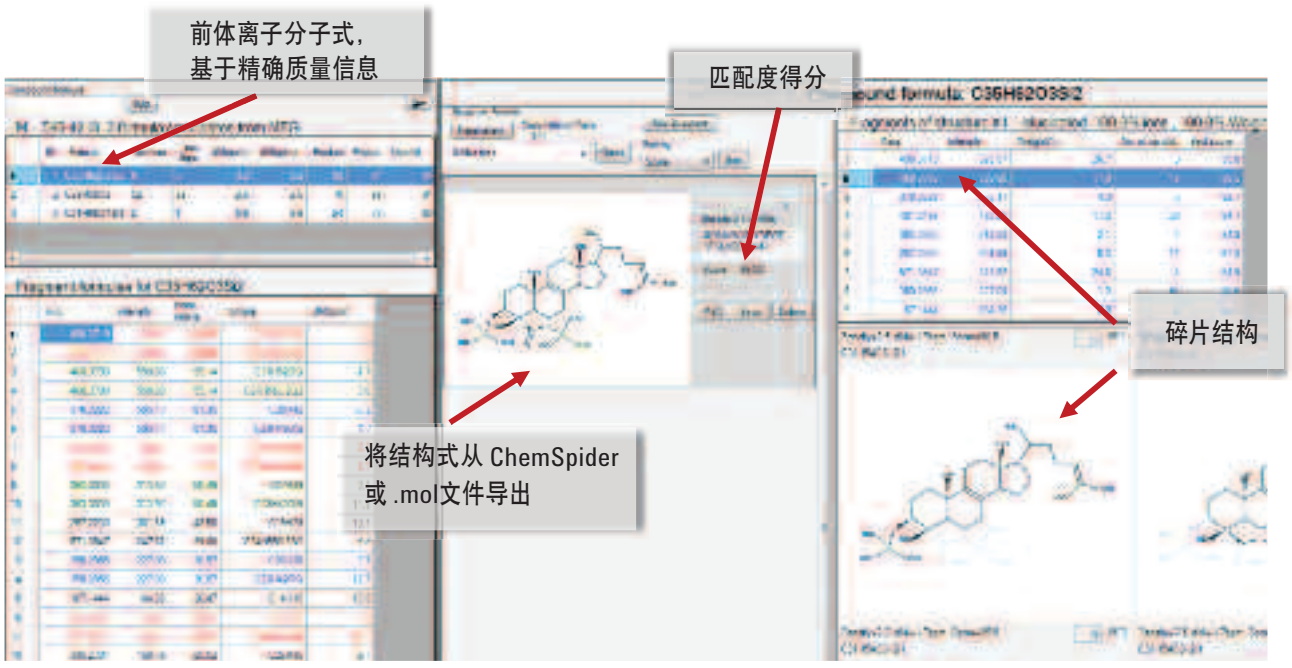

图 8. *Molecular Structure Correlator 根据 MS/MS 的每张精确质量碎片离子谱图分配分子式。通过软件工具挖掘 ChemSpider 数据库。通过 MDL Molfile 添加结构式可以对所有可能的同位素或者特定的化合物进行评估*

7200 GC/Q-TOF 全扫描模式出色的灵敏度可在一次实验中识别所有必要的代谢物，这对特异性较差的抗真菌药物的作用机理解析非常重要。图 9 总结了两种潜在抗真菌药物的代谢轮廓分析结果，说明了 ERG25 和 ERG26 分别是 NCE 1181-0519 和桃柘酮在麦角甾醇生物合成路径的靶基因。

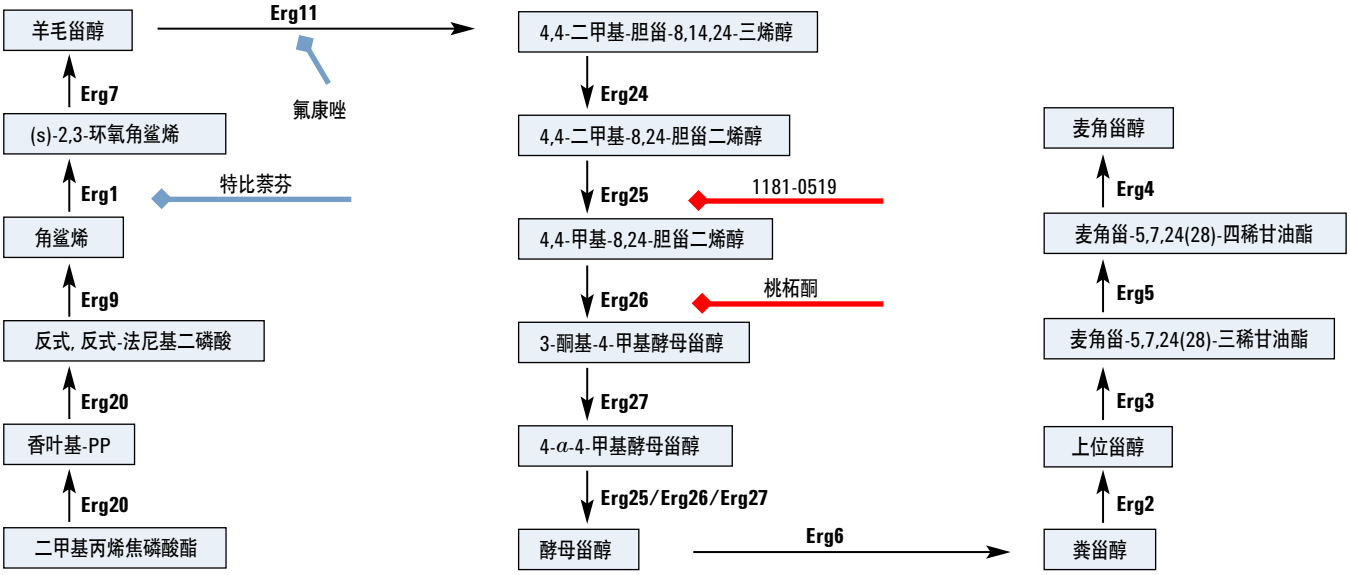

图 9.　麦角甾醇生物合成的路径图，红色标注的为研究确定的 NCE1181-0519 和桃柘酮的靶基因

结论

7200 系列 GC/Q-TOF 是一个功能强大的分析工具，用来进行酵母类固醇代谢轮廓的扫描，识别公认抗真菌药物的靶酶，与 Haploinsufficiency Profiling 一起更详尽地阐明药物抑制机理。7200 GC/Q-TOF 的精确质量信息和全谱图的灵敏度可以对目标物及药物治疗蓄积形成的未知化合物进行可靠的识别和定性。线性范围高达 5 个数量级，可以对整个细胞浓度范围内的代谢物同时进行测定。

用此方法对几种潜在抗真菌的药物包括 NCE1181-0519 和桃柘酮的作用机理进行了解析，这一过程通过经 Mass Profiler Professional 评估，中间体浓度发生显著变化的样本同时进行靶标分析和非靶标分析实现的。此外，7200 GC/Q-TOF 通过精确质量 MS/MS 产物离子谱图与 Molecular Structure Correlator 工具相结合，可对未知代谢物进行结构确认和解析。

参考文献

1. G. Giaever, P. Flaherty, J. Kumm, M. Proctor, C. Nislow, D. F. Jaramillo, A. M. Chu, M. I. Jordan, A. P. Arkin, R.W Davis. “Chemogenomic profiling: identifying the functional interactions of small molecules in yeast.” Proc Natl Acad Sci U S A. 101, 793-798 (2004).
2. J. Folch, M. Lees, G. H. Sloane Stanley. “A simple method for the isolation and purification of total lipids from animal tissues.” J Biol Chem. 226, 497-509 (1957).

更多信息

本文中的数据仅代表测定的典型结果。有关产品和服务的更多信息，请访问 www.agilent.com/chem/cn

气相色谱-四极杆-飞行时间质谱仪 (GC-QTOF) 分析大葱中多种农药残留

应用报告

作者

王雯雯　余翀天

安捷伦科技（中国）有限公司

前言

大葱不仅是中国传统的调味品，而且是一种重要的出口农产品。传统的分析方法，比如气相色谱或者气相色谱 — 单四极杆质谱仪容易受大葱当中强基质干扰，造成分析结果出现偏差。高分辨 Q-TOF GC/MS 即可以工作在单 TOF 模式下，利用采集到的碎片精确质量数对未知化合物进行定性分析，也能充分利用 MS/MS 选择性进一步增强的优势，对目标化合物进行更准确的检测，特别适用于类似大葱这样复杂的样品。本文使用安捷伦 7200 Q-TOF GCMS 对大葱当中的多种农药残留进行定性分析，以考察 7200 检测复杂样品的能力。

仪器参数

气相色谱：Agilent 7890A，色谱柱：Agilent HP-35 MS 色谱柱 (30 m×0.25 mm×0.25 μm)；程序升温：80 °C 保留 1.0 min，25 °C • min^{-1} 升到 170 °C，6 °C • min^{-1} 升到 300°C，保留 10 min；载气：氦气，载气流量：1.1 mL • min^{-1}；进样口温度：270 °C，进样体积：1.0 μL，进样模式：不分流。

质谱系统：7200 Q-TOF。离子源：EI，离子化能量：70 eV，离子源温度：250 °C，气质接口温度：280 °C，溶剂延迟：5.0 min，工作模式：全扫描和 MS/MS，扫描范围：m/z 45-450。

结果及讨论

精确质量数对结果的影响

图 1（上）是大葱基质当中 100.0 ng • mL^{-1} 的 100 种农药在 TOF 模式下采集得到的 TIC 结果；图 1（中）显示的是 Procymidone 质荷比为 m/z 283.0161 的碎片在 +/-0.5 Da 提取窗口情况下得到的 EIC 结果，此时由于离子提取窗口太宽（即所要求的准确度低），其它质荷比相近的离子碎片也被提取出来了。这个结果与低分辨四极杆质谱结果类似。而如果把提取窗口进一步缩小到 +/-10 ppm，如图 1（下）所示，那么高分辨情况下得到的精确质量数碎片就可以与基质当中的干扰离子碎片明显区别开来。

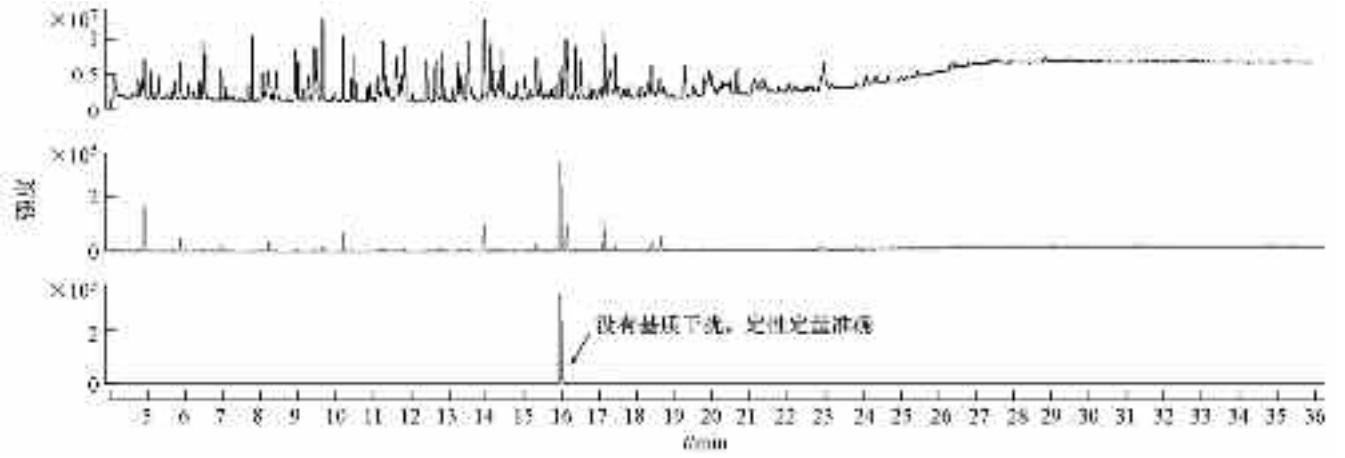

图 1.　（上）在大葱基质中 100 种农药的总离子流图 (100 ng • mL^{-1})；（中）在单 TOF 扫描模式下，提取离子流图 (283.0161 +/-0.50 Da)；（下）在单 TOF 扫描模式下，提取离子流图 (283.0161 +/-10 ppm)

质量准确性

表 1 显示了部分被检测农药在 10.0 ng • mL^{-1} 添加水平时的分辨率和质量精度。即使是在如此低浓度的情况下，7200 GC-Q/TOF 也表现出了非常优异的质量检测精度和分辨率，特别是长时间的整机性能的稳定性（仪器调谐是 2d 之前做的，而且在数据采集过程当中没有使用内标来实时校准质量轴）。

校准曲线

在大葱基质当中添加了 100 种农药，添加水平分别为 10.0、20.0、50.0、100.0 和 200.0 ng • mL^{-1}。结果显示，绝大多数农药都有很好的线性响应。图 2 中，敌稗在 10.0 ng • mL^{-1} 添加水平 EIC 结果，信噪比为 63.39；敌稗标准曲线，相关系数 0.9992。

表 1.　　部分农药碎片离子的分辨率和检测精度

名称	分子式	精确质量数（理论）	精确质量数（实测）	分辨率	精确度/ppm
异丙甲草胺	$C_{11}H_{16}N$	162.1277	162.1272	11327	3.24
二苯胺	$C_{12}H_{11}N$	169.0886	169.0879	11036	4.14
达草灭	$C_{12}H_9ClF_3N_3O$	303.0381	303.0369	12448	3.88
腐霉利	$C_{13}H_{11}Cl_2NO_2$	283.0161	283.0154	12686	2.6
p,p′-DDD	$C_{13}H_9Cl_2$	235.0076	235.0076	12207	-0.08
o,p′-DDT	$C_{13}H_9Cl_2$	235.0076	235.0068	12274	3.33
o,p′-DDD	$C_{13}H_9Cl_2$	235.0076	235.0068	12274	3.33
嘧菌环胺	$C_{14}H_{14}N_3$	224.1182	224.1177	12138	2.34
灭蚁灵	C_5Cl_6	269.8126	269.8119	12364	2.47
四氯硝基苯	C_5HCl_4	200.8824	200.882	11686	3.42
五氯硝基苯	$C_6^{35}Cl_4^{37}ClNO_2$	294.8337	294.833	12288	2.27
HCB	$C_6^{35}Cl_5{}^{37}Cl$	283.8096	283.8096	13151	0.06
Gamma-BHC	$C_6H_4Cl_3$	180.9373	180.9369	11576	2.26
Delta-BHC	$C_6H_4Cl_3$	180.9373	180.9368	11489	2.82
三氯杀螨砜	C_6H_4ClOS	158.9666	158.9662	10728	2.45
五氯苯	C_6HCl_5	247.8515	247.8509	12734	2.58
西玛津	$C_7H_{12}ClN_5$	201.0776	201.0769	11692	3.35
戊炔草胺	$C_7H_3OCl_2$	172.9555	172.9554	10809	0.85
噻嗪酮	C_7H_7N	105.0573	105.057	9159	2.86
抗蚜威	$C_8H_{12}N_3O$	166.0975	166.0971	11369	2.34

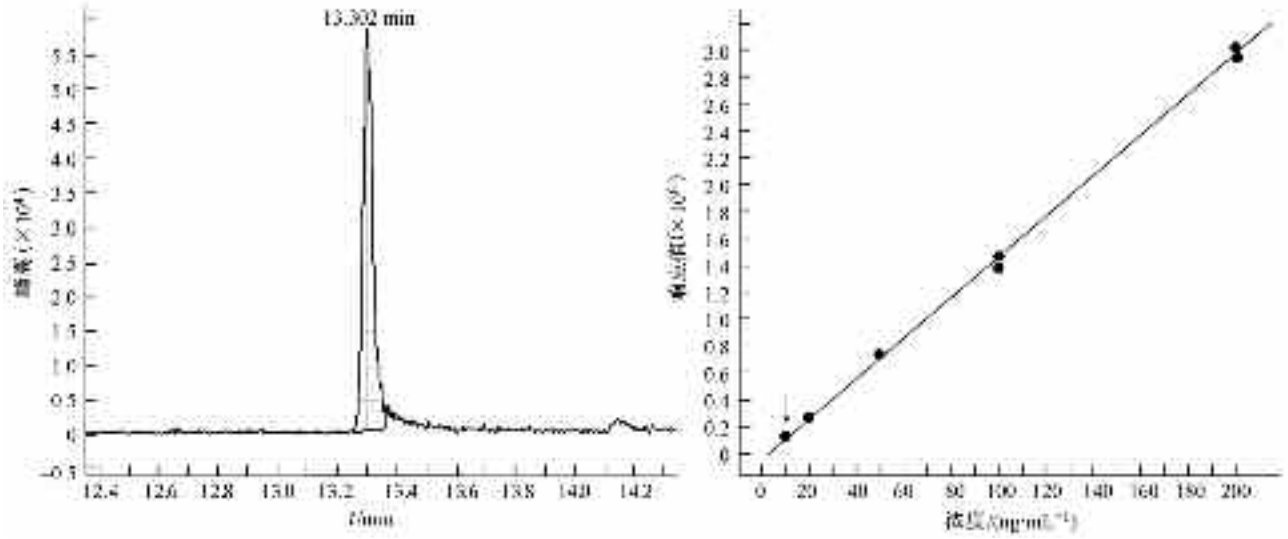

图 2.　　大葱当中敌稗基质匹配的标准曲线

为了考察 7200 在全扫描模式下的灵敏度，选择最低添加水平 (10.0 ng • mL^{-1}) 结果计算所有农药的信噪比，所有农药的 S/N 都大于 3。表 2 列出了部分农药的线性相关系数及信噪比结。

表 2.　　部分农药标准曲线相关系数及信噪比

农药名称	碎片离子精确质量数	R^2	信噪比	农药名称	碎片离子精确质量数	R^2	信噪比
四氯硝基苯	200.8824	0.991	156.55	腐霉利	283.0161	0.998	21.76
氯苯胺灵	152.9976	0.995	17.8	氯丹	405.7972	0.994	5.38
戊炔草胺	172.9555	0.993	22.9	氟酰胺	173.0209	0.991	29.73
莠去津	200.0697	0.998	27.59	p,p′-DDE	315.9375	0.999	101.25
西玛津	201.0776	0.992	21.04	o,p′-DDT	235.0076	0.993	63.66
野麦畏	268.0324	0.999	32.86	o,p′-DDD	235.0076	0.993	61.63
gamma-六六六	180.9373	0.996	170.07	三氯杀螨砜	158.9666	0.992	22.37
delta-六六六	180.9373	0.998	46.18	氯苯嘧啶醇	138.9945	0.985	7.46
敌稗	160.9794	0.999	63.39	哒螨灵	147.1168	0.997	21.72
异丙甲草胺	162.1277	0.994	43.16	醚菊酯	163.1117	0.99	25.13

根据 EU 法规对农药残留检测的要求，高分辨质谱需要至少两个精确质量数碎片才能对目标化合物进行确认。图 3 显示的是在 10.0 ng • mL^{-1} 浓度水平下部分农药的两个精确质量数的 EIC 重叠结果。可以看出即使浓度很低，但是仍能很容易对农药进行准确的定性分析。

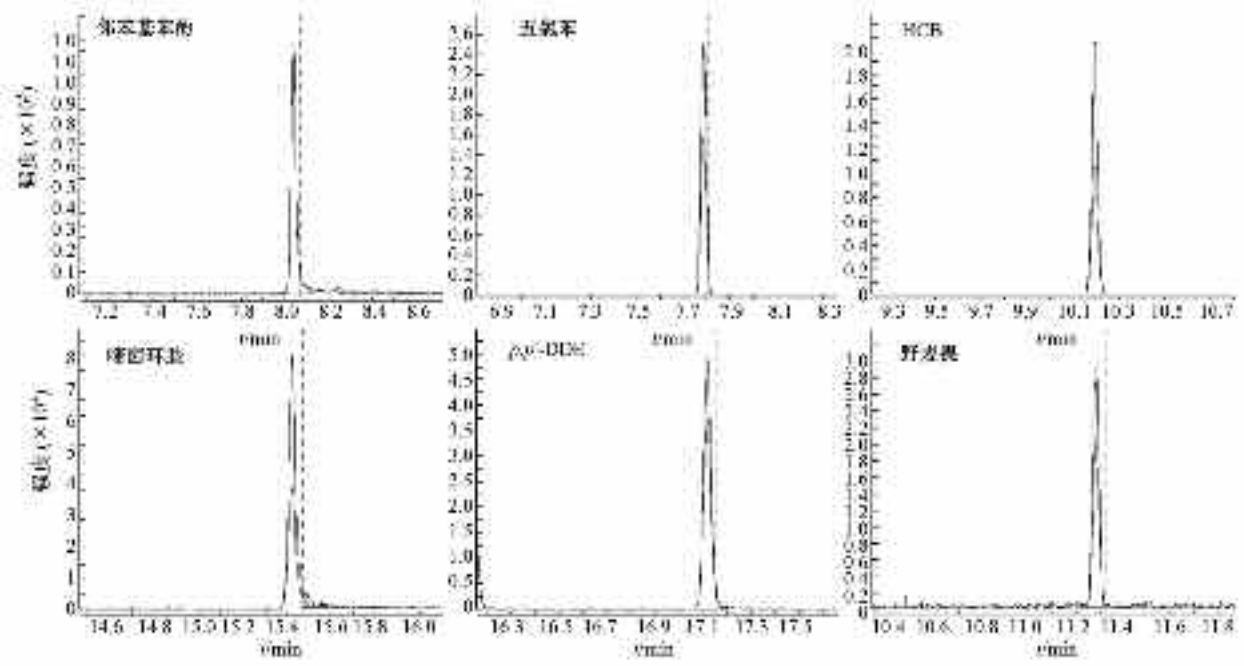

图 3.　　在 10.0 ng • mL^{-1} 浓度水平下部分农药的两个精确质量数的 EIC 重叠结果

MS/MS 选择性及精确质量采集

一些基质非常复杂的样品，或者由于某种原因，样品的前处理步骤比较简单，都会导致大量高浓度离子碎片进入到质谱检测器当中。如果这些碎片的保留时间和质荷比与被检测的目标化合物非常接近，单纯的 TOF 工作模式也不能满足检测的需要，此时可以使用 Q-TOF 模式，首先用低分辨四极杆选择性地只让某一种碎片离子通过，在碰撞池碎裂后，再进入 TOF 进行高分辨条件下精确质量数的采集。这样可以有效排除干扰问题。下图当中 Atrazine 在离子提取窗口为 20 ppm 时，旁边仍然有干扰离子出现。采用 Q-TOF 模式进行检测，则可以得到非常干净的结果。

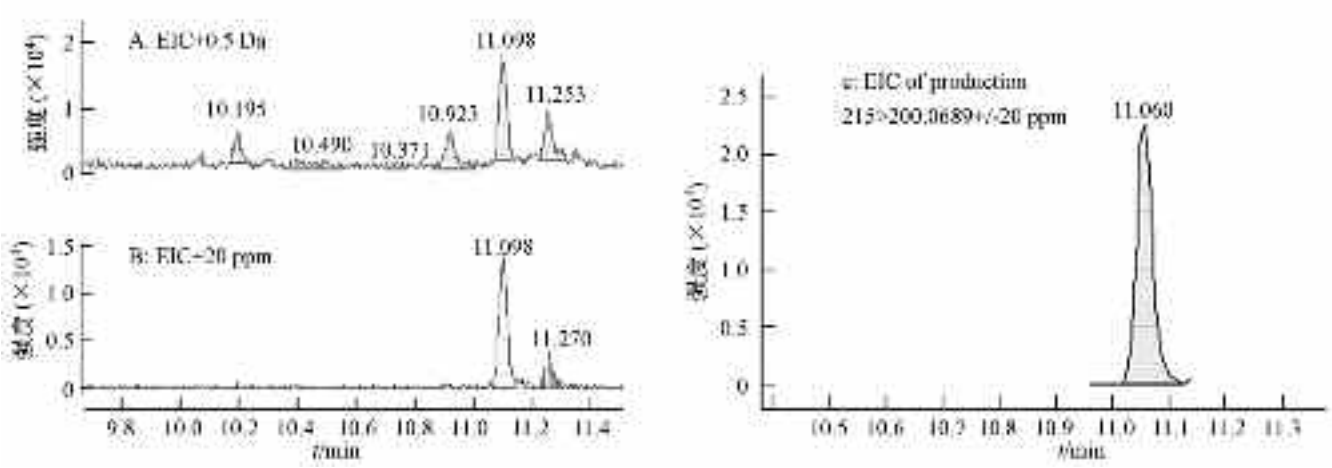

图 4.　TOF 模式下 10.0 ng • mL^{-1} Atrazine 在不同提取窗口范围时 EIC 结果
A：m/z (215.0932 ± 0.50) Da；B：m/z (215.0932 ± 20) ppm；
C：MS/MS 模式下以 m/z 215 为母离子，做子离子扫描得到的 EIC 结果 (215 > (200.0689 ± 20) ppm)

结论

(1) 凭借高分辨和出色的离子碎片精确质量数采集能力，7200 Q-TOF GC/MS 在面对类似大葱这样复杂样品当中农药残留任务时表现出了高灵敏度和高准确性的特点。

(2) 7200 在高分辨条件下的长期工作稳定性会极大方便用户的日常使用。

(3) Q-TOF 两种工作模式可以确保用户面对不同检测状况采取不同的检测方法，取得同样高可靠性的实验结。

ASMS 2012

M 486

Structural Elucidation and Predictive Model Generation of Oliver Oil Classification using a GC/Q-TOF MS and Multivariate Analysis

Stephan Baumann and Sofia Aronova

Agilent Technologies, Santa Clara, CA

Overview

A model was constructed to predicts whether an olive oil would pass the extra virgin sensory test. Running a GC/Q-TOF MS in both electron impact (EI) and positive chemical ionization (PCI) modes identified a large number of compounds in olive oil. Multivariate software was then used to perform statistical analysis and construct a classification model utilizing the presence of five specific compounds to accurately predict whether an olive oil would fail the sensory test.

Introduction

The demand for olive oil is growing rapidly in the United States. The US market is expected to surpass $1.8 billion by 2013. The International Olive Council (IOC) and USDA have established standards for the classification of extra virgin olive oil (EVOO), including a sensory test conducted by a tasting panel, as well as chemical tests. However, recent studies have stated that imported olive oils, which account for 99% of the EVOO on the US market, often fail the sensory test for EVOO classification. Multivariate software can be used to model olive oil classification and a GC/Q-TOF can be used to determine the identity of markers that correlate with a failed sensory test.

In this experiment we demonstrated that untargeted compound analysis done on an accurate mass GC/Q-TOF could be used with an EI spectral library to help identify markers that correlate with a failed sensory test. We also showed that orthogonal techniques such as positive chemical ionization could be used to collaborate the EI identifications.

Experimental

Sample Preparation Procedure

Ten olive oil samples were obtained from the UC Davis Olive Center. All of these samples had been subjected to IOC sensory test using a panel sanctioned by the IOC to determine if they passed or failed the criteria for EVOO. The samples were stored in the dark at room temperature. The samples were diluted 1:10 in cyclohexane and injected into the GC/Q-TOF with a 1:10 split. The results were evaluated using multivariate analysis and a model was developed that accurately predicted if an EVOO would fail the sensory test. Representative samples were then analyzed in PCI and EI Product Ion Scan modes to aid in Structural Elucidation.

Experimental

Figure 1: 7890 GC / 7200 Q-TOF instrumentation.

GC Run Conditions	
Column	DB-5 MS, 30 meter, 0.25 mm ID, 0.25 µm film (P/N 122-5532)
Injection volume	1 µL
MMI Injector	50 °C for 0.01 min 600 °C/min to 300°C
Purge to split vent	80 mL/min at 1 minute
Oven Temperature Program	45 °C for 4.25 min 5 °C/min to 75 °C, 0 min hold 10 °C/min to 320 °C, 10 min hold
Carrier gas	Helium at 1.3mL/min constant flow
Transfer line temperature	290 °C
MS Conditions	
Ionization mode	EI, positive CI (20 % methane flow)
Source temperature	230°C
Quadrupole temperature	150°C
m/z scan	40 to 800 m/z
Spectra acquisition rate	5 Hz, collecting both in scan and profile modes

Table 1: A cold splitless injection was used to minimize thermal decomposition.

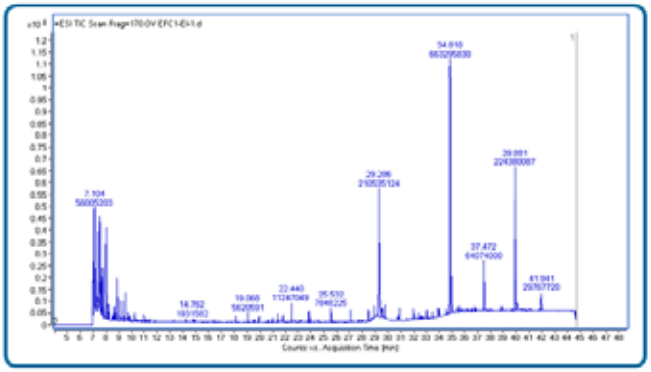

Figure 2: Typically, about 150 peaks are identified by chromatographic deconvolution with a relative area filter of 0.1% of largest peak.

Results and Discussion

Statistical Evaluation

Mass Profiler Professional (MPP) was used for statistical evaluation of the data. This software provides the possibility of using a guided workflow that helps the user evaluate the analytical data. The guided approach efficiently reduces the data set from 442 components to five statistically relevant compounds in a few steps. The steps were as follows:

1. Define the experiment type, workflow, and organism.
2. Select the data source as MassHunter Qual.
3. Import CEF files from MassHunter Qual.
4. Set abundance and model ion filters.
5. Define retention and match factor alignment parameters. (Total Compounds: 442)
6. Select internal, external, or no calibration.
7. Choose baseline correction.
8. Set condition filter flags. (Total Compounds: 91)
9. Filter based on Volcano Plot. This combines the Student's t-test for significance ($p < 0.05$) with fold change threshold = 4. (Total Compounds: 5)

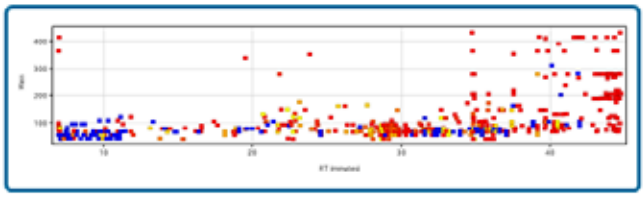

Figure 3: This mass vs. retention time plot shows that 442 unique compounds were distinguished by chromatographic deconvolution, most of which occurred only once or twice and were filtered out by MPP. The low frequency components are shown in red while the higher frequency components are shown in blue.

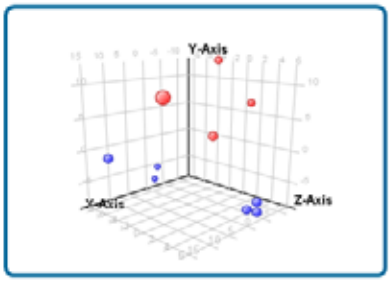

Figure 4: Principal Component Analysis (PCA) shows how data clusters. The samples that failed the sensory test are marked in red and the ones that passed are blue.

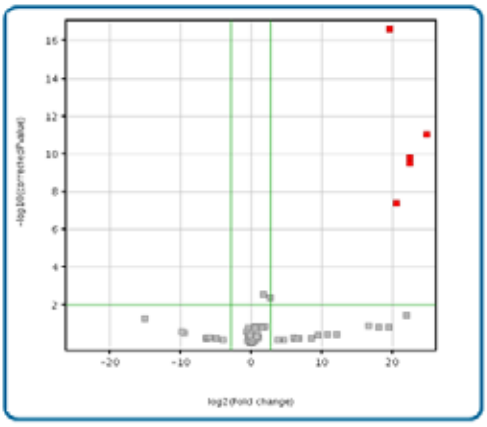

Figure 5: The Volcano Plot shows fold-change for each entity on the x-axis and significance on the y-axis. The five compounds in the upper right hand corner are accumulated in the samples that failed the sensory test.

Class Prediction

Through multivariate analysis we identified five compounds that correlated with a failed sensory test; the next step was to build a class prediction model that could be run independently of MPP. To do this we had to train the model with the data.

There are several classification models that can be applied however Partial Least Square (PLS) analysis is particularly adapted to situations where there are fewer observations (i.e. number of samples) than measured variables (e.g. detected entities, *m/z*). Its use has become very popular due to its ability to deal with many correlated and noisy variables. Therefore, PLSDA was used to construct the olive oil classification model.

Identifier	Training	Predicted(Training)	Confidence
CSCI-E1: lg2	[F, Training]	[F, Training]	1.000
FSW2-E1: lg2	[F, Training]	[F, Training]	1.000
ESCI-E1: lg2	[P, Training]	[P, Training]	1.000
ESC2-E1: lg2	[P, Training]	[P, Training]	1.000

Table 2: PLSD training set which contains representatives from each of the three clusters found in the PCA plot.

We can see in table three that a small data set such as this one is capable of identifying lower grade olive oil being misclassified as EVOO, a larger model could also determine if an olive oil has any of the characteristic compounds related to 'fusty', rancid, musty or vinegary flavor notes.

Results and Discussion

Identifier	Grade	Training	Predicted (Class Prediction)	Confidence
PAC1-EI: Ig2	F	None	[F, Training]	1.000
ESC2-EI: Ig2	P	Training	[P, Training]	1.000
ESCI-E1: Ig2	P	Training	[P, Training]	1.000
SAC1-EI: Ig2	F	None	[F, Training]	1.000
RFC2-EI: Ig2	P	None	[P, Training]	1.000
RSA2-EI: Ig2	P	None	[P, Training]	1.000
CSC1-EI: Ig2	F	Training	[F, Training]	1.000
RSA1-EI: Ig2	P	Training	[P, Training]	1.000
EFC1-EI: Ig2	P	None	[P, Training]	1.000
FSW2-EI: Ig2	F	Training	[F, Training]	1.000

Table 3: The model correctly predicted the pass or fail status of all samples, including those not used to construct the model. The samples that were not used for building the prediction model are listed with the Training variable set as 'None'.

Compound Identification/Structure Elucidation

While it is not necessary to know the identity of the compounds used in the classification model, identification could lead to an understanding of the mechanism by which those chemical components might adversely affect the sensory qualities of olive oil. The advantage of the 7200 GC/Q-TOF is that it can collect data in EI, CI, and Product Ion Scan modes. These orthogonal modes of operation aid confirmation. EI spectra allow library searching and provide fragmentation data, CI provides information about the empirical formula, and Product Ion Scan MS/MS generates data for an accurate mass substructure search that can be applied to EI or CI generated ions.

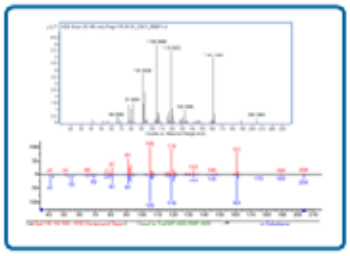

Figure 6: Commercial unit mass EI spectral libraries like Wiley and NIST can be searched using accurate mass EI GC/Q-TOF data to identify compounds.

As we see in Figure 7, the Molecular Structure Correlator (MSC) performs a substructure search of the ChemSpider database using MS/MS product ion scan data. MSC correlates the product ion scan results to all the possible structural isomers. Each individual fragment ion is ranked based on mass error corresponding to the proposed formula, along with a penalty based on how many bonds needed to be broken to generate that proposed formula. An isomer's individual compatibility score is a weighted average of the fragment ion scores, taking into account the intensity and the mass of each fragment ion.

Figure 7: MSC performs a ChemSpider substructure search on the product ion scan fragments of ethyl octadecanoate's molecular ion peak and generates a compatibility score. Note that this substructure is equally compatible with eicosanoic acid as to ethyl octadecanoate. The EI fragmentation pattern is what allows us to distinguish between structural isomers.

Exact Mass

NIST ID	Formula	EI[M*]+ Measured	Mass Error (PPM)	PCI [M+H]+ Measured	Mass Error (PPM)
n-Hexadecanoic acid	$C_{16}H_{32}O_2$	256.2385	4.7	257.2470	1.9
Octadecanoic acid, ethyl ester	$C_{20}H_{40}O_2$	312.3008	4.8	313.3091	3.2
Squalene	$C_{30}H_{50}$	410.39037	0.8	411.3987	0.5
α-Cubebene	$C_{15}H_{24}$	204.1883	4.9	205.1945	2.9

Table 4: PCI spectral data provided confirmatory accurate mass information for molecular ions of the four up-regulated compounds that had molecular ion peaks and were identified through EI library searching.

Conclusions

Using accurate mass EI and positive CI scan data generated by a GC/Q-TOF system, a model can be constructed that accurately predicts whether an olive oil will pass the EVOO sensory test. Although a study constructed using a very small sample set generates an incomplete model, it demonstrates the feasibility of the approach. A predictive model constructed using a significantly larger sample size would give olive oil producers a quick determination as to whether their oil would fail the sensory test and the defects present.

Structure elucidation of four of the model compounds was accomplished by EI library searching combined with Molecular Formula Generation, Isotopic Pattern Filtering, and Molecular Structure Correlation.

ASMS 2012

Th 600

Negative Chemical Ionization and Accurate Mass −A Novel Approach to the Analysis of Pesticides by GC/Q-TOF

Moritz Hebestreit, Jörg Riener, Bernhard Rothweiler

Agilent Technologies, Waldbronn, Germany

Introduction

Abstract

Analysis of pesticide residues in feed and food is an ongoing challenge. Especially in "QuEChERS-times", highly selective methods are obligatory to eliminate matrix interferences. GC/MS with high mass accuracy and full scan acquisition opens up the possibility of highly selective determination of a theoretically unlimited number of compounds. Negative chemical ionization is adding additional selectivity and increases the molecular ion response for lower detection limits than electron impact or positive chemical ionization for dedicated pesticides like halogenated pyrethroides.
We present preliminary data for the analysis of γ-BHC, γ-chlordane, α-chlordane and trans-nonachlor in various food matrices.

Experimental

Standards

Calibration solutions of γ-BHC, γ-chlordane, α-chlordane and trans-nonachlor were prepared in ethyl acetate at 20 fg/µL (ppt), 50 fg/µL, 100 fg/µL, 200 fg/µL, 500 fg/µL, 1000 fg/µL, 2000 fg/µL and 5000 fg/µL. Calibration curves were generated from 20 fg/µL to 1000 fg/µL.

Samples

Food samples were prepared by Eurofins Food Testing UK Limited using a QuEChERS-like method to yield 1 g/mL matrix in acetonitrile. The following matrices were provided:
a) Parsley b) Mint c) Tomato d) Grapes e) Brussel Sprouts f) Kale g) Swede h) Orange i) Cucumber j) Sage
Aliquots of each 90 µL of the extracts were spiked with 10 µL of calibration solutions to yield concentrations of 50 fg/µL, 100 fg/µL, 200 fg/µL and 500 fg/µL.

GC/MS System

The GC and MS configurations and conditions were as shown in Table 1. To ensure mass accuracy, recalibration of the TOF was performed automatically within the sequence. No further mass correction was applied.

Data Analysis

Agilent MassHunter Qualitative and Quantitative Analysis were used. γ-Chlordane, α-chlordane and trans-nonachlor showed molecular ions. For γ-BHC, the most abundant ion is the chlorine fragment. Quantifier ions are listed in table 2. At least two further ions served as qualifiers (not shown). Quantitative Analysis was performed with extraction windows of ± 50 ppm.

Experimental

Gas chromatograph	Agilent 7890A
Inlet	Air cooled multimode inlet (MMI), equipped with an ultrainert splitless liner with glass wool
Columns	Two 15.0 m x 0.25 mm ID x 0.25 µm HP-5MS Ultra Inert were connected to the MS via a pressure controlled tee.
Carrier gas	Helium
Carrier gas mode	Constant flow
Column flows	1.25 mL/min (col. 1) and 1.45 mL/min (col. 2) (retention time locked to chlorpyriphos methyl at 18.111 min)
Autosampler	Agilent 7693A
Injection mode	Cold splitless, purge flow 50.0 mL/min at 2.0 min
MMI Temperature program	70 °C (0.02 min), 600 °C/min to 300 °C (1 min), 100 °C/min to 280 °C Backflush: 280 °C
Injection volume	1.0 µL
Oven program	60 °C (1 min), 40 °C/min to 120 °C, 5 °C/min to 285 °C
Backflush conditions	Post run, 2.4 min, oven 280 °C, 40 psi at pressure controlled tee, inlet 1 psi
Transfer line	280 °C
Mass spectrometer	Agilent 7200 Q-TOF
Ionization	Negative chemical ionization (NCI)
Reactant gas	Methane at 40% (2 mL/min)
Source temperature	150 °C
Quadrupole temperature	150 °C
Quadrupole mode	Total ion transmission, cutoff at m/z 50
Collision gas	Nitrogen @ 1.5 mL/min
Scan range	m/z 65 to 600
Acquisition rate	5 Hz
Acquisition mode	2 GHz dual gain

Table 1. GC/MS Conditions

Compound	Chemical Formulae of Ions used for Quantification	Exact Mass (Da)
γ-BHC	$[^{35}Cl_2]^{\cdot-} = [M\text{-}C_6H_6Cl_4]^{\cdot}$	69.93825
γ-Chlordane	$[C_{10}H_6{}^{35}Cl_6{}^{37}Cl_2]^{\cdot-} = [M+4]^{\cdot}$	409.79242
α-Chlordane	$[C_{10}H_6{}^{35}Cl_6{}^{37}Cl_2]^{\cdot-} = [M+4]^{\cdot}$	409.79242
trans-Nonachlor	$[C_{10}H_5{}^{35}Cl_8{}^{37}Cl]^{\cdot-} = [M+2]^{\cdot-}$	441.75640

Table 2. Chemical formulae and exact masses of quantifier ions; chlorine isotopes are indicated

Results and Discussion

Calibration Solutions

All compounds were detectable at the lowest calibration level and showed linear responses.

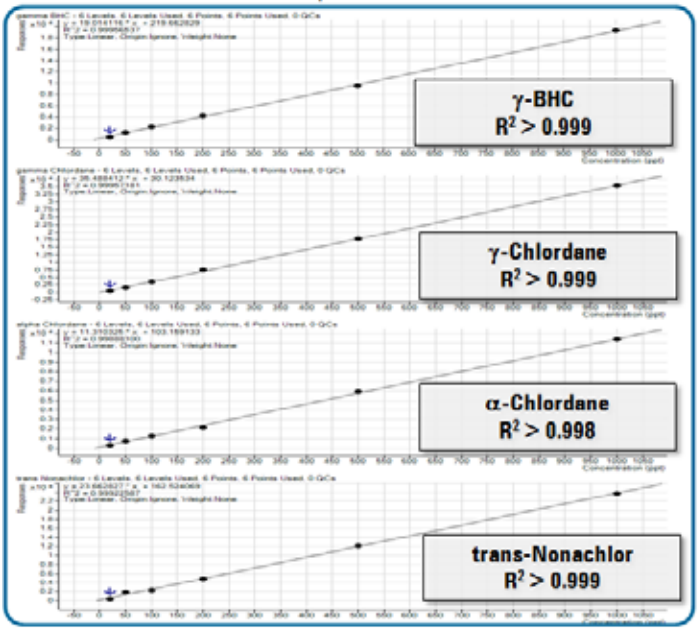

Figure 1. Calibration curves of target compounds

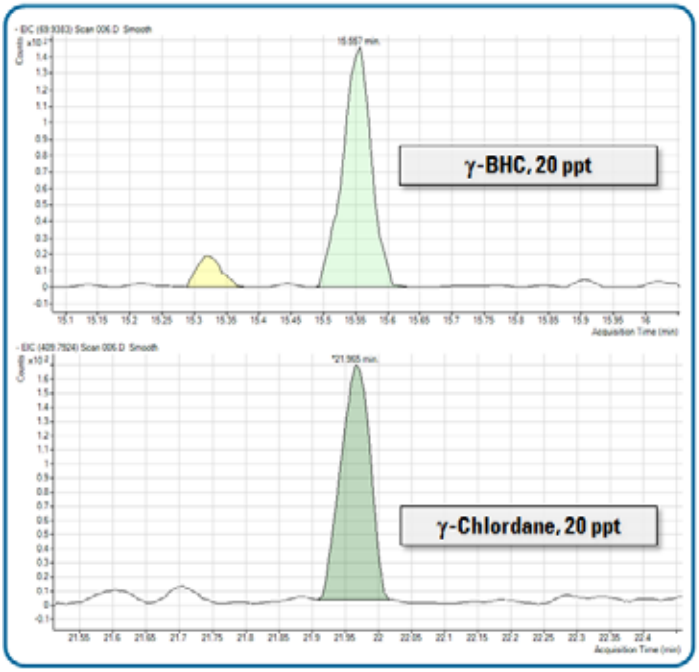

Figure 2. Quantifier response of γ-BHC and γ-chlordane at 20 fg/µL (i.e. lowest calibration level)

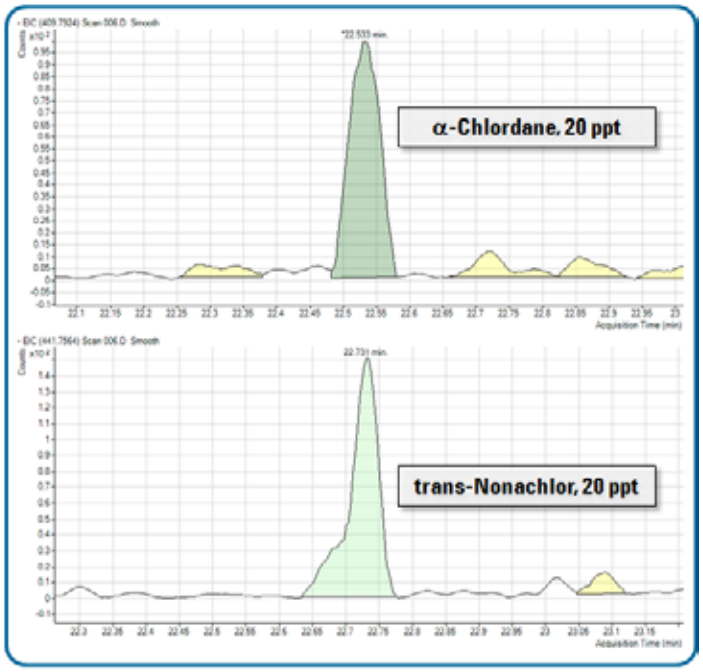

Figure 3. Quantifier response of α-chlordane and trans-nonachlor at 20 fg/µL

Samples

The quantifier ions with extraction windows of ± 50 ppm were sufficiently selective in all matrices. All targets could be detected at the lowest spiked level (50 ppt) and higher, except of γ-chlordane and α-chlordane in parsley as well as γ-BHC in mint. γ-Chlordane and α-chlordane in parsley as well as γ-BHC in mint were detectable at 100 ppt or higher. S/N ratios (peak to peak) at the lowest detectable levels are shown in table 3.

Matrix	γ-BHC	γ-Chlordane	α-Chlordane	trans-Nonachlor
Parsley	6*	7 (100 ppt)	48 (100 ppt)	4
Mint	63 (100 ppt)	61	69	7
Tomato	64	133	46	73
Grapes	6	130	49	85
Brussel Sprouts	37*	133	27	92
Kale	82*	124	45	78
Swede	62*	188	63	149
Orange	23	47	70	28
Cucumber	38	207*	60	73
Sage	4	72	46	7

* Very low residues already detectable in unspiked sample

Table 3. S/N ratios (peak to peak) in matrix at 50 ppt if not indicated differently

Results and Discussion

Mass Accuracy

The following figures illustrate obtained mass accuracy of the quantifier ions at different concentrations in the calibration solutions and in the matrices.
No post-acquisitional recalibration was applied.

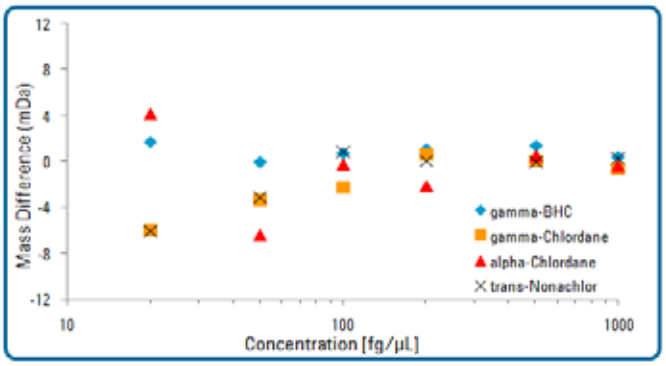

Figure 4. Mass difference of measured mass minus exact mass vs. concentration in calibration solutions

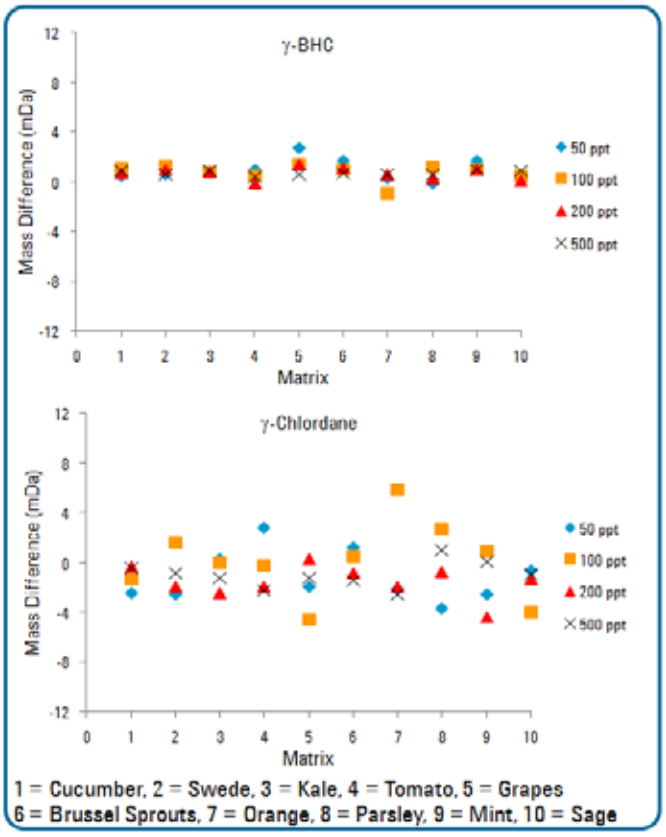

Figure 5a. Mass difference of measured mass minus exact mass of γ-BHC (top) and γ-chlordane (bottom) in the ten different matrices

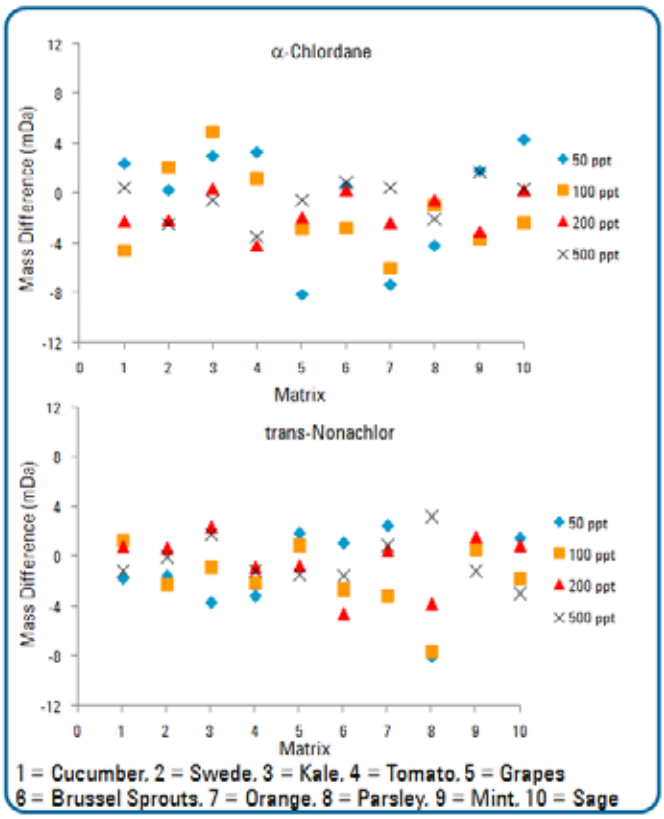

Figure 5b. Mass difference of measured mass minus exact mass of α-chlordane (top) and trans-nonachlor (bottom) in the ten different matrices

Fig. 4 shows the influence of the concentration on mass accuracy. At low ion counts, higher errors are most probably due to the ion statistics. At higher concentrations, mass accuracy is stable for all ions (-0.03 mDa ± 0.46 mDa (n = 4) at 1 ppb for the four different quantifier ions).
Figures 5a and 5b illustrate mass accuracy depending on the matrix. Mass differences are within few mDa in all matrices at all spiked levels. As expected, mass accuracy in matrix is better at higher levels (-0.25 mDa ± 1.44 mDa (n = 40) at 500 ppt for all quantifiers in all matrices).

Conclusions

The results of this preliminary study let us confirm, that negative chemical ionization combined with high mass accuracy and sufficient resolving power can provide excellent selectivity and sensitivity for organochlorine pesticides regarding GC/MS analyses.

Acknowledgements

The authors would like to gratefully acknowledge Jonathan Horner from Eurofins Food Testing UK Limited for providing the QuEChERS extracts used for this study.

ASMS 2012

Th 602

Dissecting the Mechanism of Antifungal Drug Action by GC/Q-TOF

[1]Sofia Aronova, [1]Stephan Baumann, [2]Manhong Wu, [3]Bob St. Onge, [3]Sundari Suresh, [3]Ron Davis and [2]Gary Peltz

[1]Agilent Technologies, Santa Clara, CA, Stanford University Departments of [2]Anesthesia, School of Medicine and [3]Biochemistry and Genome Technology Center

Overview

Metabolic profiling of yeast sterols was performed to precisely determine enzymatic targets for new potential antifungal drugs. Targeted analysis of the relative levels of ergosterol biosynthesis pathway intermediates was combined with an untargeted approach, empowered by accurate mass high resolution GC/Q-TOF technology, to obtain the most comprehensive results. Full scan electron ionization (EI) spectral information was complemented with MS/MS accurate mass product ion scan data to confirm the identity of the compounds accumulated in yeast as a result of drug treatment.

Introduction

Budding yeast *Saccharomyces cerevisiae* is widely used as a model genetic organism because of its simplicity and availability of strains with individual deletions in all of the genes in its genome. To evaluate new antifungal agents that target a key component of yeast membrane – ergosterol – complementary genetic and analytical approaches were utilized. As a first-tier high throughput approach HaploInsufficiency Profiling (HIP) screening was performed. HIP involves the growth of gene-depleted yeast against a drug where resulting sensitivity of the strain suggests that the enzyme product of heterozygous locus is being a target of the inhibitor. Furthermore, an analytical approach involving accurate mass high resolution GC/Q-TOF metabolic profiling of yeast sterols was used to specifically identify enzymatic targets of the potential drugs.

Based on the relative levels of targeted intermediates of the ergosterol biosynthesis pathway as well as accumulated untargeted metabolites in drug-treated *versus* untreated samples, the mechanisms of several potential antifungal therapeutic agents affecting sterol metabolism in yeast were proposed. In addition, the MS/MS accurate mass product ion spectra were used in conjunction with the Molecular Structure Correlator (MCS) tool for structural confirmation of some of the accumulated metabolites.

Experimental

Sample Preparation

Wild type yeast cultures (strain BY4743) were incubated with drug concentrations that inhibited growth by 10%. Yeast lipids were extracted by the Folch method (Folch et al., *J Biol Chem*, 1957, 226, 497). The lower chloroform aliquots were dried by speed vacuum, and the

Experimental

active functional groups were derivatized with 40 mg/mL hydroxyamine hydrochloride in pyridine followed by silylation using MSTFA + 1 % TMCS, prior to analysis by Agilent 7200 series GC/Q-TOF.

Analytical Conditions

This study was performed using an Agilent 7890 GC coupled to an Agilent 7200 series Quadrupole-Time-of-Flight (Figure 1). GC and MS conditions are described in Table 1.

Figure 1. 7200 series GC/Q-TOF system.

GC and MS Conditions:	
Column	HP-5 MS UI, 30 meter, 0.25 mm ID, 0.25 µm film
Injection volume	1 µL
Split ratio	20:1
Split/Splitless inlet temperature	250 °C
Oven temperature program	60 °C for 1 min 10 °C/min to 325 °C, 3.5 min hold
Carrier gas	Helium at 1 mL/min constant flow
Transfer line temperature	280 °C
Ionization mode	EI
Source temperature	230°C
Quadrupole temperature	150°C
Scan range	50 to 600 m/z
Spectral acquisition rate	5 Hz, collecting both in centroid and profile modes

Table 1. GC-MS conditions used in the study.

Data Processing

The chromatographic deconvolution was performed using MassHunter Unknowns Analysis software. Metabolites of interest were identified by comparison with the NIST11 mass spectral library. The multivariate software package Mass Profiler Professional (MPP) was used to determine compounds present at distinct levels in drug-treated *vs* untreated samples. Quantitation was performed using MassHunter Quantitative software B.05.

Results and Discussion

Proof of Concept

At the first stage of this study the analytical approach utilizing GC/Q-TOF was validated using two well-described antifungal drugs followed by the examination of novel drugs with potential therapeutic properties. Both Terbinafine and Fluconazole are widely used antifungal drugs that target distinct steps in the ergosterol biosynthesis pathway and whose mechanisms of yeast sterol pathway inhibition are well understood. Terbinafine inhibits the ERG1 gene product, squalene epoxidase, thus preventing the conversion of squalene to the next intermediate of the pathway. Therefore, squalene accumulation and depletion of downstream intermediates of the pathway is an expected outcome in this case. Data obtained by GC/Q-TOF were consistent with this expectation (Figure 2).

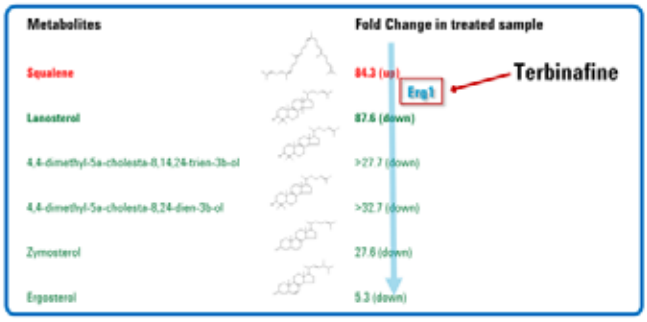

Figure 2. Squalene accumulation was observed in yeast treated with Terbinafine as compared to untreated control. The numbers represent fold change.

Similarly, in the case of an azole antifungal agent Fluconazole, that inhibits ERG11 gene product, the cytochrome P450 14α-demethylase, or lanosterol demethylase, accumulation of lanosterol is expected.

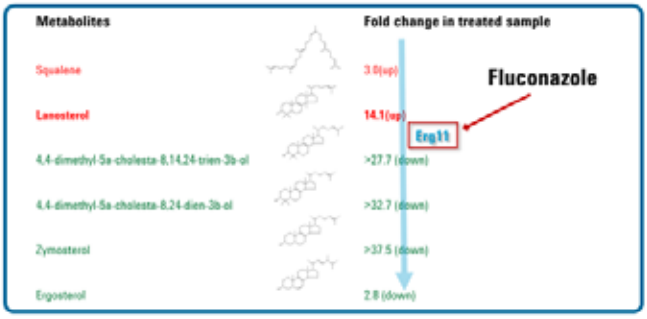

Figure 3. Significant accumulation of lanosterol as well as depletion of several targeted downstream metabolites was observed following Fluconazole treatment.

Unexpected Observation Revealed by Untargeted Approach

In addition to accumulation of lanosterol and depletion of other targeted downstream metabolites (Figure 3), untargeted approach revealed a buildup of several 14α-methyl sterols that are not usually detected in yeast (Table 2).

Component (m/z @ RT)	Compound	Formula	MI of Derivatized Species (m/z)	Accurate Mass of MI (m/z)	Mass Error (ppm)
469 @ 28.08	14α-desmethyl episterol	$C_{29}H_{48}O$	484.4095	484.4101	1.24
379 @ 28.26	14α-desmethyl 4α-methyl zymosterol	$C_{29}H_{48}O$	484.4095	484.4107	2.48
487 @ 28.39	14α-desmethyl 3-keto-4-methylzymosterol	$C_{29}H_{46}O$	482.3938	482.3931	-1.45

RT – Retention Time
MI – Molecular Ion

Table 2. Results of Untargeted Analysis of Fluconazole Treatment.

The empirical formulas of the accumulated 14α-methyl sterols were determined based on EI fragmentation spectra and accurate mass information. Accumulation of 14α-methyl sterols suggested that some of the downstream enzymes in the ergosterol biosynthesis pathway are rather "promiscuous" and are able to utilize sterols with an extra methyl group as their substrates.

Metabolic Profiling for Characterization of Potential Antifungal Drugs

A few potential inhibitors of ergosterol biosynthesis pathway such as Totarol and New Chemical Entity (NCE) 1181-0519 were evaluated. Statistical analysis performed in MPP helped to easily identify specific steps of the pathway affected by a drug. In the case of NCE 1181-0519 only 4,4-dimethyl-8,24-cholestadienol met the significance criteria for a biologically significant fold-change (Figure 4). When taking into account downregulation of the downstream intermediates (Figure 5), the results strongly suggested that the NCE specifically inhibited Erg25.

Totarol treatment resulted in the accumulation of another sterol, 4α-carboxy-4β-methyl-5α-cholesta-8,24-dienol, suggesting Erg26 being a specific target of Totarol (Figure 6). This sterol was not originally targeted since it is a biologically unstable intermediate present only at trace levels and was revealed only in an untargeted approach.

Results and Discussion

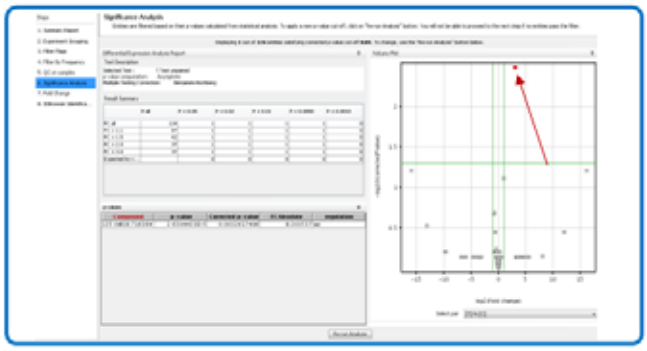

Figure 4. Significance analysis performed in MPP shows that only one compound (4,4-dimethyl-8,24-cholestadienol) is accumulated in response to treatment with NCE 1181-0519.

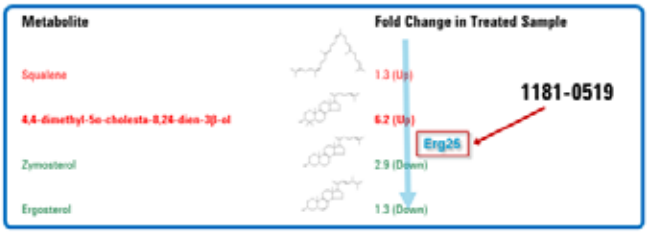

Figure 5. Significant accumulation of 4,4-dimethyl-8,24-cholestadienol as well as downregulation of downstream metabolites in response to treatment with NCE 1181-0519 strongly suggest Erg25 as its target.

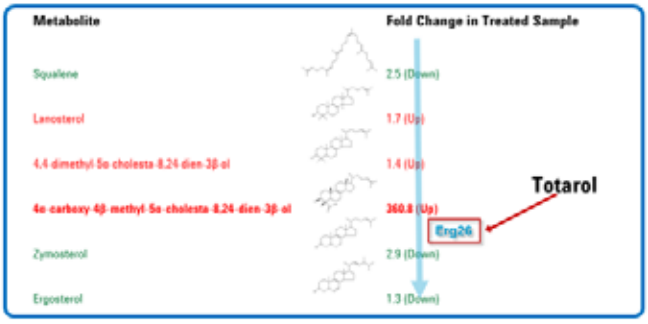

Figure 6. Buildup of 4α-carboxy-4β-methyl-5α-cholesta-8,24-dienol is consistent with Erg26 being the specific target for Totarol.

The structure of 4α-carboxy-4β-methyl-5α-cholesta-8,24-dienol was confirmed using accurate mass product ion spectra information (Figure 7) since NIST library spectrum is not available for this compound.

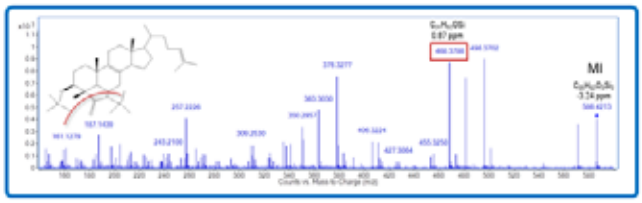

Figure 7. MS/MS product ion spectrum helps to confirm the structure of one of the compounds identified by untargeted approach, 4α-carboxy-4β-methyl-5α-cholesta-8,24-dienol.

Molecular Structure Correlator (MSC) was further used to predict the substructures of the resulting MS/MS fragments and evaluate best candidate structures of accumulated compounds (Figure 8).

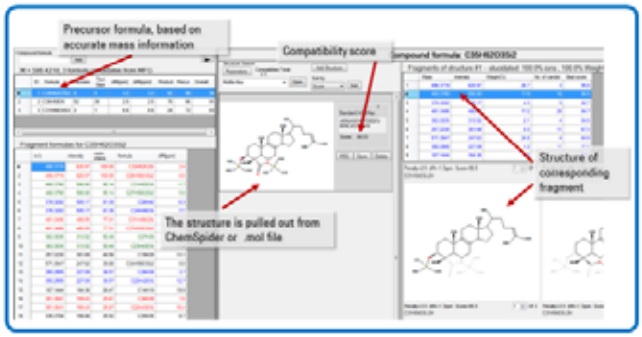

Figure 8. MCS helps to assign formulas to each accurate mass fragment from product ion scan. Compounds structures are extracted from ChemSpider database or from *.mol* file to visualize fragmentation and provide the score that reflects the probability of each fragment structure being formed. Finally, it assigns a compatibility score to each possible compound structure.

Conclusions

Metabolic profiling of yeast sterols is a powerful approach for identifying enzymatic targets of antifungal drugs, and can be used in combination with HIP to elucidate the mechanism of drug inhibition in more details. The accurate mass information and full spectrum sensitivity of GC/Q-TOF enabled reliable identification of targets as well as unknown compounds that accumulated as a result of the treatments. The accumulation of several intermediates of yeast sterol biosynthesis pathway in drug treated *vs* untreated samples helped to elucidate the mechanisms of several potential antifungal agents including NCE 1181-0519 and Totarol.

Analytica Chimica Acta 757 (2012) 39–47

Contents lists available at SciVerse ScienceDirect

Analytica Chimica Acta

journal homepage: www.elsevier.com/locate/aca

Rapid simultaneous screening and identification of multiple pesticide residues in vegetables

Fang Zhang [a], Chongtian Yu [b], Wenwen Wang [b], Ruojing Fan [a], Zhixu Zhang [b], Yinlong Guo [a,*]

[a] Shanghai Mass Spectrometry Center, Shanghai Institute of Organic Chemistry, Chinese Academy of Sciences, Shanghai 200032, China
[b] Agilent Technologies (China) Co., Ltd., 140 Tianlin Road, Shanghai 200233, China

HIGHLIGHTS

- The method was set up for a universal screening of pesticide residues.
- The database included retention time, a single characteristic ion and a pair of ions.
- GC–QTOF MS as a new instrument system was applied due to its improving sensitivity and accuracy.
- Limit of identification of the database was at 5 ppb in this case and accurate mass errors less than 2.5 mDa.
- Thirteen pesticides were found in the vegetables (11 in celery, 9 in rape, 3 in scallion and 2 in spinach).

GRAPHICAL ABSTRACT

ARTICLE INFO

Article history:
Received 5 September 2012
Received in revised form 22 October 2012
Accepted 26 October 2012
Available online 2 November 2012

Keywords:
Pesticide residues
Database
Screening
Structural identification
Gas chromatography–quadrupole time-of-flight mass spectrometry (GC–QTOF MS)

ABSTRACT

A method for the rapid simultaneous screening and identification of multiple pesticide residues in vegetables was established using a novel database and gas chromatography in combination with hybrid quadrupole time-of-flight mass spectrometry (GC–QTOF MS). A total of 187 pesticides with different chemical species were measured by GC–QTOF MS to create the database, which collected the retention time and exact masses of ions from the first-stage mass spectrum (MS^1 spectrum) and second-stage mass spectrum (MS^2 spectrum) for each pesticide. The workflow of the created database consisted of "MS^1 screening" for possible pesticides by chemical formula match and "MS^2 identification" for structural confirmation of product ion by accurate mass measurement. To evaluate the applicability of the database, a spinach matrix was prepared by solid phase extraction, spiked with a mixture of 50 pesticides at seven concentrations between 0.1 and 10 ppb, and analyzed by GC–QTOF MS. It was found that all of the 50 pesticides with concentrations as low as 5 ppb were detected in the "MS^1 screening" step and accurate masses were identified with errors less than 2.5 mDa in the "MS^2 identification" step, indicating high sensitivity, accuracy, selectivity and specificity. Finally, to validate the applicability, the new method was applied to four fresh celery, rape, scallion and spinach vegetables from a local market. As a result, a total of 13 pesticides were found, with 11 in celery, 9 in rape, 3 in scallion and 2 in spinach. In conclusion, GC–QTOF MS combined with an exact mass database is one of the most efficient tools for the analysis of pesticide residues in vegetables.

1. Introduction

Agriculture in the world has changed greatly in the past 100 years. Many farmers pursue high yields by utilizing cheap energy,

* Corresponding author. Tel.: +86 021 54925300; fax: +86 021 54925314.
E-mail address: ylguo@sioc.ac.cn (Y. Guo).

0003-2670/$ – see front matter © 2012 Elsevier B.V. All rights reserved.
http://dx.doi.org/10.1016/j.aca.2012.10.048

plentiful water supplies, effective chemical fertilizers and pesticides. Pesticides achieve their intended control of pests; on the other hand, bring unintended and adverse impact to the health of humans and animals as well. For example, recent studies showed a link between heavy pesticidal use in rural areas and incidence of childhood leukemia [1–3]. The wide use of pesticides in agriculture contributes to environmental pollution, affecting land, water, and food products in particular. Some pesticide residues can survive foods and reach consumers, imposing a potential threat to human and animal health, even after the applied pesticides were thought to dissipate. Research reveals that prolonged exposure to pesticide residues may increase the risk of various cancers and neurological disorders, and impair the immune system [4–7]. The increased exposure to pesticide residues from food sources has caused serious concerns in food safety. The Pesticide Residues Committee, an independent organization established in many countries, has repeatedly advised the governments to establish a nationwide program monitoring pesticide residues in food and drink.

To monitor the pesticides residues left on the raw food products, many approaches have been taken using various analytical techniques including spectrophotometry [8], polarography [9], atomic absorption spectrometry [10], thin layer chromatography [11], isotopic tracer method [12], gas/liquid chromatography [13,14], and mass spectrometry [15] etc. At present, gas chromatography–mass spectrometry (GC–MS) and liquid chromatography–tandem mass spectrometry (LC–MS/MS) are the two most powerful techniques for multi-residue pesticides analyses [16–19]. For GC-amenable semi-volatile pesticides GC methods are still preferred over LC methods due to its higher resolution. With the rapid development of MS technique, gas chromatography–tandem mass spectrometry (GC–MS/MS) has been increasingly used to minimize signal interferences in complicated sample matrices. For examples, Tao et al. used a GC–ion trap mass spectrometer (GC–IT MS) and detected multi-residues of pesticides in vegetables [20]. Salquebre et al. used a GC–triple quadrupole mass spectrometer (GC–TQ MS) and detected 22 pesticidal residues in human hair [21].

Although many approaches have been successfully taken for the analysis of pesticides in food or other matrices [19,22–25], accurate and reliable improvement for high-throughput applications of untargeted residue remains an elusive goal. A method featured with higher accuracy, resolution, and detection sensitivity as well as fast speed is being explored for monitoring multi-residues of pesticide residues, especially the banned or severely restricted poisonous pesticide residues even in trace amounts and complicated matrices. The application of single-stage quadrupole MS or IT MS is limited because of the low resolution and disturbances by the high matrix burden and co-eluting peaks. By using TQ MS or more preferably TQ-linear ion-trap mass spectrometer, the low scan speed and the minimum dwell times for each multi-reaction monitoring transition limit the number of substances in one measurement cycle. GC coupled with tandem high-resolution QTOF MS is a powerful analytical tool for the identification of unknown compounds and provides increased selectivity for the determination of target compounds, even when they are nested in complicated sample matrices. Compared with other traditional tandem MS (TQ MS) or high-resolution MS (TOF MS), the elevated mass resolution of QTOF MS enables the performance of the extracted ion chromatograms using narrow mass windows and measure of the characteristics ions at accurate mass seen in MS^1 and MS^2 spectra. Such narrow mass windows lead to a remarkable improvement of sensitivity due to the decrease of the background noise and the improvement of the signal-to-noise ratio. In addition, QTOF MS possesses a high-speed spectral acquisition rate, which can rate as fast as 50 Hz to perform effective MS^2 dissociations of multiple precursor ions in one measurement cycle. Considering these advantageous features for improving sensitivity and accuracy, GC–QTOF MS as a new instrument system could have a promising future for routine monitoring of targeted and non-targeted pesticides. Prior to this study, Portoles et al. reported a pesticide residue analysis using an atmospheric pressure chemical ionization source in GC–QTOF MS [26]. In this study, we present a rapid, simultaneous, and multi-species screening and identification method capable of monitoring multi-residues of pesticide remaining in vegetables using GC–QTOF MS.

2. Experimental

2.1. Chemicals and reagents

One hundred and eighty-seven references of pesticides included in the database were purchased from J&K Scientific Ltd. (Beijing, China). Standard solutions of pesticide were prepared in n-hexane (HPLC grade) supplied by Fisher Scientific (Santa Clara, USA). Bond Elut Carbon/NH_2 cartridges (500 mg/500 mg, 6 mL) were purchased from Agilent Technologies (Santa Clara, USA). Other solvents and reagents used for sample preparations were obtained from Shanghai Reagent Company (Shanghai, PR China) in analytical grade purity.

2.2. Instrument and software

All measurements were performed with a 7200 accurate-mass GC–QTOF MS instrument (Agilent Technologies, Santa Clara, USA), using a fused silica DB-35MS capillary column of 30 m × 0.25 mm i.d. The injector was operated at 250 °C in splitless mode and helium (purity > 99.999%) was used as the carrier gas at 1.2 mL min^{-1}. The GC oven temperature was programmed from an initial temperature of 80 °C held for 1 min, ramped at 25 °C min^{-1} to 170 °C, and then at 6 °C min^{-1} to final 300 °C held for 10 min, resulting in a total run time of 36.267 min. Injection volume was 1 μL. The other optimized parameters included a transfer line temperature of 300 °C and an ion source of 250 °C. TOF for MS was operated at 5.0 spectra/s acquiring the mass range *m/z* 50–600 and about 13,500 (FWHM). The MS^2 conditions were fixed for each compound with a quadrupole for isolation of precursor ion at a medium MS resolution and a linear hexapole collision cell with nitrogen at 1.5 mL min^{-1} as the collision gas. Perfluorotributylamine (PFTBA) was utilized for daily MS calibration. MassHunter Acquisition B.06 and MassHunter Qualitative Analysis B.05 were applied for the control of the equipment, and the acquisition and treatment of data. In addition, Microsoft Excel software was applied to create a CSV file for the database of pesticides.

2.3. Sample source

The fresh vegetables of celery, rape, scallion and spinach were purchased from a local market in Shanghai, China.

2.4. Sample preparation

2.4.1. Extraction

The sample of each 20 g chopped vegetable was transferred into an 80 mL centrifugal tube, 40 mL acetonitrile added, and blended at a 15,000 rpm for 1 min with 5 g of sodium chloride added during the blending. After that, the sample homogeneity was centrifuged at 4200 rpm for 5 min. The acetonitrile layer of 20 mL was transferred into a 100-mL rotary evaporator flask and concentrated to 1 mL at 40 °C for further clean-up.

2.4.2. Clean-up

A Bond Elut Carbon/NH_2 cartridge (500 mg/500 mg, 6 mL) was added with 2 cm anhydrous sodium sulfate and conditioned with 4 mL of acetonitrile/toluene (3:1). Then, the solution obtained from

the extraction step was applied to the cartridge and eluted with 25 mL of acetonitrile/toluene (3:1). The entire volume of effluent was collected and concentrated to 0.5 mL at 40 °C. The residue was dissolved in n-hexane to make a 10 mL solution for detection. For the spiked spinach sample, each residue was added a pesticide mixture of known concentrations and mixed thoroughly, then added n-hexane to make a 10 mL solution for separation and detection.

3. Results and discussion

3.1. Creation of the database

Because the database of pesticides was created for simultaneous multi-species screening, it was important to include as many species of pesticides as possible. A total of 187 pesticides, such as organophosphate insecticides, organochlorine insecticides, organic fluorine insecticides, pyrethroid insecticides, glyphosate herbicide, and azole fungicides, were collected and divided into 11 groups at 200 ppb for GC–QTOF MS analysis. TOF MS was calibrated first by using PFTBA to achieve a typical mass resolution >13,000 and mass accuracy <5 ppm. Then 1 μL of each group standard solution was injected into the system for detection.

According to the European Council Directive 96/23/EC 4, a minimum of four identification points per pesticide are required to ensure its confirmation [27]. To adhere to this Directive, retention time plus a single characteristic ion and an ion pair (precursor–product ions) for each pesticide was included in the database. Among them, the same chromatographic separation ensured a nearly identical retention time. The precision of retention time was evaluated by the GC–MS measurements of all pesticides groups each in six replications. The standard deviation of each pesticide's retention time was between ±0.00 and ±0.04 min. The selection of characteristic ion for pesticide is a critical element for the application of the database. The best candidate of characteristic ion is derived from characteristics fragmentation and owns the most abundance. But in actual cases, many pesticides have no ideal characteristic ions meeting both features. Hence, in our design, sensitivity was preferred to selectivity in the selection of the characteristic ion. The most abundant ion from a MS^1 full scan spectrum was selected as the characteristic ion and precursor ion in order to achieve the best sensitivity. This also provided a maximum possibility to avoid missing the identification of pesticide in question. Moreover, the accurate masses of the selected ions could increase the selectivity of the method. The ion pair (precursor–product ions) would be utilized for the confirmation of pesticide. Of course, in case that the more abundant ion had a lower *m/z* ratio below 100 normally due to a poor selectivity, the precursor ion would be replaced by the ion with higher *m/z* and lesser abundance. The precursor ion theoretically calculated from its formula was separated in the quadrupole and submitted to collision-induced dissociation (CID). The precursor ion undergoes repeated collisions with the collision gas, building up potential energy in the molecule, until eventually the fragmentation threshold is reached and the product ions are formed [28]. The types of fragmentation that occur vary considerably with the type of product ion and the amount of energy involved. Each product ion has its specific fragmentation threshold called as the optimal CID energy. Normally, it is best to work at around the optimal CID energy, or just above, to maintain most control over and obtain the highest intensity of the proposed product ion. Hence, for each pesticide, the optimization of collision energy was necessary to achieve an optimal abundance level of the product ion selected. At lower energies, the proposed fragmentation did not occur. When the energy was too high, other fragmentations may occur instead. Corresponding, the intensity of the proposed product ion would be decreased at a lower or higher CID energy. As an example, Fig. 1a shows a mass spectrum of triadimefon. The most abundant ion at *m/z* 57 was selected as the characteristic ion, while the lesser abundant ion at *m/z* 208 was selected as the precursor ion due to its higher *m/z* ratio. Among the three CID mass spectra of this precursor ion (Fig. 1b–d), the most abundant ion at *m/z* 127 was generated at 10 eV, rapidly reduced at 20 eV, and nearly disappeared at 30 eV. The ions at *m/z* 111 and *m/z* 99 replaced the ion at *m/z* 127 as the most abundant ion at 20 eV and 30 eV, respectively. Comparing the signal intensities of three ions with CID energies from 5 eV to 30 eV, the ion at *m/z* 127 with the maximum abundance and its optimal CID energy at 10 eV was regarded as the best choice for inclusion in the database (Fig. 1e). The obtained optimal CID energy was included in the database as an important parameter for the GC–MS^2 measurement in order to achieve the greatest possible sensitivity. Finally, all three selected ions were identified by their chemical formula, and the exact masses of them were calculated and used to create the database. In some cases, retention time or exact ion masses of one pesticide in the database would match other pesticides. However, by expanding to four criteria of retention time, a characteristic ion, a precursor ion, and its product ion for each pesticide, it is possible to completely distinguish one from another.

3.2. Workflow of the database

GC–QTOF MS is selected as the analytic instrument for the application of the database in the workflow because it combines the high resolution of TOF analyzer with the capability to perform MS^1 (GC–TOF mode) and MS^2 experiments (GC–QTOF mode). Thus, it is possible to acquire full scan spectra of MS^1 and MS^2 with accurate mass, which drastically increases the selectivity of the method due to the high amount and quality of the structural information produced. Fig. 2 illustrates the whole workflow of database in two steps. Step one is GC–MS^1 measurement in GC–TOF mode and "MS^1 screening" for possible pesticides by chemical formula match. Software named "Compounds Find by Formula Match" is applied to post-run analysis of a GC–MS^1 file measured in a full scan mode. Both the retention time and exact mass of the characteristic ion from the database are used to determine the pesticide match. In addition, the spacing and relative abundance of the ion's isotope detected are also considered to estimate the accuracy of the match. After the search, all matched compounds are listed in one table called "Compound List" and their extracted ion chromatograms with the average spectra can be generated. Search criteria are specified in two key options including mass tolerance and retention time window. Depending on the precision of retention time, the retention window would be set to 0.1 min or less. However, the matrix effect could cause retention time shifting [29]. As an extreme example, by our estimation, the retention time of methamidophos in the celery matrix was shifted 0.18 ± 0.05 min in six replicates compared with the calibration standard. Considering the effect induced by the different matrix, the retention time window was optimized to 0.25 min to avoid a false negative on the screening. The mass tolerance was optimized to 5 mDa. Although the TOF MS had been well calculated for high resolution and mass accuracy before measurements, some factors known as dead time of detector and abundance of ions, could affect measurement accuracy and cause mass error [30]. Thus, the mass tolerance could not be set as expected (normally ≤5 ppm), or some target pesticides would be missed. Signal-to-noise ratio (S/N) here was calculated as the peak height from the extracted ion chromatogram of each characteristic ion to the background noise. Noise here was measured "peak-to-peak" from the highest to the lowest intensity over two ranges of 0.1 min before peak start and after peak end. All compounds satisfying S/N ≥ 3 would be viewed as the proposed pesticides for the further verification in the second step. Step two was GC–MS^2

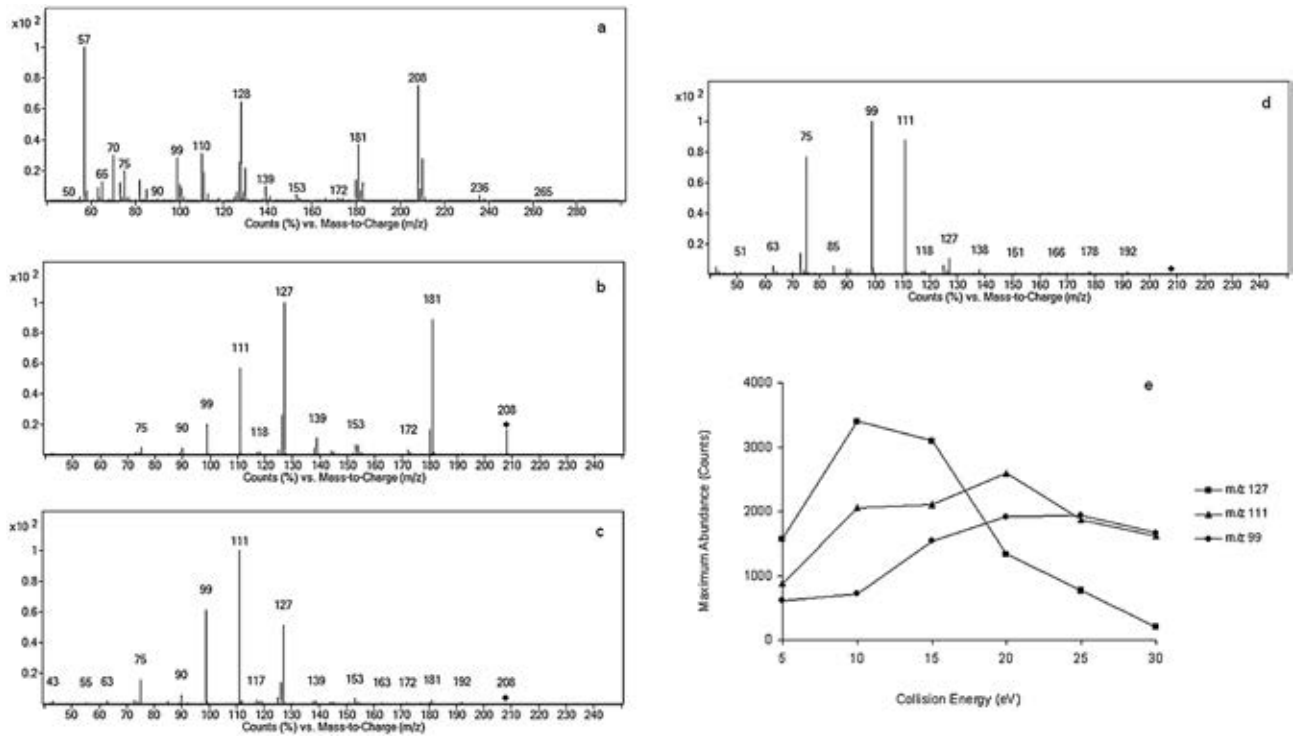

Fig. 1. (a) Mass spectrum of triadimefon at 200 ppb, showing the characteristic ion at *m/z* 57 (low *m/z*) with the highest abundance and the precursor ion at *m/z* 208 (higher *m/z*) with a lesser abundance. (b) CID mass spectrum of the precursor ion at *m/z* 208 at the energy of 10 eV, showing the most abundant ion at *m/z* 127. (c) CID mass spectrum of the precursor ion at *m/z* 208 at the energy of 20 eV, showing the most abundant ion at *m/z* 111. (d) CID mass spectrum of the precursor ion at *m/z* 208 at the energy of 30 eV, showing the most abundant ion at *m/z* 99 and the ion at *m/z* 127 nearly disappearing. (e) Plot of the maximum abundance versus the collision energy in the range of 5–30 eV for the ions at *m/z* 127, 111 and 99.

measurement in GC–QTOF mode and "MS^2 identification" for structural confirmation of product ion. All proposed pesticides in "Compound List" were acquired MS^2 data in one analytical run using a targeted MS^2 mode specified in the retention time and retention time window. The precursor ions with corresponding optimal collision energies were referred to the database. The windows of retention time were unified to a 0.3 min time length and the acquired times were optimized to 100 ms/spectrum to give the best sensitivity for all pesticides in one run. In post-run analysis, an exact ion chromatogram of GC–MS^2 was extracted for each product ion to generate an average spectrum, which was then utilized to perform the mass match of the product ion in the database. The tolerance for accurate mass extraction was limited to within 5 mDa range.

3.3. Qualitative validation of the database

Because the main purpose of the qualitative screening was to distinguish between negative and positive samples at a determined level, the method proposed here would be considered satisfactorily validated at a certain concentration level only when the target ion was detected and correctly identified based on the matrix-spiked samples tested, regardless of their recovery rate and precision. One spinach sample was spiked with 50 test pesticides (Table 1)

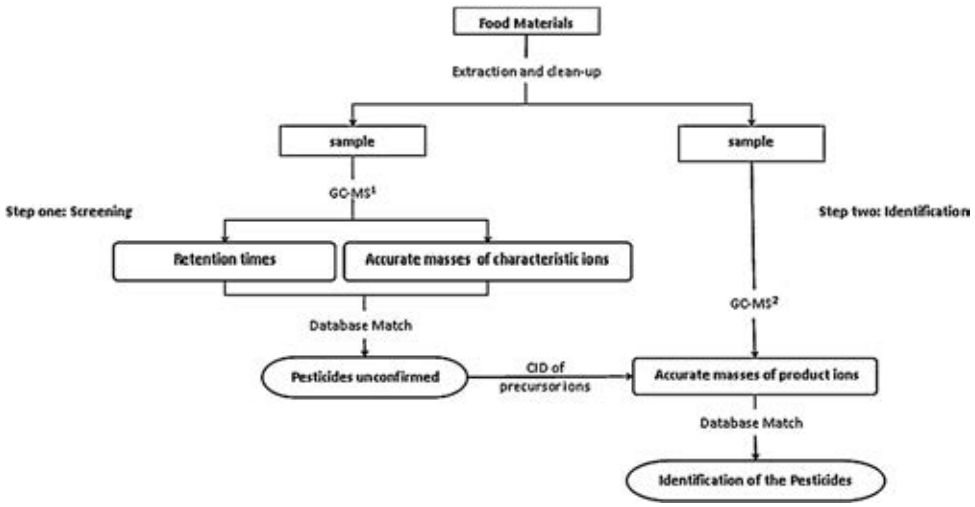

Fig. 2. Workflow of the database.

Table 1
Information of 50 test pesticides and their measured mass errors in "MS^2 identification".

Pesticide	MS^1 screening		MS^2 identification		
	RT (min)	Characteristic ion (*m/z*)	Precursor–product ions (*m/z*)	LOD (ppb)	Measured mass error (mDa)
Etridiazole	6.74	210.9494	210.9494–182.9181	1	0.5
Chlorpropham	8.86	127.0183	127.0183–65.0386	5	−0.1
Propoxur	8.90	110.0362	110.0362–64.0308	1	−1
Cadusafos	9.08	158.9698	158.9698–96.9508	1	−0.6
Ethoxyquin	9.97	202.1226	202.1226–174.0913	1	−2.2
Pronamide	10.39	172.9555	172.9555–144.9606	1	−0.5
Diazinon	10.48	137.0709	137.0709–84.0444	2	−0.4
Dinitramine	10.77	305.0856	305.0856–261.0594	20	−1.8
Simazine	10.80	201.0776	201.0776–173.0463	1	−1.6
Carbofuran	11.23	164.0832	164.0832–149.0597	5	0.5
Pentachlorobenzonitrile	11.34	272.8468	272.8468–237.8779	2	1.9
Vinclozolin	12.17	186.9586	186.9586–123.9949	5	−0.1
Pirimicarb	12.17	166.0975	166.0975–96.0444	2	−0.4
delta-BHC	12.73	180.9373	180.9373–144.9606	2	−1.4
Propanil	12.81	160.9794	160.9794–98.9996	2	−0.1
Tolclofos-methyl	13.00	264.9850	264.9850–249.9613	1	1.2
Ametryn	13.02	227.1199	227.1199–58.0651	5	0.8
Parathion-methyl	13.13	109.0049	109.0049–78.9943	10	0.1
Diethofencarb	13.58	151.0264	151.0264–123.0315	5	1.9
Dacthal	13.61	298.8831	298.8831–220.8958	2	−1.2
Chlorpyrifos	13.66	96.9508	313.9569–257.8943	5	−1.6
Dichlofluanid	13.88	123.0137	123.0137–77.0386	10	0.3
Pirimiphos-ethyl	13.94	180.1131	180.1131–152.0818	10	1.7
Fenthion	14.31	278.0195	278.0195–109.0049	5	−1.2
o, p-Dicofol	14.49	138.9945	138.9945–110.9996	2	1
Isocarbophos	14.78	120.0206	120.0206–92.0257	5	−1.5
Procymidone	15.44	283.0161	283.0161–96.0570	2	−0.8
trans-Chlordane	15.51	370.8284	370.8284–263.9062	5	−2.1
cis-Chlordane	15.81	370.8284	370.8284–263.9062	5	1.5
Hexaconazole	16.43	82.0400	213.9947–158.9763	10	−1.5
p, p′-DDE	16.58	245.9998	245.9998–176.0621	1	0.8
Oxyfluorfen	16.63	252.0393	252.0393–224.0444	20	1.6
Buprofezin	16.72	105.0573	105.0573–77.0386	20	−0.9
Bupirimate	17.13	208.1444	208.1444–165.1022	10	−1.7
Isoprothiolane	17.77	117.9905	117.9905–89.9592	5	−0.4
Endrin	17.81	260.8594	260.8594–190.9217	10	1.1
o, p′-DDT	18.05	235.0076	235.0076–165.0699	1	−0.6
Endosulfan II	18.69	234.8437	234.8437–140.9060	10	1.7
Tris(2-butoxyethyl) phosphate	18.83	85.0648	124.9998–98.9842	5	−0.1
p, p′-DDT	19.26	235.0076	235.0076–165.0699	1	−1.7
Quinoxyfen	19.36	237.0584	237.0584–208.0557	5	2.3
Triazophos	19.87	162.0662	162.0662–134.0475	2	1.4
Fenpropathrin	20.76	181.0648	181.0648–152.0621	10	1.1
Tebufenpyrad	20.85	171.0320	171.0320–87.9949	5	−1.3
Bifenazate	21.69	152.0621	152.0621–150.0464	50	−0.1
Phosmet	22.35	160.0393	160.0393–77.0386	1	−1.5
trans-Permethrin	23.83	183.0804	183.0804–153.0699	2	0
Fluquinconazole	24.93	340.0396	340.0396–298.0178	5	−0.4
Boscalid	26.73	139.9898	139.9898–111.9949	0.5	−1.7
Difenoconazole	28.86	264.9818	264.9818–202.0180	10	−0.4

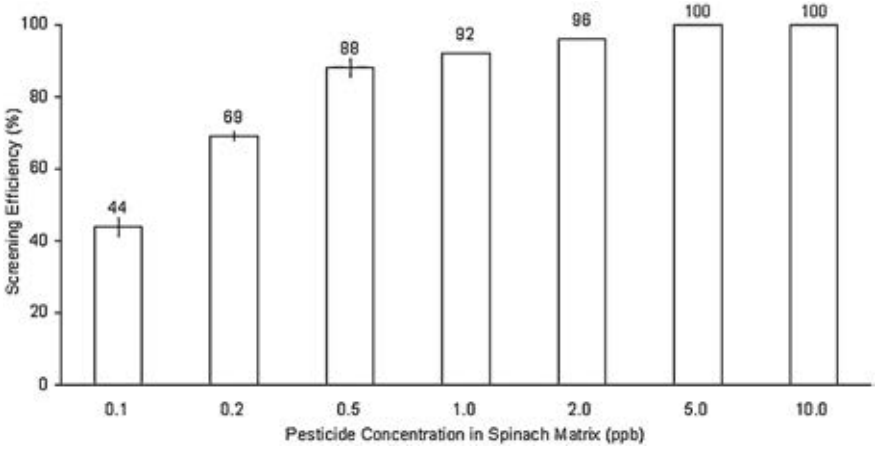

Fig. 3. Screening efficiency (SE) for "MS^1 screening" at different pesticide concentrations in a spinach matrix.

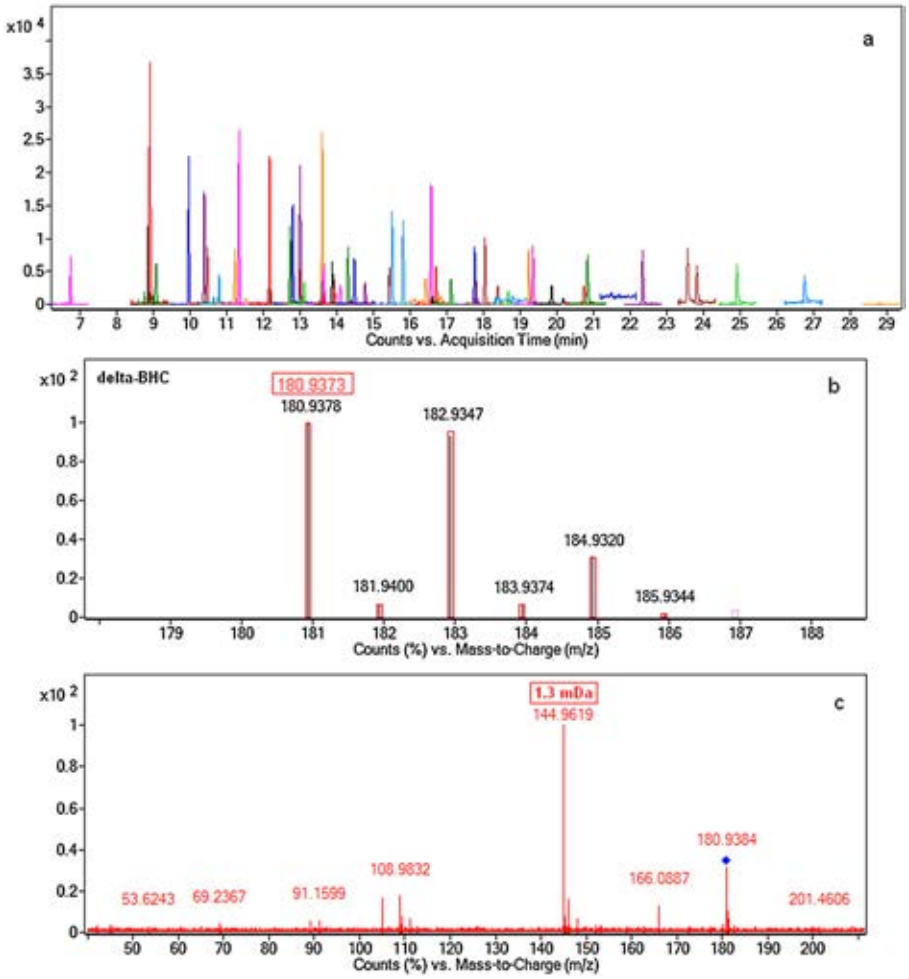

Fig. 4. (a) Multi-extracted ion chromatogram of the spiked sample at 5 ppb using the software "Find Compounds by Formula Match", showing that all 50 test pesticides were found and the signal of each pesticide met with S/N ≥ 3. (b) Average first-stage mass spectrum of peak at 12.73 min (delta-BHC), showing the characteristic ion at *m/z* 180.9378 and its isotope pattern. Compared with its theoretic value at *m/z* 180.9373 and isotope pattern in red, all ions were matched well with the spacing and relative abundance of its isotopes and the measured mass error of 0.5 mDa. (c) Average second-stage mass spectrum of peak at 12.73 min (delta-BHC), showing that the measured mass error of the product ions was 1.3 mDa in red block. (For interpretation of the references to color in figure legend, the reader is referred to the web version of the article.)

at seven concentrations of 0.1, 0.2, 0.5, 1.0, 2.0, 5.0, and 10 ppb, analyzed in two replicates together with their respective blanks according to the described procedures and submitted to a search in the database. No signals of such pesticides were obtained from the analyses of the reagent blank and spinach matrix blank, indicating that these materials were free of the 50 test pesticides. The limit of identification (LOI) was established as the lowest concentration for all test pesticides found in "MS^1 screening". The limit of detection (LOD) was established as the lowest concentration that the analytical process could differentiate from the background level with S/N ≥ 3. The capacity of "MS^1 screening" was defined by its screening efficiency (SE) which was the percentage of pesticides found out of the total pesticides tested. As shown in Fig. 3, SE was 44% at 0.1 ppb but increased to 88% at 0.5 ppb, and reached 100% at 5 ppb, which was the estimated LOI in this case. Following the "MS^1 screening", the proposed pesticides entered the "MS^2 identification" step and the mass errors of corresponding product ions were calculated. The result showed each product ion was identified successfully with the mass error below 2.5 mDa. LODs of the test pesticides in the "MS^2 identification" step were investigated using the spinach sample spiked at concentrations between 0.1 and 100 ppb. All identified pesticides had concentrations of 10 ppb or below, except dinitramine, oxyfluorfen, buprofezin, and bifenazate (Table 1).

There are four ways to evaluate the efficiency of a database for screening pesticide residues, which include sensitivity, accuracy, selectivity and specificity [31]. In the screening, the narrow windows of retention time and mass combined with the exact masses of multi-class characteristic ions in the database improved the high sensitivity and accuracy. Fig. 4a presents a multi-extracted ion chromatogram of the spiked sample at 5 ppb after "MS^1 screening", showing LODs of all test pesticides in MS^1 at 5 ppb or below. Fig. 4b shows the result of search procedure for the peak at 12.73 min in the chromatogram of Fig. 4a, which was identified as delta-BHC. This compound was well matched using the theoretic characteristic ion at *m/z* 180.9373 with the spacing and relative abundance of its isotopes. In addition, the pair of precursor–product ions at *m/z* 180.9373–144.9606 further supported the structure of this compound (Fig. 4c). Selectivity and specificity here were supported by the high separation efficiency of GC and the high resolution of QTOF MS. For example, chlorothalonil and tolclofol-methyl had close retention times and exact masses of characteristic/precursor ions (chlorothalonil: retention time at 12.86 min and ion at *m/z* 263.8810; tolclofol-methyl: retention time at 12.99 min and ion at *m/z* 264.9850). As shown in Fig. 5a, they were separated due to the combination of GC separation and exact ion extraction from the total ion chromatography in GC–MS^1, although the difference of their retention times and accurate ion masses was as narrow as

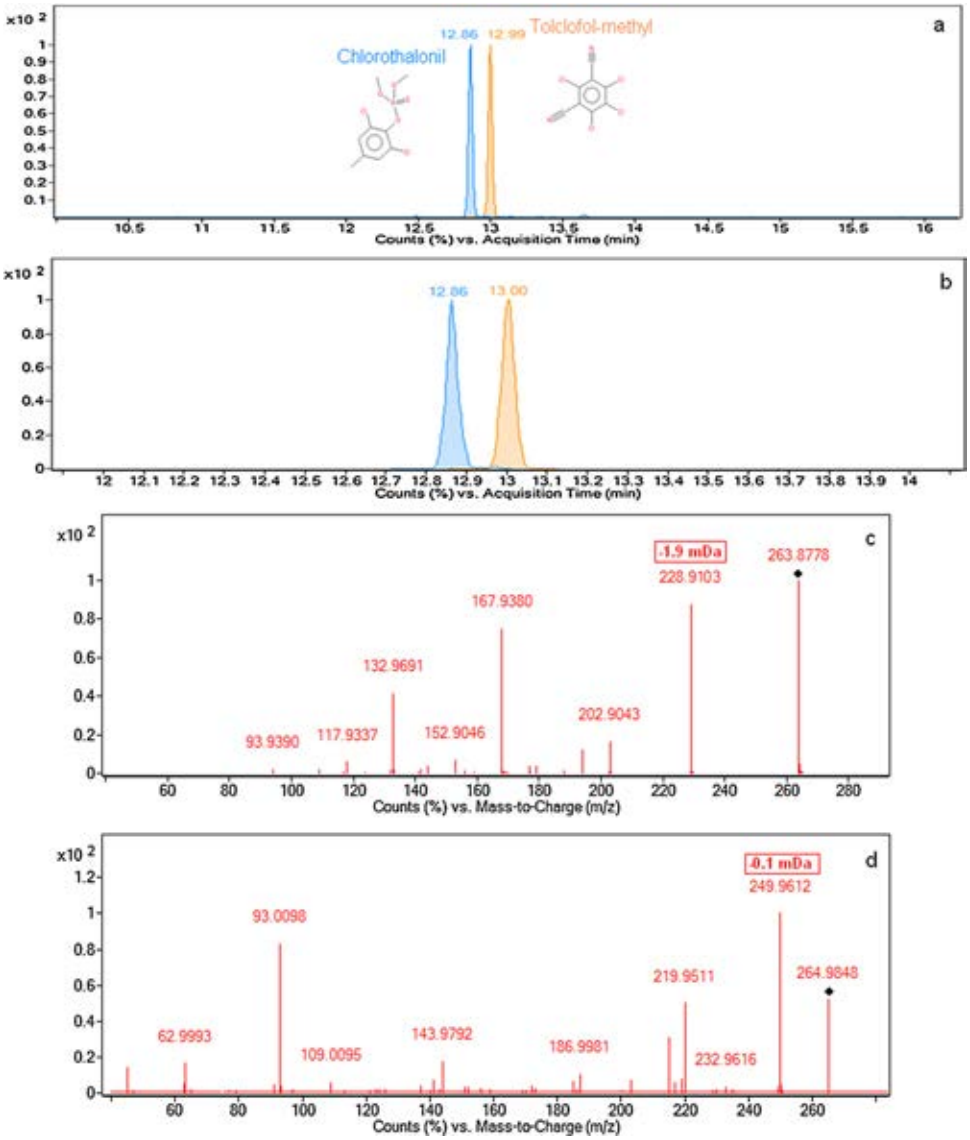

Fig. 5. (a) Multi-extracted ion chromatogram of chlorothalonil at *m/z* 263.8810 and tolclofol-methyl at *m/z* 264.9850 in GC–MS^1. The corresponding chemical structures were shown inside. (b) Multi-extracted ion chromatogram of chlorothalonil at *m/z* 228.9122 (precursor ion at *m/z* 263.8810) and tolclofol-methyl at *m/z* 249.9613 (precursor ion at *m/z* 264.9850) in GC–MS^2. (c) Average accuracy MS^2 spectrum of chlorothalonil peaked at 12.86 min, showing that the measured mass error of the product ion at *m/z* 228.9122 was 1.9 mDa in red block. (d) Average accuracy MS^2 spectrum of tolclofol-methyl peaked at 13.00 min, showing that the measured mass error of the product ion at *m/z* 249.9613 was 0.1 mDa in red block. (For interpretation of the references to color in figure legend, the reader is referred to the web version of the article.)

0.13 min and as small as 0.1040 Da. Similarly, in Fig. 5b–d, these two pesticides were also separated and accurately identified due to the exact masses of product ions in GC–MS^2 and the accurate masses of product ions with measured errors of less than 2.5 mDa. In another case where o, p′-DDT and p, p′-DDT had the same formula of characteristic ion at *m/z* 235.0076, or where vinclozolin and pirimicarb had the same retention times at 12.17 min, good results were obtained thanks to the use of the four identification criteria. We could not find the most challenging case where two pesticide compounds share the same retention times and masses of characteristic ions. However, it is predicted that their paired precursor–product ions would be most useful in achieving separate identifications of each (optical-isomers excluded).

3.4. Application to real vegetables

Four fresh celery, rape, scallion and spinach vegetables were collected from a local market. The vegetables were pretreated first according to the Chinese Official Standard Method [32]. Subsequently, a proved extraction and clean-up method for the volatile and semi-volatile pesticides was utilized for the volatile and semi-volatile pesticides [33]. In this method, solid phase extraction was applied for the clean-up, which has been universally adopted for modern residue analysis of non-fatty samples. The optimal conditions for extraction based on the references could meet the demand of this study. After extraction and clean-up, each sample was analyzed following the workflow steps. Table 2 and Fig. 6 show that a total of 13 pesticides were found in the four fresh vegetables, with 11 in celery, 9 in rape, 3 in scallion and 2 in spinach. Among them, isofenphos-methyl peaked at 20.18 min, a common phosphoramidothioate pesticide residue, was found in all four vegetables. Compared with celery and rape, scallion and spinach had less amounts of pesticide residues. Considering the vegetable processing environment, the same pesticide residues in trace amounts remaining in different vegetables might be results of environmental pollution.

Table 2
The pesticide residues in fresh celery, rape, scallion and spinach vegetables.

Pesticide	MS^1 screening		MS^2 identification	
	RT (min)	Characteristic ion (*m/z*)	Precursor–product ions (*m/z*)	Measured mass error (mDa)
Methamidophos	5.43	94.0052	141.0008–95.0131	0.4^{ce}, -0.4^{ra}
Acephate	7.31	136.0158	136.0158–94.0052	-0.7^{ce}, -0.3^{ra}
Isoprocarb	7.38	121.0648	121.0648–77.0386	0.1^{ce}
cis-1,2,3,6-Tetrahydrophthalimide	8.02	79.0542	151.0625–80.0621	-1.1^{ce}
Diphenylamine	9.06	169.0886	169.0886–167.0730	0.8^{ce}, 0.9^{ra}
Omethoate	9.47	110.0127	110.0127–78.9943	-0.1^{ce}, -0.3^{ra}
Dicrotophos	9.99	127.0155	127.0155–109.0049	-0.9^{ce}, 0.6^{ra}
Monocrotophos	10.52	127.0155	127.0155–109.0049	-0.1^{ce}, -0.6^{ra}
Isocarbamid	11.95	142.0611	142.0611–70.0287	-0.2^{ce}, -0.2^{ra}
Chlorpyrifos-methyl	12.61	285.9256	285.9256–93.0100	0.8^{sc}, -0.5^{sp}
Tetraconazole	13.93	336.0521	336.0521–218.0480	-0.2^{ce}, 1.0^{ra}
Endosulfan sulfate	20.08	269.8126	269.8126–234.8437	-1.0^{sc}
Isofenphos-methyl	20.18	121.0284	121.0284–65.0386	-1.2^{ce}, -0.9^{ra}, -0.6^{sc}, 0^{sp}

ce: found in celery; ra: found in rape; sc: found in water scallion, sp: found in spinach.

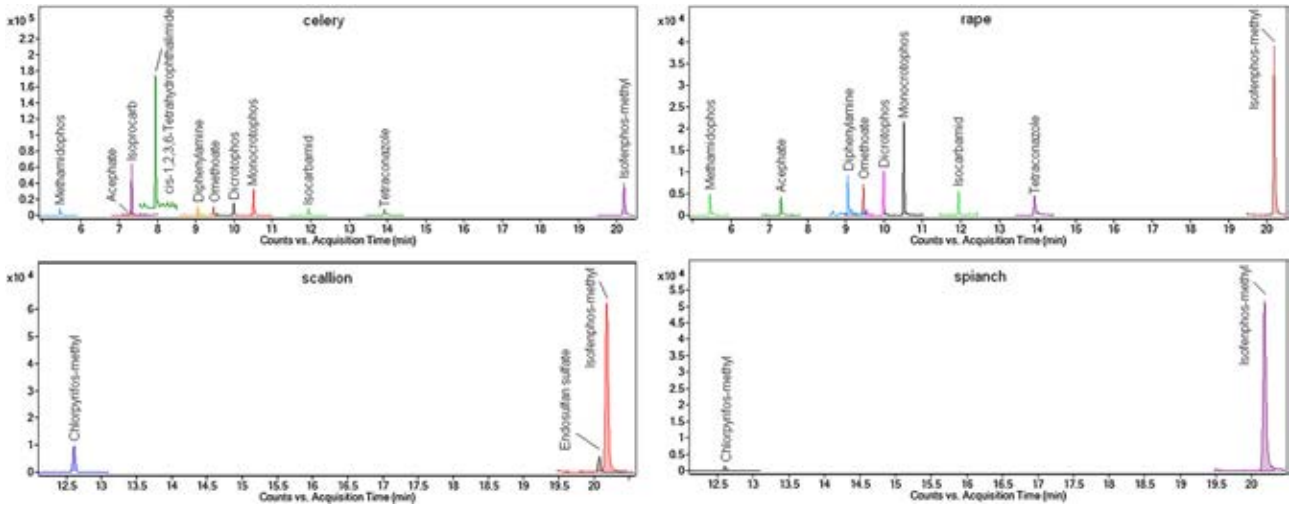

Fig. 6. Multi-extracted ion chromatogram of pesticide residues in fresh celery, rape, scallion and spinach showing that identified pesticides with 11 in celery, 9 in rape, 3 in scallion and 2 in spinach. Each pesticide met S/N ≥ 3.

4. Conclusion

An exact mass database and GC–QTOF MS were combined for the monitoring of pesticides remaining in vegetables. In the database, retention time, a single characteristic ion and an ion pair (precursor–product ions) selected from MS^1 and MS^2 spectra were included for the rapid screening and the identification of the pesticides. GC coupled with tandem high-resolution QTOF MS provided a powerful analytical method for the identification of the pesticides and increased the selectivity of the determination. The efficiency of the method was demonstrated by the lowest concentration (LOI) at 5 ppb to identify all test pesticides by using the "MS^1 screening" step and mass errors of less than 2.5 mDa by using the "MS^2 identification" step, which indicated its high sensitivity, accuracy, selectivity and specificity. Further work is in progress to find a more universal parameter to replace the retention time in the database, which varies with the chromatographic conditions. Success in finding this replacement would significantly improve the application universality of this screening and identification method.

Acknowledgements

The authors thank Agilent Technologies (China), Inc. for assistance in the sample preparation and experiments. The authors acknowledge the financial support of NSFC (Grant No. 21072215), Innovation Method Fund of China (Grant No. 2010IM030900) and CAS (Grant No. YZ200938).

References

[1] F. Vinson, M. Merhi, I. Baldi, H. Raynal, L. Gamet-Payrastre, Occup. Environ. Med. 68 (2011) 694–702.
[2] G. Van Maele-Fabry, A.C. Lantin, P. Hoet, D. Lison, Environ. Int. 37 (2011) 280–291.
[3] M.C. Turner, D.T. Wigle, D. Krewski, Cien. Saude Colet. 16 (2011) 1915–1931.
[4] M. Cohen, Aust. Fam. Physician 36 (2007) 1002–1004.
[5] A.F. Hernandez, T. Parron, A.M. Tsatsakis, M. Requena, R. Alarcon, O. Lopez-Guarnido, Toxicology (2012), June 21 (Epub ahead of print).
[6] C. Freire, S. Koifman, Neurotoxicology 33 (2012) 947–971.
[7] D.A. Jett, Neurol. Clin. 29 (2011) 667–677.
[8] K. Seshaiah, P. Mowli, Analyst 112 (1987) 1189–1190.
[9] R. Inam, E.Z. Gulerman, T. Sarigul, Anal. Chim. Acta 579 (2006) 117–123.
[10] R.J. Cassella, V.A. Salim, S. Garrigues, R.E. Santelli, M. de la Guardia, Anal. Sci. 18 (2002) 1253–1256.
[11] J. Sherma, J. Environ. Sci. Health B 46 (2011) 557–568.
[12] C.M. Reddy, N.J. Drenzek, T.I. Eglinton, L.J. Heraty, N.C. Sturchio, V.J. Shiner, Environ. Sci. Pollut. Res. Int. 9 (2002) 183–186.
[13] C. Zhang, H. Zhao, M. Wu, X. Hu, X. Cai, L. Ping, Z. Li, J. Chromatogr. Sci. 50 (2012) 940–944.
[14] C. Wang, S. Ji, Q. Wu, C. Wu, Z. Wang, J. Chromatogr. Sci. 49 (2011) 689–694.
[15] T. Cai, L. Zhang, H. Wang, J. Zhang, Y. Guo, Anal. Chim. Acta 706 (2011) 291–296.
[16] L. Alder, K. Greulich, G. Kempe, B. Vieth, Mass Spectrom. Rev. 25 (2006) 838–865.
[17] D. Stajnbaher, L. Zupancic-Kralj, J. Chromatogr. A 1015 (2003) 185–198.
[18] R. Raposo, M. Barroso, S. Fonseca, S. Costa, J.A. Queiroz, E. Gallardo, M. Dias, Rapid Commun. Mass Spectrom. 24 (2010) 3187–3194.

[19] A. Kruve, K. Herodes, I. Leito, Rapid Commun. Mass Spectrom. 24 (2010) 919–926.
[20] C.J. Tao, J.Y. Hu, J.Z. Li, S.S. Zheng, W. Liu, C.J. Li, Bull. Environ. Contam. Toxicol. 82 (2009) 111–115.
[21] G. Salquebre, C. Schummer, M. Millet, O. Briand, B.M. Appenzeller, Anal. Chim. Acta 710 (2012) 65–74.
[22] T. Vasiljevic, N. Dujakovic, M. Radisic, S. Grujic, M. Lausevic, M. Dimkic, Water Sci. Technol. 66 (2012) 965–975.
[23] T. Portoles, E. Pitarch, F.J. Lopez, F. Hernandez, J. Chromatogr. A 1218 (2011) 303–315.
[24] S. Walorczyk, Rapid Commun. Mass Spectrom. 22 (2008) 3791–3801.
[25] K. Zhang, J.W. Wong, P. Yang, D.G. Hayward, T. Sakuma, Y. Zou, A. Schreiber, C. Borton, T.V. Nguyen, B. Kaushik, D. Oulkar, Anal. Chem. 84 (2012) 5677–5684.
[26] T. Portoles, J.V. Sancho, F. Hernandez, A. Newton, P. Hancock, J. Mass Spectrom. 45 (2010) 926–936.
[27] European Commission Decision. Concerning the performance of analytical methods and the interpretation of results. Document No. L221, Implementing Council Directive 96/23/EC.
[28] L. Sleno, D.A. Volmer, J. Mass Spectrom. 39 (2004) 1091–1112.
[29] H.G. Mol, A. Rooseboom, R. van Dam, M. Roding, K. Arondeus, S. Sunarto, Anal. Bioanal. Chem. 389 (2007) 1715–1754.
[30] K. Webb, T. Bristow, M. Sargent, B. Stein (Eds.), Methodology for Accurate Mass Measurement of Small Molecules, LGC, Limited, Teddington, UK, 2004.
[31] European Commission Decision. Method validation and quality control procedures for pesticide residues analysis in food and feed. Document No. SANCO/10684/2009, Implemented on 01/01/2010.
[32] Determination of 450 pesticides and related chemicals residues in fruits and vegetables. GB/T 20769-2008. Standardization Administration of the People's Republic of China.
[33] G.F. Pang, C.L. Fan, Y.M. Liu, Y.Z. Cao, J.J. Zhang, X.M. Li, Z.Y. Li, Y.P. Wu, T.T. Guo, J. AOAC Int. 89 (2006) 740–771.

Identification of drug targets by chemogenomic and metabolomic profiling in yeast

Manhong Wu[a], Ming Zheng[a], Weiruo Zhang[b], Sundari Suresh[c], Ulrich Schlecht[c], William L. Fitch[a], Sofia Aronova[d], Stephan Baumann[d], Ronald Davis[c], Robert St.Onge[c], David L. Dill[b] and Gary Peltz[a]

Objective **To advance our understanding of disease biology, the characterization of the molecular target for clinically proven or new drugs is very important. Because of its simplicity and the availability of strains with individual deletions in all of its genes, chemogenomic profiling in yeast has been used to identify drug targets. As measurement of drug-induced changes in cellular metabolites can yield considerable information about the effects of a drug, we investigated whether combining chemogenomic and metabolomic profiling in yeast could improve the characterization of drug targets.**

Basic methods **We used chemogenomic and metabolomic profiling in yeast to characterize the target for five drugs acting on two biologically important pathways. A novel computational method that uses a curated metabolic network was also developed, and it was used to identify the genes that are likely to be responsible for the metabolomic differences found.**

Results and conclusion **The combination of metabolomic and chemogenomic profiling, along with data analyses carried out using a novel computational method, could robustly identify the enzymes targeted by five drugs. Moreover, this novel computational method has the potential to identify genes that are causative of metabolomic differences or drug targets.** ***Pharmacogenetics and Genomics*** **22:877–886** © **2012 Wolters Kluwer Health | Lippincott Williams & Wilkins.**

Pharmacogenetics and Genomics 2012, **22**:877–886

Keywords: chemogenomics, metabolomics, pharmacology

[a]Department of Anesthesia, Stanford University School of Medicine, [b]Department of Computer Science, Stanford University School of Engineering, [c]Department of Biochemistry and Stanford Genome Technology Center, Stanford University, Stanford and [d]Agilent Technologies Inc., Santa Clara, California, USA

Correspondence to Gary Peltz, MD, PhD, Department of Anesthesia, Stanford University School of Medicine, Stanford University, 300 Pasteur Drive L232, Stanford, CA 94305, USA
Tel: +1 650 721 2487; fax: +1 650 721 2420; e-mail: gpeltz@stanford.edu

Received 15 May 2012 **Accepted** 22 September 2012

Introduction

The diploid yeast collections contain ~6000 heterozygous gene deletion strains and ~5000 homozygous gene deletion strains. A reduction in the copy number of a gene within a pathway affected by a drug increases the sensitivity of a heterozygous deletion strain to the growth-inhibitory effect of the drug [1]. A chemical genomics assay was developed to exploit this effect for the characterization of drug targets; the effect of a test drug on the competitive growth of a complete collection of bar-coded heterozygous yeast deletion strains is measured in a single culture [2]. This method, and related approaches using homozygous deletion strains, was used to characterize the targets for multiple drugs and chemicals [2–5]. However, a reduction in the copy number of genes other than the actual drug target could also alter the sensitivity of deletion strains, and this could confound efforts to identify the specific drug target by this method.

Metabolomic studies have been carried out in yeast [6], but relatively few metabolomic studies have analyzed yeast gene deletion strains [7]. We investigated whether drug targets could be determined by coupling chemogenomic profiling with metabolomic analysis of drug responses in yeast. The extreme differences in physicochemical properties make it impossible to accurately measure changes in all cellular metabolites using a single extraction or analytic method. It is not even possible to dissolve all types of metabolites into a single solvent, and there is a very wide range of cellular metabolite concentrations, ranging from millimolar concentrations of triglycerides to subpicomolar levels of signaling molecules. Liquid (LC/MS) [8] or gas (GC/MS) [9] chromatography coupled with mass spectroscopy have become the standard platforms for metabolomic analysis. Although each platform can analyze a large number of metabolites, there are limitations on the number of metabolites that can be profiled reliably with a single analytic method. Therefore, to identify the cellular targets for bioactive compounds, we used chemogenomic profiling to inform targeted metabolomic profiling. Specifically, two different methods were used to profile drug-induced metabolomic changes in biosynthetic pathways that were identified

Supplemental digital content is available for this article. Direct URL citations appear in the printed text and are provided in the HTML and PDF versions of this article on the journal's Website (*www.pharmacogeneticsandgenomics.com*).

1744-6872 © 2012 Wolters Kluwer Health | Lippincott Williams & Wilkins

DOI: 10.1097/FPC.0b013e32835aa888

9 Pasikanti KK, Ho PC, Chan ECY. Gas chromatography/mass spectrometry in metabolomic profiling of biological fluids. *J Chromatogr B* 2008; **871**:202–211.
10 Guo K, Li L. Differential 12C-/13C-isotope dansylation labeling and fast liquid chromatography/mass spectrometry for absolute and relative quantification of the metabolome. *Anal Chem* 2009; **81**:3919–3932.
11 Fiehn O, Kopka J, Trethewey RN, Willmitzer L. Identification of uncommon plant metabolites based on calculation of elemental compositions using gas chromatography and quadrupole mass spectrometry. *Anal Chem* 2000; **72**:3573–3580.
12 Ghannoum MA, Rice LB. Antifungal agents: mode of action, mechanisms of resistance, and correlation of these mechanisms with bacterial resistance. *Clin Microbiol Rev* 1999; **12**:501–517.
13 Pierce SE, Davis RW, Nislow C, Giaever G. Chemogenomic approaches to elucidation of gene function and genetic pathways. *Methods Mol Biol* 2009; **548**:115–143.
14 Folch J, Lees M, Sloane Stanley GH. A simple method for the isolation and purification of total lipids from animal tissues. *J Biol Chem* 1957; **226**:497–509.
15 Kind T, Wohlgemuth G, Lee do Y, Lu Y, Palazoglu M, Shahbaz S, Fiehn O. FiehnLib: mass spectral and retention index libraries for metabolomics based on quadrupole and time-of-flight gas chromatography/mass spectrometry. *Anal Chem* 2009; **81**:10038–10048.
16 Benjamini Y, Hochberg Y. Controlling the false discovery rate: a practical and powerful approach to multiple testing. *J R Stat Soc Series B* 1995; **57**:289–300.
17 Hastie T, Tibshirani R, Friedman J. *The elements of statistical learning*. New York: Springer; 2001.
18 Romero P, Wagg J, Green ML, Kaiser D, Krummenacker M, Karp PD. Computational prediction of human metabolic pathways from the complete human genome. *Genome Biol* 2005; **6**:R2.
19 Lepesheva GI, Waterman MR. Sterol 14alpha-demethylase cytochrome P450 (CYP51), a P450 in all biological kingdoms. *Biochim Biophys Acta* 2007; **1770**:467–477.
20 Craven RJ, Mallory JC, Hand RA. Regulation of iron homeostasis mediated by the heme-binding protein Dap1 (damage resistance protein 1) via the P450 protein Erg11/Cyp51. *J Biol Chem* 2007; **282**:36543–36551.
21 Kubo I, Muroi H, Himejima M. Antibacterial activity of totarol and its potentiation. *J Nat Prod* 1992; **55**:1436–1440.
22 Gachotte D, Barbuch R, Gaylor J, Nickel E, Bard M. Characterization of the *Saccharomyces cerevisiae ERG26* gene encoding the C-3 sterol dehydrogenase (C-4 decarboxylase) involved in sterol biosynthesis. *Proc Natl Acad Sci USA* 1998; **95**:13794–13799.
23 Kim H, Sablin SO, Ramsay RR. Inhibition of monoamine oxidase A by beta-carboline derivatives. *Arch Biochem Biophys* 1997; **337**:137–142.
24 Li Y, Sattler R, Yang EJ, Nunes A, Ayukawa Y, Akhtar S, *et al*. Harmine, a natural beta-carboline alkaloid, upregulates astroglial glutamate transporter expression. *Neuropharmacology* 2010; **60**:1168–1175.
25 Jahaniani F, Ebrahimi SA, Rahbar-Roshandel N, Mahmoudian M. Xanthomicrol is the main cytotoxic component of *Dracocephalum kotschyii* and a potential anti-cancer agent. *Phytochemistry* 2005; **66**:1581–1592.
26 Rommelspacher H. The beta-carbolines (harmanes) – a new class of endogenous compounds: their relevance for the pathogenesis and treatment of psychiatric and neurological diseases. *Pharmacopsychiatria* 1981; **14**:117–125.
27 Waitzinger J, Lenders H, Pabst G, Reh C, Ulbrich E. Three explorative studies on the efficacy of the antihistamine mebhydroline (Omeril). *Int J Clin Pharmacol Ther* 1995; **33**:373–383.
28 Abadjieva A, Pauwels K, Hilven P, Crabeel M. A new yeast metabolon involving at least the two first enzymes of arginine biosynthesis: acetylglutamate synthase activity requires complex formation with acetylglutamate kinase. *J Biol Chem* 2001; **276**:42869–42880.
29 Caspi R, Altman T, Dale JM, Dreher K, Fulcher CA, Gilham F, *et al*. The MetaCyc database of metabolic pathways and enzymes and the BioCyc collection of pathway/genome databases. *Nucleic Acids Res* 2010; **38 (Database issue)**:D473–D479.
30 Smith DA, Obach RS. Metabolites in safety testing (MIST): considerations of mechanisms of toxicity with dose, abundance, and duration of treatment. *Chem Res Toxicol* 2009; **22**:267–279.
31 Guengerich FP, MacDonald JS. Applying mechanisms of chemical toxicity to predict drug safety. *Chem Res Toxicol* 2007; **20**:344–369.

by chemogenomic profiling. A recently developed dansyl [5-(dimethylamino)-1-napthalene sulfonamide] derivatization method [10] was coupled with LC/MS analysis to analyze drug-induced changes in metabolites with primary or secondary amines (and some other reactive groups). Dansylation increases metabolite detection sensitivity by 10–1000-fold, and improves metabolite retention and separation on reversed-phase columns [10]. In addition, trimethylsilyl derivatization and GC/MS [11] analysis were used to profile drug-induced metabolite changes in the yeast ergosterol biosynthesis pathway. Ergosterol in yeast is the functional equivalent of cholesterol in mammalian cells; multiple antifungal agents target this biosynthetic pathway [12].

Methods

Chemicals

Individual amino acids, a mixture of amino acid standards (LAA21), dansyl chloride, and sodium decahydrate, were purchased from Sigma-Aldrich (St Louis, Missouri, USA). HPLC grade acetonitrile and water were purchased from Honeywell Burdick and Jackson (Morristown, New Jersey, USA), and LC/MS grade formic acid were from ProteoChem Inc. (Denver, Colorado, USA). Mebhydrolin (mebhydrolin 1,5-naphthalenedisulfonate salt; M5279-1G), fluconazole (M5279-1G), and totarol (532657-100MG) were purchased from Sigma-Aldrich. Harmine (286044-1G) was purchased from Sigma-Aldrich. Terbinafine (SRP01197t) was purchased from Sequoia Research Products (Pangbourne, UK).

Chemogenomic screening protocol and data analysis

Chemogenomic profiling of yeast deletion strains was carried out as described previously [4]. Briefly, yeast pools were grown in the presence of chemical inhibitor at concentrations that inhibited the growth of a wild-type strain by ~10–20%. The homozygous pool (~5000 strains representing nonessential genes) and heterozygous pool (~1100 strains representing genes essential for viability) were grown in YPD + 25 mmol/l HEPES (pH adjusted to 6.8) for 5 and 20 generations, respectively. Genomic DNA extraction, PCR amplification of molecular tags, and Genflex tag16k array (Affymetrix, Santa Clara, California, USA) hybridization, washing, and scanning were carried out as described previously [4,13] Chemogenomic data were analyzed as described previously [4,13]. Briefly, quantile-normalized fluorescence values for each tag were $\log_2$ transformed, and then z-scores were calculated as follows: Tag z-score = [(average of controls) – (experimental value)]/(SD of controls), where controls are 12 DMSO-treated samples. Each strain contains two molecular tags, and the final z-score is the average of the two scores associated with that strain.

Yeast growth assays

Isogenic cultures (100 µl) of yeast deletion strains were inoculated at a concentration of 0.01 OD_{600}/ml and grown in 96-well microtiter plates at 30°C. Optical density was measured every 15 min over the course of several hours (as indicated in graphs) using a GENios microplate reader (Tecan, Mannedorf, Switzerland). The growth rate of each culture was then determined as the average doubling time (AvgG) by recording the time (Δt) from the start of growth until the optical density of the culture reached the calibrated five-generation point and dividing this by the number of generations (i.e. five). We quantified the effect of drug on each strain (relative growth) by dividing AvgG at each concentration tested by AvgG at a noninhibitory concentration of the compound (1.472, 0.098, and 0.071 µmol/l for totarol, harmine, and mebhydrolin, respectively).

Yeast cell preparation

The *Saccharomyces cerevisiae* strain, BY4743, was inoculated into 50 ml of YPD media (10 g/l yeast extract, 20 g/l peptone, and 20 g/l dextrose, supplemented with 25 mmol/l HEPES; pH 6.8) and grown to saturation overnight at 30°C. Cells were then diluted to 0.25 OD_{600}/ml in 50 ml of fresh media. To these cultures, DMSO was added to a final concentration of 1% or a chemical inhibitor was added at concentrations predetermined to inhibit growth by ~10–20%. Cultures were grown for ~4 h at 30°C, at which point a concentration of ~1 OD_{600}/ml was reached. Six 5 ml aliquots of each culture were collected by centrifugation at 3000 rpm for 5 min. Supernatants were removed and each cell pellet was washed with 5 ml of PBS. Samples were centrifuged as above, the supernatant of each sample was carefully removed, and cell pellets were frozen at −80°C until further use.

Metabolite extraction

Yeast pellets were homogenized in PBS buffer with 0.5 mg of 0.5 mm glass beads in a tube by vortexing for a total of 6 min, and the tubes were returned to the ice bath every 2 min for recooling. The homogenized mixture was extracted using the Folch method [14]. The upper aqueous layers of the chloroform : methanol : water mixture, which contained the polar metabolites extracted from the yeast cell pellet, were removed and dried in a Speedvac (Thermo Scientific, Waltham, Massachusetts, USA). The dried extract was then resuspended in water.

Dansylation

Dansylation was carried out using a modification of the procedures developed by Guo and Li [10]. A volume of 50 µl of the polar metabolites were dissolved in 0.1 mol/l sodium tetraborate buffer, and then combined with 50 µl of 20 mmol/l dansyl chloride and vortexed. The mixture was incubated at room temperature for 30 min before the addition of 50 µl of 0.5% formic acid to stop the reaction. The supernatant of the reaction mixture was then placed in an autosampler vial.

LC/MS analysis

All samples were analyzed on an Agilent Technologies Inc. (Santa Clara, California, USA) accurate mass Q-TOF 6520 coupled with an Agilent UHPLC infinity 1290 system. The chromatography runs were carried out using a Phenomenex (Torrance, California, USA) Kinetex reversed-phase C18 column (dimension 2.1×100 mm, 2.6 mm particles, 100 Å pore size). Solvent A was HPLC water with 0.1% formic acid and solvent B was LC/MS grade acetonitrile with 0.1% formic acid. A 30-min gradient at 0.5 ml/min was as follows: $t = 0.5$ min, 5% solvent B; $t = 20.5$ min, 60% solvent B; $t = 25$ min, 95% solvent B; and $t = 30$ min, 95% solvent B. The column was equilibrated at 5% solvent B for 5 min. All data were acquired by positive ESI (electrospray ionization) using Masshunter acquisition software (Agilent Technologies Inc.). Molecular feature extraction on all data was carried out using Masshunter qualitative software. Six independently prepared extracts were analyzed for each yeast strain, and 700–900 different ion features were identified in each extract. The metabolite abundance, which is a measure of the metabolite concentration in an extract, was determined using Agilent Masshunter software, which integrates the peak area for the indicated metabolite on the extracted ion chromatogram for each sample.

GC/MS analysis

The trimethylsilyl-derivatized sterols were analyzed using a 7890GC/7200 Q-TOF instrument (Agilent Technologies Inc.). The samples were analyzed on an HP-5 ms UI (Agilent Technologies Inc.), $30\,\text{m} \times 0.25\,\text{mm} \times 0.25\,\text{mm}$, with 1 µl injection, a split 20 : 1, and a column flow rate of 1.0 ml/min. The split/splitless inlet temperature was 250°C, transfer line was 290°C, source temperature was 230°C, and quad temperature was 150°C. The oven ramp was programmed to maintain the temperature at 60°C for 1 min, increase at 10°C/min to 325°C, and then held for 3.5 min. The scan range was 50–600 amu, and the speed was 5 Hz. The data were acquired using Masshunter acquisition software. The key ergosterol pathway intermediates were identified by searching against a unit mass resolution retention time locked metabolite library [15]. Chromatographic peak deconvolution and quantification were carried out using Masshunter software.

Statistical analyses

For the targeted analysis of metabolites in the ergosterol pathways (Supplemental digital content, Table S1, *http://links.lww.com/FPC/A529*) and in the yeast *arg1*Δ, *arg3*Δ, *arg4*Δ, and *arg*7Δ gene deletion strains (Supplemental digital content, Table S2, *http://links.lww.com/FPC/A530*), the individual chromatograms of metabolites with abundances that were below the detection limit (BDL) were inspected manually to ensure that the metabolite was not present in the sample. If so, the abundance of these metabolites was set to 0 (on the log scale) and a standard two-sample two-sided *t*-test was used to identify metabolites with a significant differential abundance between all of the control and the drug-treated (or gene deletion) extracts on the log scale. The raw *P* values from the *t*-test were then adjusted for multiple testing [16].

All metabolites that were present in more than one sample were analyzed when the wild-type and deletion (ARG4, ARG5,6, or ARG8) strains were analyzed in the presence or absence of mebhydrolin [Supplemental digital content, Tables S3 (*http://links.lww.com/FPC/A531*) and S4 (*http://links.lww.com/FPC/A532*)]. For this analysis, the minimum threshold abundance was empirically set to 1000. If a metabolite was not detected in a sample (i.e. its abundance was below the threshold), it was assumed that its true abundance was uniformly located between 0 and 1000, and its abundance in that sample was assumed to be one-half of the threshold value. It then had an SD: (lower detection limit)/sqrt(12). When the SEM of the metabolite abundance was estimated from the variance in the data, this amount of variation was added to the formula to account for the uncertainty introduced by the estimation of this value. Therefore, the SEM reported in Supplemental digital content, Table S3 (*http://links.lww.com/FPC/A531*) was larger than the SEM estimation obtained by artificially setting all BDL values as equal to half of the lower detection limit. When the statistical significance of these differences was evaluated, a nonparametric Wilcoxon's rank-sum test was used to avoid the artifact induced by the BDL observations. Using this method, all BDL values were treated as equal to each other and smaller than those values that were above the detection limit. The raw *P* values from Wilcoxon's test were then adjusted for multiple testing [16]. It is noteworthy that 12 samples were analyzed for each comparison of metabolite levels in wild-type yeast versus a deletion strain. For each analyzed metabolite, usually all samples (but at least nine of the 12 analyzed samples) for each condition had detectable levels of the analyzed metabolite; the only exception was *N*-acetylornithine levels in the Arg5,6 deletion strain, which was BDL for obvious reasons.

Principal component analysis (PCA) was used to determine the pattern of metabolite changes in an unbiased and unsupervised manner. For this analysis, the BDL observations were treated as described above and the data were then subjected to a $\log_{10}$-based transformation, and PCA [17] was used to display the data. All analyses were carried out using R (*http://www.r-project.org*).

Metabolomic network analysis

A curated (YeastCyc) metabolic pathway database that covers 947 reactions and 694 chemical species is used to analyze yeast metabolomic datasets [18]. The analysis algorithm constructs a table that predicts, for each enzyme-encoding gene and each metabolite in the yeast

metabolic database, whether a decrease in the activity of an enzyme would increase or decrease the concentration of a metabolite. (As many factors are not modeled in the available metabolic networks, not all of these predictions will be correct. However, our testing indicates that the results are valid most of the time.) The analysis assumes that the flux of metabolites through a network is constant and that the concentrations of metabolites will change to partially counteract the effects of altering the activity of an enzyme, either because of reversible reactions or through regulation of the network. Suppose that only the activity of a single enzyme differs between two samples, and that the enzyme activity is lower in the second sample. The concentrations of the reactants for the reaction catalyzed by that enzyme reaction will be reliably greater in the second sample, and the concentrations of products will be less. Consider a reactant A whose concentration is increased in the second sample. Other reactions that consume that reactant could increase in velocity, partially consuming reactant A, and reactions that produce A could decrease in velocity to produce less of it. These changes will alter the concentrations of other substrates of those reactions, and these changes will propagate through additional reactions.

These considerations are used to predict the changes in metabolite concentrations that would occur if an allelic effect (or if an inhibitor or another factor) reduced the activity of each enzyme in the network. Initially, the algorithm predicts that the reactants of the reaction associated with that enzyme increase and the products decrease. It then iteratively propagates the predictions of increased and decreased metabolites through the reaction network. When evaluating the propagation of changes in metabolite concentrations across a network, it is possible that the reactant and product concentrations may be altered in conflicting directions. To cope with this, increases and decreases in metabolite concentrations are propagated separately, and the algorithm assigns to each predicted change a 'reliability' factor that is between 0 and 1, which heuristically represents our confidence in the prediction. More precisely, the algorithm separately calculates the reliabilities for predictions on the basis of increased and decreased metabolite concentrations. During iterative propagation, the algorithm maintains a queue of recent updates that have not yet been propagated through reactions. For each iteration, it removes the update from the queue with maximum reliability, and propagates it through all directly connected reactions to update the concentrations of other metabolites. This is repeated until the queue of updates is empty or the reliability of the updates falls below a specified threshold, at which point the algorithm terminates.

To propagate a change through a reaction, let the metabolite be m and the reliability of the metabolite change be r. All propagated changes will have reliability r/d, where d is the number of reactions that have m as a substrate, on the basis of the reasoning that changes to metabolites involved in many reactions will be diffused by being distributed among those reactions. Hence, changes in the concentration of metabolites such as glucose, which are involved in many reactions, will have lower reliabilities than changes to metabolites that are substrates of very few reactions. Metabolites with degrees of 50 or more are ignored. Without loss of generality, assume that m is a product of a reaction, and that the change in m is an increase. Then, decreases will be propagated for all reaction products and increases will be propagated for all reactants. A change will only be propagated further if the previously computed reliability was less than r/d. The other cases, where m is a reactant of the reaction or where m decreases, are treated similarly.

After propagation terminates, each metabolite will usually have predictions for both increases and decreases. The next step of the algorithm chooses a direction of change by picking whichever has the greatest reliability, and the change is given that reliability, and the reliabilities of decreases are multiplied by -1. If a metabolite has equal reliabilities for increases and decreases, it is assigned a reliability of 0, which is effectively 'no prediction'. By repeating the above computation for each gene that codes for an enzyme, a prediction table is constructed with genes as rows and metabolites as columns. Each row consists of the predictions computed for the reaction controlled by the enzyme coded by that gene. Given a list of measured fold changes for metabolites in different samples, this table is used to calculate a score and rank the genes that are most likely to explain the differences.

The scoring function, which measures the match between the measured and the predicted differences for each analyzed reaction, is calculated as follows: $\sum_{m=1}^{M} rm \log_2 x_m/y_m$, where M is the number of metabolites and x_m and y_m are the measured concentrations of metabolite m in the first and the second samples, respectively. This scoring formula rewards predictions whose direction matches the measured differences and penalizes predictions that oppose the measured differences. Predictions with high reliability and large measured fold changes contribute more toward the score than those with lower reliability and smaller fold changes. The reactions are sorted by decreasing scores for presentation. Genes are then ranked in descending order of their scores.

Results

Metabolomic profiling of drugs that are known to inhibit ergosterol biosynthesis

To determine whether the measurement of drug-induced metabolomic changes in yeast could identify the known target for a drug, we examined the changes in the abundance of metabolites in the ergosterol biosynthetic pathway in wild-type yeast cultures after incubation with

Fig. 1

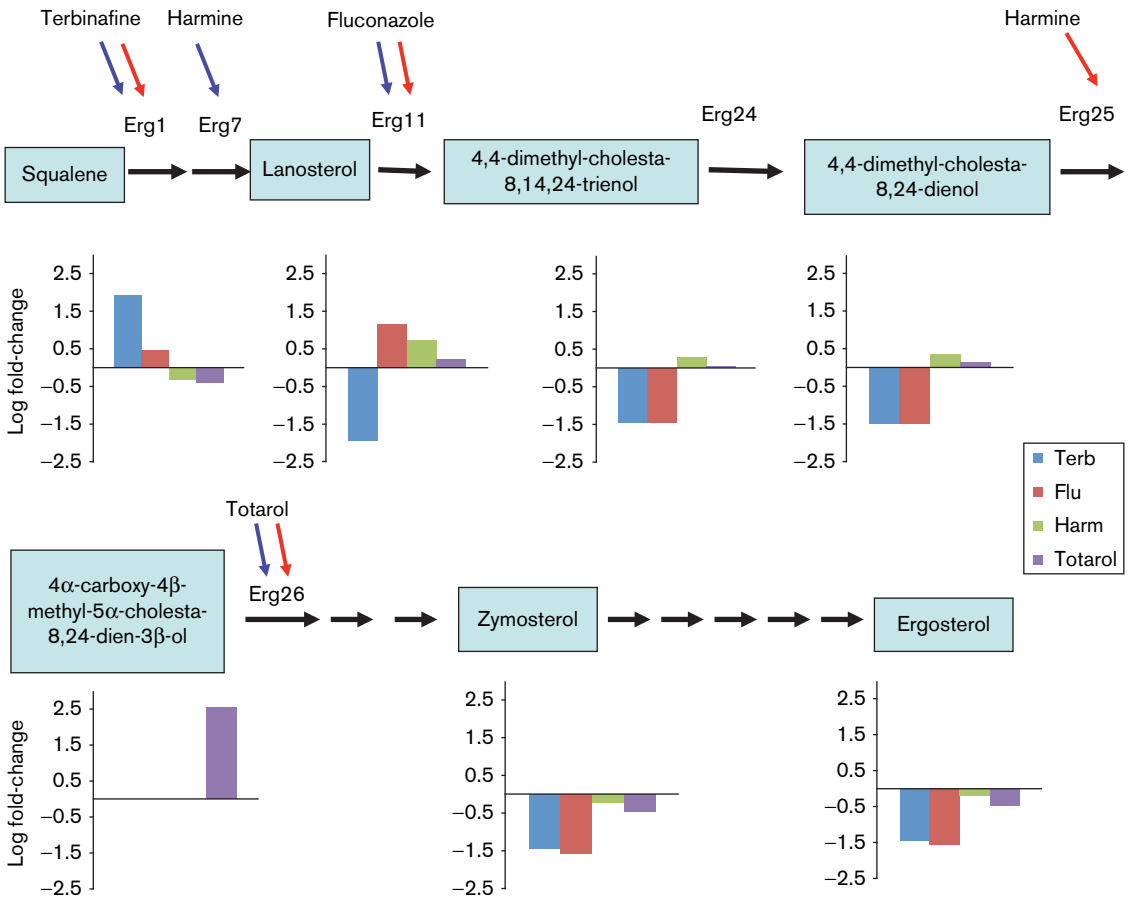

A simplified diagram of the yeast ergosterol pathway from squalene to ergosterol. The boxes represent the seven metabolites that were measured in this study, and the enzymes are listed above each step. The red and blue arrows indicate the targets that were identified by chemogenomic and metabolomic profiling, respectively, for each of the indicated drugs. The insets below each metabolite show the logarithm of the fold-change (relative to control) in the abundance of that metabolite in wild-type yeast after incubation with the drug that is indicated by the corresponding colored bar. Flu, fluconazole; Harm, harmine; Terb, terbinafine.

fluconazole, which is an azole antifungal that is known to inhibit yeast lanosterol 14-α-demethylase (ERG11) [19]. This enzyme is a P450 monooxygenase that catalyzes a critical step in the ergosterol biosynthesis pathway [20] (Fig. 1). Previously obtained chemogenomic profiling results indicated that fluconazole inhibits ERG11 [4]. Therefore, wild-type yeast cultures were incubated with a fluconazole concentration (70 μmol/l for 6 h) that induced a 10% growth inhibition. The abundance of ergosterol pathway metabolites in control and fluconazole-treated cultures was then compared. Fluconazole induced a significant increase in squalene (three-fold, $P = 1.3 \times 10^{-3}$) and lanosterol (14-fold, $P = 3 \times 10^{-7}$) abundance, and significant decreases ($\sim$30-fold) in multiple other downstream ergosterol biosynthesis pathway metabolites, including 4,4-dimemethyl-5α-cholesta-8,14,24-trien-3β-ol, 4,4-dimethyl-5α-cholesta-8,24-dien-3β-ol, and zymosterol (Supplemental digital content, Table S1, *http://links.lww.com/FPC/A529*). These metabolomic changes are consistent with its known ability to inhibit ERG11 (Fig. 1).

The same analysis was also carried out on yeast cultures incubated with terbinafine, an allylamine antifungal agent that inhibits an earlier step in the ergosterol biosynthesis pathway (reviewed in [12]). Previously obtained chemogenomic profiling results indicated that the growth of ERG1 haploinsufficient strains was specifically inhibited by terbinafine [3]. Consistent with it having a different site of action than fluconazole, terbinafine induced a different pattern of metabolomic alterations. Terbinafine (20 μmol/l) caused an 84.3-fold increase (P value $= 3 \times 10^{-9}$) in squalene abundance and an 87.6-fold ($P = 6 \times 10^{-9}$) decrease in lanosterol abundance, along with an $\sim$30-fold decrease in the abundance of multiple other downstream metabolites (Supplemental digital content, Table S1, *http://links.lww.com/FPC/A529*). This pattern

Fig. 2

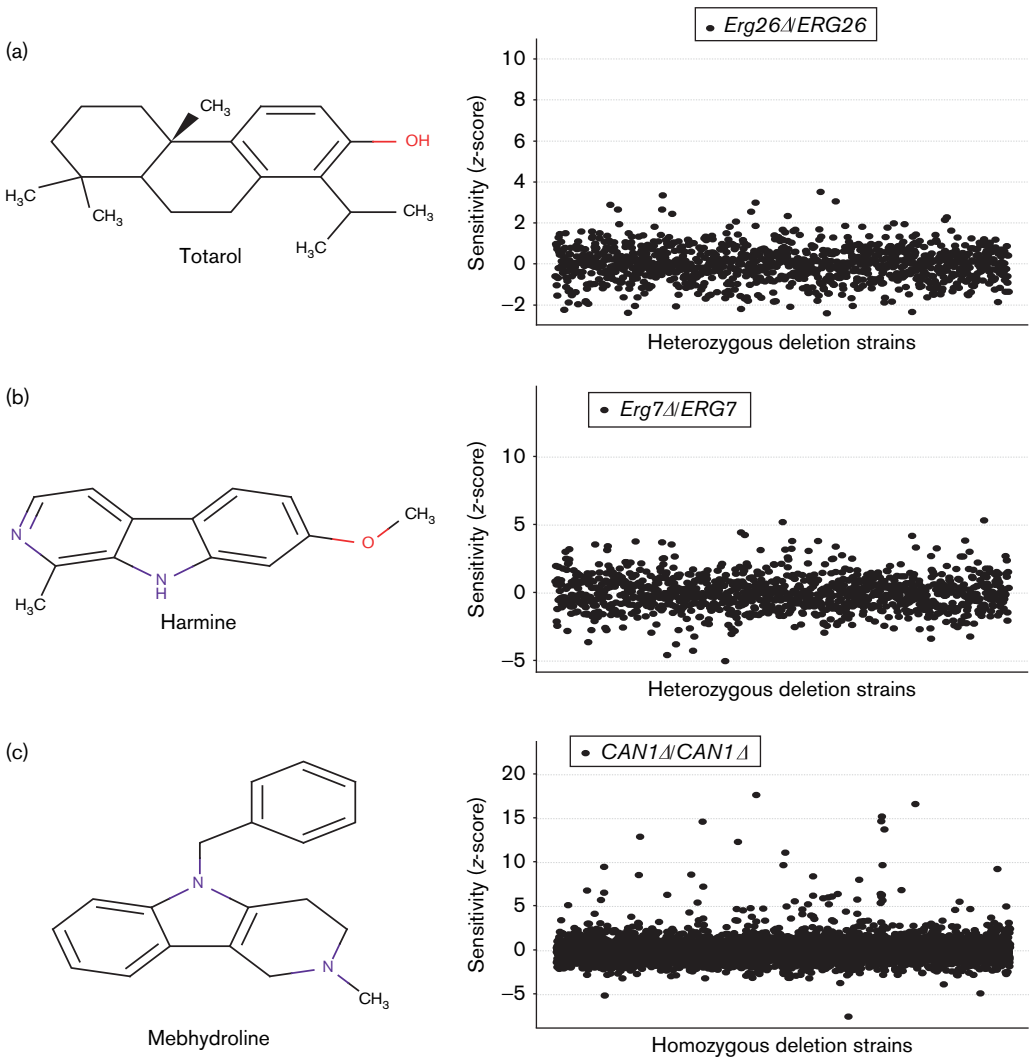

Chemogenomic profiling identifies novel inhibitors of the yeast ergosterol pathway. The chemical structures of totarol, harmine, and mebhydrolin are shown on the left. (a and b) The sensitivity of 1147 yeast heterozygous deletion strains (representing the essential yeast genome) was measured in the presence of totarol or harmine, respectively. The sensitivity of each deletion strain to the compound is plotted on the *y*-axis and the heterozygous deletion strains are arranged alphabetically on the *x*-axis. The most sensitive heterozygous strains in each experiment are labeled. Erg26 is identified as the potential target of totarol and Erg7 as the potential target of harmine. (c) The sensitivity of 4886 homozygous deletion strains was measured in the presence of mebhydrolin. A strain carrying deletions in the *CAN1* gene (encoding an arginine permease) was identified as the strain most sensitive to mebhydrolin.

of metabolomic changes indicates that terbinafine inhibits squalene epoxidase (ERG1) (Fig. 1), which is consistent with the chemogenomic profiling results.

Chemogenomic and metabolomic profiling of two compounds, totarol and harmine, whose mechanism of action has not been characterized previously, was carried out. Chemogenomic profiling indicated that totarol, a natural product with antimicrobial activity [21], inhibited ERG26 (Fig. 2 and Supplemental digital content, Fig. S1, *http://links.lww.com/FPC/A525*). Consistent with the chemogenomic profiling result, totarol (20 μmol/l) induced a 360-fold ($P = 4.3 \times 10^{-11}$) increase in 4α-carboxy-4β-methyl-5α-cholesta-8, 24-dien-3β-ol abundance, whereas the abundance of downstream metabolites (zymosterol and ergosterol) was decreased (Supplemental digital content, Table S1, *http://links.lww.com/FPC/A529*). The proteins encoded by the *ERG25*, *ERG26*, and *ERG27* genes [22] form a multienzyme complex. This complex includes the C-3 sterol dehydrogenase (ERG26), which converts 4α-carboxy-4β-methyl-5α-cholesta-8, 24-dien-3β-ol into zymosterol (Fig. 1). Thus, the measured pattern of metabolite changes indicates that totarol inhibits ERG26. Harmine is a β-carboline alkaloid found in many middle

Fig. 3

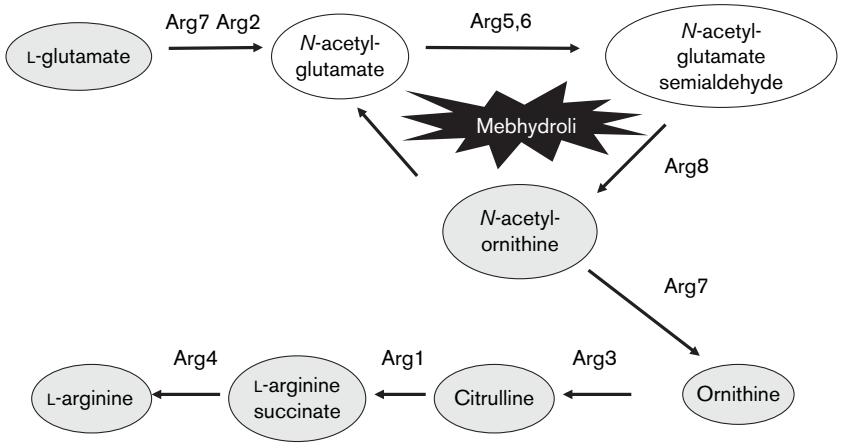

A diagram of the metabolites and reactions catalyzed by yeast deletion mutants in the arginine biosynthesis pathway is shown. The consecutive reactions catalyzed by ARG8 and ARG5,6 are the probable sites for mebhydrolin inhibition. Two metabolites that could not be measured by dansyl derivatization appear in unshaded circles. For harmine, metabolomic profiling implicates a reaction (ERG25) as the target of harmine that is downstream of that identified by chemogenomic profiling (ERG7).

eastern plant families. It has a variety of bioactivities, including inhibition of monoamine oxidase A [23]; altering cellular gene expression [24], DNA topoisomerase inhibition, and induction of cytotoxicity in cancer cell lines [25]. It has been considered as an anticancer agent [25] and for the treatment of Parkinson's and neuropsychiatric diseases [26]. Chemogenomic profiling indicated that harmine selectively altered the growth of a yeast strain with an ERG7 (lanosterol synthase) haploinsufficiency (Fig. 2 and Supplemental digital content, Fig. S1, *http://links.lww.com/FPC/A525*). However, metabolomic profiling indicated that incubation with harmine (200 µmol/l) increased lanosterol abundance by 5.4-fold ($P = 7.5 \times 10^{-8}$) (Supplemental digital content, Table S1, *http://links.lww.com/FPC/A529*), and induced lesser increases in the abundance of the next two metabolites in this pathway. This indicates that harmine inhibits a reaction that is downstream of ERG7 (Fig. 2), which could be the reactions catalyzed by the ERG25–27 complex or another downstream enzyme. Chemogenomic and metabolomic profiling identified closely related steps in the ergosterol pathway as the target for totarol. However, the metabolomic data indicate that an enzymatic step that was downstream of the target identified by chemogenomic profiling is the actual target. It is likely that the proximity of ERG7 to the actual target explains why the growth of a strain with an ERG7 haploinsufficiency would be inhibited by harmine.

Analysis of inhibitors of arginine biosynthesis

To determine whether dansyl derivatization coupled with LC/MS analysis could identify key metabolomic changes, the abundances of arginine biosynthesis pathway metabolites in extracts prepared from four *S. cerevisiae* strains with gene deletions (*arg1*Δ, *arg3*Δ, *arg4*Δ, and *arg*7Δ) were compared with a wild-type strain. The analyses described in the supplement show that the deleted genes could be identified using this metabolomic profiling method (Supplemental digital content, Table S2, *http://links.lww.com/FPC/A530*; Fig. 3). We next examined a chemical with a previously unknown target. Mebhydrolin is an antihistamine that was used previously for the treatment of allergies [27]. Chemogenomic profiling indicated that mebhydrolin selectively affected the growth of a yeast strain with an arginine permease deletion (CAN1D) (Fig. 2 and Supplemental digital content, Fig. S2, *http://links.lww.com/FPC/A526*). Wild-type yeast cultures incubated with a mebhydrolin concentration (150 µmol/l, 6 h) mebhydrolin that caused a 10% decrease in their growth rate showed 4.4-fold and 3.1-fold decreases in the abundances of *N*-acetylornithine ($P = 0.01$) and ornithine ($P = 0.01$), respectively (Supplemental digital content, Table S3, *http://links.lww.com/FPC/A531*). These metabolomic changes indicate that mebhydrolin affected arginine biosynthesis, but its site of action is distinct from the pattern of metabolomic changes in the ARG1, ARG3, ARG4, or ARG7 deletion strains (Fig. 3). Notably, the *neo1*Δ/*NEO1* heterozygous strain also showed sensitivity to mebhydrolin (Supplemental digital content, Fig. S2, *http://links.lww.com/FPC/A526*), indicating that this drug may have multiple cellular targets in yeast.

A computational method for metabolomic network analysis

To facilitate the identification of the mebhydrolin target, a novel computational algorithm for automated analysis of metabolomic datasets was developed. It analyzes the metabolomic changes measured in a set of samples and

Table 1 The 10 highest-ranked genes output by the metabolic network analysis program after analysis of metabolomic datasets for the indicated yeast gene deletion strains and drug treatments

	Deletion							
	ARG1		ARG3		ARG4		ARG7	
	Gene	Score	Gene	Score	Gene	Score	Gene	Score
	ARG1	2.34	*ARG3*	1.65	*ARG4*	1.88	*ARG7*	1.90
	CAR2	1.48	*SPE1*	1.65	*FUM1*	1.19	*ARG3*	0.63
	SPE1	1.47	*ARG7*	1.30	*SPE1*	1.08	*ARO9*	0.63
	ASP1	1.14	*LYS1*	1.30	*CAR2*	1.08	*GDH2*	0.63
	ASP3-2	1.14	*CAR2*	1.14	*URA2*	0.95	*BAT2*	0.63
	ASP3-3	1.14	*ACS1*	0.68	*CAR1*	0.68	*BAT1*	0.63
	ASP3-1	1.14	*ACS2*	0.68	*PRS2*	0.48	*IDP1*	0.63
	ASP3-4	1.14	*ARO9*	0.63	*PRS1*	0.48	*IDP2*	0.63
	ADK2	0.85	*BAT2*	0.63	*PRS3*	0.48	*IDP3*	0.63
	ADK1	0.85	*BAT1*	0.63	*PRS4*	0.48	*SPE1*	0.63
Mebhydrolin		Fluconazole		Totarol		Harmine		Terbinafine	
Gene	Score	Gene	Score	Gene	Score	Gene	Score	Gene	Score
ARG8	2.45	*ERG11*	3.24	*ERG26*	2.71	*ERG25*	0.61	*ERG7*	4.01
AAT2	1.11	*FDH1*	1.74	*ERG27*	1.76	*ERG27*	0.24	*ERG1*	3.05
AAT1	1.11	*ADE3*	1.73	*ERG11*	1.63	*ERG24*	0.24	*ERG27*	1.24
CAR1	1.11	*MIS1*	1.73	*HEM14*	1.35	*ERG11*	0.19	*MHT1*	0.37
ALT1	0.94	*ERG27*	1.44	*FMS1*	1.35	*ERG26*	0.13	*FDH1*	0.37
GLT1	0.88	*ERG24*	0.71	*POX1*	1.35	*FDH1*	0.09	*ADE3*	0.36
LYS20	0.80	*SOD2*	0.64	*CAT5*	1.35	*ADE3*	0.09	*MIS1*	0.36
LYS21	0.80	*CTA1*	0.64	*HEM13*	1.35	*MIS1*	0.09	*COQ5*	0.36
STR2	0.79	*CTT1*	0.64	*ADI1*	1.35	*ERG9*	0.08	*COQ3*	0.36
ARG2	0.78	*SOD1*	0.64	*COQ6*	1.35	*MHT1*	0.05	*SPE2*	0.36

Of note, the relatively lower scores for the genes identified from analysis of the harmine dataset are because of the smaller changes in metabolite abundance that were induced by harmine.

identifies the genes that could be responsible for the measured changes in metabolite concentrations. A curated (YeastCyc) metabolic pathway database that covers 947 reactions and 694 chemical species is used to analyze yeast metabolomic datasets [18]. In brief, this algorithm uses this yeast metabolic database to predict the effect that a change in the activity of each enzyme would have on the concentration of each metabolite in the database. The metabolomic differences measured in a sample dataset are then compared with these predictions to compute a score that assesses the match between the predicted and the measured metabolite changes for each gene. To test this computational method, the metabolomic data generated from four yeast strains with gene deletions in the arginine biosynthesis pathway were analyzed. For each of these datasets, this algorithm correctly identified the deleted gene as the one that was most likely to cause the measured metabolomic changes (Table 1). For example, ARG4 (argininosuccinate lyase) was the highest-ranking gene for the ARG4 deletion mutant data (score 1.88). The next highest-scoring gene was FUM1 (score 1.19), which is an enzyme that acts on a product (fumarate) of the ARG4 reaction. A more detailed description of the analysis of ARG3 and ARG4 gene deletions is provided in Supplemental digital content, Fig. S4 (*http://links.lww.com/FPC/A528*). We next assessed the ability of this algorithm to analyze the metabolomic changes induced in wild-type yeast after incubation with four different drugs, which provided a more rigorous test of this software. The algorithm correctly identified ERG11 and ERG26 as the genes that were most likely to be inhibited by fluconazole and totarol, respectively. ERG25 was the highest-scoring gene when the harmine data were analyzed. ERG1 had the second-highest ranking when the terbinafine data were analyzed (Table 1). Taken together, the results from analyzing metabolomic changes in yeast with four different gene deletions, and after treatment with four different drugs indicate that this computational method has the potential to correctly identify the factors responsible for metabolomic differences in yeast.

Analysis of the mebhydrolin-induced metabolomic changes

When the mebhydrolin-induced metabolite changes were evaluated using the computational method, it identified ARG8 as the gene that was most likely to be inhibited by mebhydrolin (Table 1). To examine this possibility, we characterized mebhydrolin-induced metabolomic changes in ARG4, ARG5,6, and ARG8 deletion strains (Supplemental digital content, Table S4, *http://links.lww.com/FPC/A532*). The ARG5,6 and ARG8 enzymes catalyze consecutive steps in the arginine biosynthesis pathway, which convert *N*-acetylglutamate into *N*-acetylornithine (Fig. 3). The pattern shown by PCA indicated that mebhydrolin treatment induced a large number of metabolomic changes in the wild-type strain, but exerted a much smaller effect on the ARG5,6 and ARG8 deletion strains (Supplemental digital content, Fig. S3, *http://links.lww.com/FPC/A527*). Importantly, the mebhydrolin-induced changes in arginine biosynthesis pathway metabolites (citrulline, ornithine, *N*-acetylornithine) that were

observed in the wild-type strain did not occur in the drug-treated ARG5,6 and ARG8 deletion mutants (Supplemental digital content, Table S3, *http://links.lww.com/FPC/A531*). Mebhydrolin induced a larger number of metabolomic changes in the ARG4 strain (Supplemental digital content, Fig. S3, *http://links.lww.com/FPC/A527*), a strain that has a gene deletion in a more distal segment of the arginine biosynthesis pathway (Fig. 3). Taken together, the metabolomic profiling results in the wild-type and in the deletion strains indicate that mebhydrolin targets an early step in the arginine biosynthesis pathway, which is catalyzed either by ARG5,6 or by ARG8. As dansyl derivatization cannot measure an intermediate (*N*-acetylglutamate) in the reaction cascade catalyzed by these enzymes, the metabolomic profiling data cannot determine which of these two enzymes is the specific target. The kinase encoded by *ARG5,6* forms a complex with the acetylglutamate synthase that is produced by *ARG7* and *ARG2*, which regulates the early steps in the arginine biosynthesis pathway [28].

Discussion

Metabolomic profiling cannot systematically quantify all cellular metabolites, and we believe that it is best applied in a targeted manner. Conversely, chemogenomic profiling can interrogate a wide range of genes systematically, but the resulting sensitivity profiles do not unambiguously identify the target for the chemical in question. For most of the drugs analyzed here, metabolomic and chemogenomic profiling identified concordant targets. However, in the case of harmine, chemogenomic and metabolomic profiling identified different targets, both of which were in the ergosterol pathway. Thus, we argue that a combination of the two approaches, comprehensive chemogenomic profiling, followed by targeted metabolomic profiling, provides a superior strategy for drug target identification than the use of either method alone.

The basis for the different mebhydrolin targets identified by metabolomic and chemogenomic profiling is quite clear. As arginine is present in the growth medium, the growth of a yeast strain with an arginine transporter gene deletion would be highly sensitive to an inhibitor of arginine biosynthesis, which explains why chemogenomic profiling would identify CAN1D as sensitive to mebhydrolin. However, metabolomic profiling identified the enzymes in the arginine biosynthesis pathway that could be the direct target for this drug. Thus, the results from the two methods are actually confirmatory of each other; the chemogenomic and the metabolomic results indicate that mebhydrolin affects arginine biosynthesis.

Although we analyzed yeast metabolomic data, the metabolomic network analysis program could also be used to analyze metabolomic data obtained from mouse, rat, or human sources. This capability is enabled by the availability of metabolomic networks that have been prepared for multiple other mammalian species [29]. Of note, the accuracy of the results produced by the metabolic network analysis program is limited by the accuracy and completeness of the available metabolic networks. There are still many interactions between metabolites and enzymes that are not modeled in the existing metabolic networks, and there are many metabolites that are yet to be discovered. However, the functioning of this program will undoubtedly improve as the holes in the available networks are filled in. Related to this, it will be important to determine how efficiently drug targets identified in yeast translate into mammalian systems. This can be assessed by evaluating the effect that the drugs have on rodent tissues *in vivo* or on human cells *in vitro*. A limitation for the utility of this yeast system is the fact that it is most often a drug metabolite, rather than the parent drug itself, that induces an unexpected drug-induced toxicity [30,31]. As yeast lack human drug-metabolizing enzymes, it is likely that the 'off-target' effects induced by human drug metabolites will be difficult to identify using a yeast-based system. However, the targets of the parent drug, which are identified using this yeast-based system, are more likely to translate to mammalian systems.

Acknowledgements

G.P. and M.W. were partially supported by funding from a transformative RO1 award (1R01DK090992-01). D.L.D. and W.Z. were supported by a King Abdullah University of Science and Technology (KAUST) research grant under the KAUST Stanford Academic Excellence Alliance program. S.S., U.S., R.D. and B.S. were partially supported by funding from the National Human Genome Research Institute (2R01HG003317-05) provided to R.D.

Conflicts of interest

There are no conflicts of interest.

References

1 Giaever G, Chu AM, Ni L, Connelly C, Riles L, Veronneau S, *et al.* Functional profiling of the *Saccharomyces cerevisiae* genome. *Nature* 2002; **418**: 387–391.
2 Giaever G, Flaherty P, Kumm J, Proctor M, Nislow C, Jaramillo DF, *et al.* Chemogenomic profiling: identifying the functional interactions of small molecules in yeast. *Proc Natl Acad Sci USA* 2004; **101**: 793–798.
3 Lum P, Armour C, Stepaniants S, Cavet G, Wolf M, Butler J, *et al.* Discovering modes of action for therapeutic compounds using a genome-wide screen of yeast heterozygotes. *Cell* 2004; **116**:121–137.
4 Hoon S, Smith AM, Wallace IM, Suresh S, Miranda M, Fung E, *et al.* An integrated platform of genomic assays reveals small-molecule bioactivities. *Nat Chem Biol* 2008; **4**:498–506.
5 Parsons AB, Lopez A, Givoni IE, Williams DE, Gray CA, Porter J, *et al.* Exploring the mode-of-action of bioactive compounds by chemical-genetic profiling in yeast. *Cell* 2006; **126**:611–625.
6 Crutchfield CA, Lu W, Melamud E, Rabinowitz JD. Mass spectrometry-based metabolomics of yeast. *Methods Enzymol* 2010; **470**:393–426.
7 Cooper SJ, Finney GL, Brown SL, Nelson SK, Hesselberth J, MacCoss MJ, *et al.* High-throughput profiling of amino acids in strains of the *Saccharomyces cerevisiae* deletion collection. *Genome Res* 2010; **20**:1288–1296.
8 Want EJ, Nordstrom A, Morita H, Siuzdak G. From exogenous to endogenous: the inevitable imprint of mass spectrometry in metabolomics. *J Proteome Res* 2007; **6**:459–468.

如需了解更多咨询
www.agilent.com/chem/cn

查找当地的安捷伦客户服务中心：
www.agilent.com/chem/contactus:cn

安捷伦客户服务中心：
免费专线：800-820-3278
400-820-3278（手机用户）

联系我们：
customer-cn@agilent.com

在线询价：
www.agilent.com/chem/quote:cn

2013 年 2 月 1 日中国印刷

Agilent Technologies